April 2021

BUCKLING OF THIN CYLINDRICAL SHELLS: IMPERFECTION SENSITIVITY, NON-DESTRUCTIVE TECHNIQUE FOR CAPACITY PREDICTION AND APPLICATION FOR WIND TURBINE TOWERS

Kshitij Kumar Yadav
University of Massachusetts Amherst

BUCKLING OF THIN CYLINDRICAL SHELLS: IMPERFECTION SENSITIVITY, NON-DESTRUCTIVE TECHNIQUE FOR CAPACITY PREDICTION AND APPLICATION FOR WIND TURBINE TOWERS

A Dissertation Presented

by

KSHITIJ KUMAR YADAV

Submitted to the Graduate School of the
University of Massachusetts Amherst in partial fulfillment
of the requirements for the degree of

DOCTOR OF PHILOSOPHY

February 2021

Civil & Environmental Engineering

BUCKLING OF THIN CYLINDRICAL SHELLS: IMPERFECTION SENSITIVITY, NON-DESTRUCTIVE TECHNIQUE FOR CAPACITY PREDICTION AND APPLICATION FOR WIND TURBINE TOWERS

A Dissertation Presented

by

KSHITIJ KUMAR YADAV

Approved as to style and content by:

Simos Gerasimidis, Chair

Sanjay R. Arwade, Member

Matthew A. Lackner, Member

John Tobiason, Department Head
Civil & Environmental Engineering

ACKNOWLEDGMENTS

This dissertation is the manifestation of my intellectual and personal growth, accumulated since the starting of my formal education. Many people helped me, directly or indirectly, to reach this stage; this thesis allows me to remember them and to express my gratitude. Naming them all is not possible partly due to the limit of the dissertation, and mainly due to my fear that I may miss some of them! Their support, encouragement, guidance, and inspiration are acknowledged and appreciated. I am profoundly grateful to all. However, few names deserve to be mentioned, whose influence on me is notable during my pursuit of the Ph.D.

First, I would like to thank my supervisor, Dr. Simos Gerasimidis, for giving me the opportunities to work with him on the challenging and fascinating field of thin shell stability. His emphasis on communication—both verbal and written— helped me to improve my presentation and writing skills; without these skills, this thesis would not have been written. Moreover, thank you, Dr. Gerasimidis, for funding me so that I could not only continue my study but also live a decent life at Amherst. I recognize and appreciate your intellectual and financial supports. I thank the members of my thesis committee Professor Sanjay R. Arwade and Professor Matthew A. Lackner, for readily agreeing to participate, giving valuable comments and contributions. I was immensely benefited by the courses offered by Professor Sanjay R. Arwade on Advanced Solid Mechanics and Probabilistic Methods in Structural Mechanics. These courses not only strengthen and refined my understanding but also gave me a new perspective on the subjects.

UMass, Amherst gave me many opportunities to grow through teaching assistant and tutor positions: developing course curriculum, creating and grading assignments, organizing discussions and debates in the class and moderating them, identifying

students who face difficulty and helping them to resolve their problems, and many more. These opportunities make me not only better teacher, researcher, and organizer, but also a better person; thank to the College of Engineering, and particularly the Department of Civil and Environmental Engineering.

I am fortunate to have wonderful colleagues at UMass; they made my stay at Amherst joyful and comfortable. I thank my group members Panos, George, and Fani, for their support and for the quality time we spend in the office and outside the office. Discussions with Alaa on Finite Element Methods have always been informative and educational. I thank Alaa for his technical and emotional supports and to Abbas and Hernan for making the office a fun place.

I would like to thank my friends and flatmates Akash, Abhilash, and Chetan; It was incredible to debate, travel, and cook with you. Your help during my initial transition is commendable. Discussing with Satyam on a wide range of topics, from physics to metaphysics and from politics to history, during the morning tea and the dinner time is enlightening. I thank to Rohan and Santosh for the quality time we shared during the last two years of my stay at Amherst. You people make my life at Amherst memorable.

Finally, I would like to thank, my family. Their unconditional love and support have always been a source of encouragement and inspiration; without that, it would have not been possible for me to pursue a Ph.D. and write this thesis. I especially thank my wife, for all her sacrifices and support.

ABSTRACT

BUCKLING OF THIN CYLINDRICAL SHELLS: IMPERFECTION SENSITIVITY, NON-DESTRUCTIVE TECHNIQUE FOR CAPACITY PREDICTION AND APPLICATION FOR WIND TURBINE TOWERS

FEBRUARY 2021

KSHITIJ KUMAR YADAV

B.Tech., MADAN MOHAN MALAVIYA ENGINEERING COLLEGE

GORAKHPUR, INDIA

M.Tech., INDIAN INSTITUTE OF TECHNOLOGY KANPUR, INDIA

Ph.D., UNIVERSITY OF MASSACHUSETTS AMHERST

Directed by: Dr. Simos Gerasimidis

The presence of imperfections significantly reduces the load-carrying capacity of thin cylindrical shells and the reduction depends on the shape and the size of the imperfections. As a result, the prediction of the shells' buckling capacity requires a priori knowledge about the imperfections—a difficult, expansive, and time-consuming adventure, if not impossible. Consequently, thin cylindrical shells are designed conservatively using the knockdown factor approach that accommodates the uncertainties associated with the imperfections present in the cylinders; almost all the design codes follow this approach explicitly or implicitly. However, cylindrical shells can be designed more efficiently by making them insensitive to imperfections, or by knowing their exact capacity without the difficult task of measuring the imperfections. This dissertation examines these two approaches for the efficient designing of thin cylindrical shells. In addition, we investigate buckling behavior and imperfection sensitivity of thin cylindrical shells under pure bending along with their applications in tall wind turbine towers.

For making thin cylindrical shells insensitive to imperfection, wavy cross-sections are proposed instead of circular cross-sections. Past studies have demonstrated the effectiveness of wavy cylinders to reduce imperfection sensitivity under axial compression assuming linear elastic material behavior and using eigenmode imperfections. In this dissertation, using a realistic dimple-like imperfection, new insights are presented into the response of wavy cylinders under uniform axial compression and bending. We found that thin cylindrical shells can be made imperfection insensitive by manipulating their cross-section geometry. For high-fidelity estimates of the capacity of thin cylindrical shells without measuring the imperfections, a novel procedure is proposed based on the probing of the axially loaded cylinders. Computational implementation of the proposed procedure yields accurate results when the probing is near the imperfection; however, the procedure over-predicts the capacity when the probing is away from the imperfection. It demonstrates the crucial role played by the probing location and shows that the prediction of imperfect cylinders is indeed possible if the probing is at the proper location.

The behavior of cylindrical shells under bending and their imperfection sensitivity have not been fully understood for all the range of dimensions. In this dissertation, we investigate the buckling behavior and imperfection sensitivity of thin steel cylindrical shells under pure bending, focusing on a specific range of slenderness, which is found in energy structures such as tall wind turbine towers ($60 < R/t < 120$). We found that strain-hardening models play an impactful role on the bending behavior; moreover, the presence of imperfections reduces the collapse curvature more than the reduction in peak moment. Further, we propose wavy wind turbine towers to make wind turbine towers efficient. The imperfection sensitivity of the wavy towers is evaluated, and we found that the sensitivity of the wavy towers is small compared to that of the circular towers.

PREFACE

Published Content:

This thesis has been partially adapted from [1–4]:

1. **Yadav, K.K.**, Gerasimidis, S. (2019), Instability of thin steel cylindrical shells under bending, *Thin-Walled Structures*, 137: 137: 151-166.
   Author's contributions: Conception and design of study, performed finite element simulations, analyzed and interpreted data, wrote manuscript.

2. **Yadav, K.K.**, Gerasimidis, S. (2020), Imperfection Insensitivity of Thin Wavy Cylindrical Shells Under Axial Compression or Bending, *Journal of Applied Mechanics*, 87(4): 041003.
   Author's contributions: Conception and design of study, performed finite element simulations, analyzed and interpreted data, wrote manuscript.

3. **Yadav, K.K.**, Gerasimidis, S. (2020), Imperfection insensitive thin cylindrical shells for next generation wind turbine towers, *Journal of Constructional Steel Research*, 172: 106228.
   Author's contributions: Conception and design of study, performed finite element simulations, analyzed and interpreted data, wrote manuscript.

4. **Yadav, K.K.**, Nicholas, C., Emmanuel, V., Rubinstein, S.M., Gerasimidis, S. (2020), Imperfection A non- destructive technique for the evaluation of thin cylindrical shells axial buckling capacity, *Manuscript in preparation.*
   Author's contributions: Performed finite element simulations, analyzed data, wrote manuscript.

TABLE OF CONTENTS

LIST OF TABLES

LIST OF FIGURES

Figure **Page**

CHAPTER 1

INTRODUCTION

1.1 Overview

From aircraft fuselages to roofs of large buildings and from boat hulls to tall wind turbine towers, thin shell structures are used extensively due to their structural efficiency and appeal to aesthetics. Owing to the ease of construction, thin cylindrical shells occupied a prominent place among thin shell structures. However, the high sensitivity of thin cylindrical shells to imperfections diminishes their structural efficiency and induces an element of uncertainty. The presence of imperfections in thin cylindrical shells reduces their load carrying capacity significantly, and extensive studies have been followed to understand this peculiar nature[5–14]. All thin cylindrical shells contain imperfections in one form or another, and thus potential of thin cylinders is not utilized fully. As a result, thin cylindrical shells are designed conservatively using the knockdown factor approach; almost all the design codes follow this approach explicitly or implicitly, e.g., Eurocode [15]. In this way, we learnt to live with the problem, but the problem has not yet been solved and long been an obstacle for the efficient use of thin cylindrical shells. Nonetheless, the quest to reduce the imperfection sensitivity of the thin shells has been continued for a long time. Moreover, recently, attempts are being made for high-fidelity estimates of the capacity of imperfect thin shells.

Among the many applications of thin cylindrical shells, wind turbines are the ones with continuously increasing use, and it is anticipated that this trend will accelerate in the coming future. The need for more vigorous wind harvesting has given impetus not only to many technological advances but also to the design of more efficient wind

turbines. One of the many technical goals of today's wind energy industry is to develop solutions for taller wind turbine towers because the increase in their height is imperative to achieve more efficiency as the wind profile is stronger and more stable at higher elevations [16]. However, tall and super tall wind turbine towers pose numerous design challenges to structural engineers. Tall wind turbine towers are generally made of thin steel cylindrical shells with the radius-to-thickness ratios (R/t) varying from 60 to 120 [17–20]. The primary load on the towers is bending and thus understanding the bending behavior of thin steel cylindrical shells within this range of slenderness is essential to the design challenges. Another challenge is imperfection sensitivity of thin tapered cylinders, which are traditionally used to make the wind turbines towers, and are responsible for the conservative design of the towers. The efficient tall and super-tall wind turbines can not be made using the traditional conservative methods. Innovative designs are needed.

1.2 Literature review

1.2.1 Review of cylindrical shells under bending

The phenomenon of buckling of thin cylindrical shells under bending has been among the most interesting instability mechanics problems. It is a complex phenomenon due to the interaction of two different modes of failure, namely, ovalization and bifurcation. Ovalization is the phenomenon in which the cross-section of the cylindrical shell changes from circle to oval under the application of bending moment [21]. The primary consequence of ovalization is the non-linear moment-curvature relationship that is represented as:

$$M = EI(M)\frac{d^2u}{dx^2} \tag{1}$$

Where M is the applied bending moment, I is the moment of inertia, E is Young's modulus and $\frac{d^2u}{dx^2}$ is the curvature. Due to the non-linearity of equation 1, there exists a curvature $\left(\frac{d^2u}{dx^2}\right)$ at which the moment reaches its peak value and starts reducing even when the curvature increases. This peak moment is known as the limit moment, and it could happen in elastic or inelastic range depending on the value of R/t and the material properties. Brazier [21] derived the equation for the limit moment in the elastic range that is expressed as:

$$M_{limit} = 2\sqrt{2}\frac{E\pi Rt^2}{9} \tag{2}$$

Many researchers studied the elastic ovalization of cylindrical shells under different loading conditions using the refined shell theory [22–28]. Later, the study of inelastic ovalization was motivated by offshore gas pipelines, which always fail due to inelastic buckling [17]. The group of Kyriakides [29–31] and Karamanos and Tassoulas [32] studied the inelastic ovalization under combined bending and external pressure.

All the above-mentioned studies are related to one aspect of thin cylindrical shells under bending, i.e., ovalization. Bifurcation instability and its interaction with ovalization are other important aspects of the phenomenon. This prebuckling nonlinear ovalization phenomenon is the main difference between thin cylindrical shells under pure bending and thin cylindrical shells under pure compression. For cylindrical shells under pure axial compression, buckling appears in the form of wrinkles when stresses reach a critical stress σ_{cr}. The value of σ_{cr} is [13]:

$$\sigma_{cr} = \frac{E}{\sqrt{3(1-\nu^2)}}(\frac{t}{R}) \tag{3}$$

Neglecting imperfection effects, this equation can only be applied for very short cylindrical shells under bending, for which the ovalization is constrained by the end

boundary conditions [33]. Ovalization can also be prevented for longer cylinders by stiffening techniques such as stiffening rings. For these cases, the critical moment can be defined as:

$$M_{Bifurcation} = \frac{E\pi Rt^2}{\sqrt{3(1-\nu^2)}} \tag{4}$$

Where ν is the Poissons ratio. Equations 3 and 4 are valid only if the cross-section of the cylinder does not change, i.e., ovalization is prevented. If ovalization is allowed, the interaction between ovalization and bifurcation takes place and the value of σ_{cr}, given by Axelrad [34], is:

$$\sigma_{cr} = \frac{E}{\sqrt{3(1-\nu^2)}}(\frac{t}{R_{local}}) \tag{5}$$

Where R_{local} is the local radius at the ends of the minor axis of the ovalized cross-section, at the region of maximum curvature (compressive side). It is essentially the same formula that Hutchinson [35] found for the elastic buckling of oval shape cylinder under axial compression. The value of R_{local} is always more than R and thus due to pre-buckling ovalization, the moment required for bifurcation is reduced. The bending capacity of cylindrical shells in the elastic range is the smallest of the two: $M_{Bifurcation}$ and M_{limit}. Numerous studies aimed to understand the interaction between ovalization and bifurcation in the elastic range and varied loading conditions [36–45]. The interaction between ovalization and bifurcation is more complex in the inelastic range. Failure could occur due to the ovalization or bifurcation depending on the R/t ratio and material properties. Studies had been done to understand the interaction between ovalization and bifurcation in inelastic range [33, 46–52], but for lower R/t ratio (< 60).

The interest in the bending behavior of thin steel cylindrical shells, with higher R/t, has been increased recently due to the demand of tall wind turbine towers, tubular pipes etc [17–19, 53–58]. The dimensions of the cylindrical shells used in

these applications are different from gas pipelines and thus new studies are needed focusing on higher R/t. Although with these studies, the progress has been made to understand the bending behavior of thin cylindrical shells under bending, which are used in tall and super tall wind turbine towers. But, these studies does not attempt to understand, thoroughly, the effect of material hardening models on the bending capacity. This aspect is crucial as these cylinders fail inelastically, i.e, at the peak bending moment, the stresses at some part of cylinders are more than yield stress limit. A part of this study is an attempt to fill this gap.

A highly important characteristic of the instability of thin cylindrical shells stems from their imperfection sensitivity. Cylindrical shells are highly sensitive to imperfections and the presence of imperfections can reduce the load carrying capacity disproportionally to the size of imperfections. Koiter [8] demonstrated the reason of imperfection sensitivity of thin cylindrical shells in his celebrated thesis. Extensive study had been done to understand the imperfection sensitivity of thin cylindrical shells [17, 33, 59–63]. The current practice to deal with the imperfection sensitivity of cylindrical shells is to use conservative knockdown factors, which were developed by NASA in the late sixties. The capacity of perfect cylinders is reduced by the knockdown factor and assigned as the design capacity. The values of the knockdown factor are provided by NASA [64] and shown in figure 1.1. To tackle the imperfection sensitivity, Eurocode [15] recommends inducing equivalent geometric imperfections in the perfect cylinder, the amplitude of which is specified based on the fabrication quality. The imperfection sensitivity of thin cylindrical shells depends on many factors, i.e., R/t ratio, material properties, loading scenarios, type and amplitude of imperfection. Thus knockdown factor must take account of these parameters, which is not the case with current design practices.

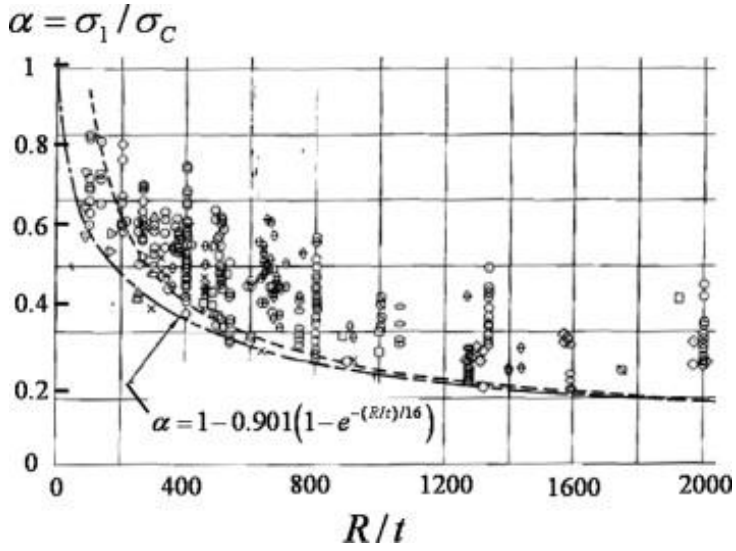

Figure 1.1: Distribution of experimental value of knockdown factor against the R/t ratio along with NASA [64] recommendation for lower bound knockdown factor. Reproduced from the report of Seide et al. [65].

1.2.2 Review of imperfection insensitive thin wavy cylinders

Due to high sensitivity of thin cylindrical shells to imperfections, almost all design codes, as discussed in the previous subsection, [15, 64] use the knockdown factor approach. In this approach, the theoretical capacity of thin cylindrical shells is reduced by a factor, known as the knockdown factor and the resulting value is assigned as the basis for calculating the design capacity. This way, the effect of imperfections is incorporated into the design. In figure 1.1, the experimental values of axial compressive capacity and bending capacity of thin cylindrical shells are plotted against radius to thickness ratio (R/t) along with the lower bound curves. These lower bound curves are the empirical knockdown factor which are used to calculate the design capacity. In figure 1.2, the empirical knockdown factor for axial compression and bending are plotted separately for more clarity. The capacity of a thin cylinder is reduced significantly, around 41% and 32% for axial compression and bending load scenarios

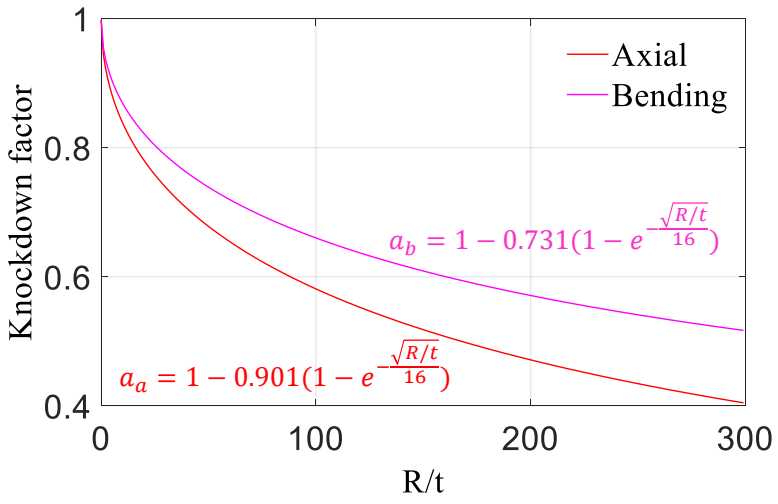

Figure 1.2: The lower bound knockdown factor [64, 65] for bending and axial compression without experimental data for clarity.

respectively for $R/t = 100$. European codes [15] also recommend similar reductions based on construction quality. These reductions are conservative, but necessary, as many uncertainties are associated with the shape and the size of imperfections.

With the developments in manufacturing processes and the sophistication in construction, the empirical formulas for knockdown factor could potentially be reconsidered [66] and become less conservative. With these improvements, the quality of manufactured cylinders has improved, but the sensitivity of cylinders to imperfections is still there. In other words, advanced manufacturing techniques have reduced the presence and amplitude of imperfections, but they cannot eliminating the sensitivity of thin cylinders to imperfections. An alternative way to increase the capacity of thin cylinders and to reduce their sensitivity to imperfections, is the use of stiffeners along the axial and circumferential directions. However, these stiffeners increase the required volume of material and the cost of construction [66]. In all the attempts to improve the design of thin cylinders, the fundamental problem which is the sensitivity to imperfections, is always present and dominating.

Recently, an alternative approach has emerged to reduce the imperfection sensi-

tivity and to increase the load carrying capacity of thin cylindrical shells [66–68, 76]. Wavy cross-sectional shapes are explored instead of circular cross-sections. The wavy cross-section shape reduces the effective slenderness (R/t) of cylindrical shells as the local radius of curvature is reduced and consequently, the imperfection sensitivity of thin cylindrical shells is also reduced. Furthermore, the stiffness developed by the waviness and the periodic change in the direction of curvature also play an important role to make wavy cylinders insensitive to imperfections. This approach changes the characteristic of thin cylindrical shells fundamentally and consequently, the response of thin cylinders to imperfections is altered.

Ning and Pellegrino [66, 67], have carried out a computational and experimental study to investigate the imperfection sensitivity of wavy shape cross-sectional cylindrical shells and they have presented highly promising results. In their computational work, thin cylinders are subjected to axial compression, the material is linear elastic and the shape of imperfection is the first eigenmode. In their experimental work, they have validated this new approach by measuring the geometric imperfection by a photogrammetry technique and then incorporating the imperfection in the computational models. These experiments confirmed that the wavy shells are not sensitive to imperfections and have put thin cylindrical shells in a new light which has opened up new avenues of exploration.

1.2.3 Review of imperfection insensitive next generation wind turbine towers

As energy sources are tilting more toward renewable sources, the demand for efficient and inexpensive wind turbines has been increasing in recent decades. The demand for efficient tall and super- tall wind turbine towers poses numerous challenges to structural engineers. One of the challenges is the imperfection sensitivity of thin

tapered cylinders, which are traditionally used to make the wind turbines towers. The imperfection sensitivity of thin tapered cylinders is responsible for the conservative design of the towers. The efficient tall and super-tall wind turbines can not be made using the traditional conservative methods; innovative designs are needed to avoid the roadblocks.

In this scenario, wavy tapered wind turbine towers, made by wavy tapered cylinders, can be used as an alternative to the traditional circular tapered wind turbine towers. Past studies have evaluated the imperfection sensitivity of wavy cylindrical shells and presented promising results: Ning and Pellegrino [66] studied the wavy cylinders under axial compression, and Yadav and Gerasimidis [2, 68] studied the wavy cylinders under bending. But these studies are limited to simple cylindrical shells, and no attempt has been made to evaluate the effectiveness of the wavy cylinders in a real application. Further, the response of tapered wavy cylinders (an important structural element and used in many applications such as wind turbine towers) to imperfections have also not been investigated. An important application of tapered cylinders, i.e., wavy tapered wind turbine towers made of wavy tapered cylinders, is explored to assess the practical utility of wavy cylinders.

1.2.4 Review of non-destructive techniques for the evaluation of thin cylindrical shells axial buckling capacity

The reduction in the cylinders' axial buckling capacity depends on the shape and the size of the imperfections that is present in the cylinders. Thus, *a priori* knowledge about the imperfections is required for the capacity prediction. However, measuring imperfections is a difficult, expensive, and time-consuming adventure. This makes the prediction of shells' capacity difficult, if not impossible. Nonetheless, the quest for high-fidelity estimates of the buckling capacity has been continued for a long time,

and is getting immense attention recently. Indeed, a promising path has emerged for the evaluation of the buckling capacity of thin cylindrical shells based on energy barrier [69–75]. In this method, thin cylindrical shells are probed under different axial loads to explore the probing profile. Probe force-displacement curves contain significant information, which can be used to predict the buckling capacity of thin cylinders [69–72, 75]. However, this method is still in the infant state, and rigorous studies are needed before the method is implemented for practical applications. Furthermore, many hurdles have to be overcome: the development of experimental and computational frameworks for the prediction, the role of probing location, the influence of the imperfection's size and shape, the impact of the interaction among imperfections, etc. These issues have to be studied and recorded before the non-destructive technique for the evaluation of thin cylindrical shells buckling capacity becomes a reality.

1.3 Objective and scope

This dissertation has four objectives: 1) understanding the bending behavior of thin steel cylindrical shells, and find a rational knockdown factors within the range of slenderness used in tall wind turbine towers, 2) throw new light into the response of imperfection insensitive wavy cylinders under uniform axial compression and bending, 3) implement the idea of wavy cylinders for making wind turbine towers, and assess the practical utility of wavy cylinders, and 4) development of a non-destructive technique for the evaluation of thin cylindrical shells buckling capacity.

To address the first objective, bending behavior of thin steel cylindrical shells with specific dimensions is investigated. R/t varies from 60 to 120, the young modulus E is 210 Gpa, the Poisson's ratio ν is 0.30 and the yield stress σ_y is 355 Mpa. These values are commonly used in tall and super tall wind turbine towers. The overall relative slenderness λ_{ov} (i.e., $\sqrt{\frac{M_p}{M_{cr}}}$ [15, 45]) varies from 0.46 to 0.65 for the dimensions and

the material properties considered. The inelastic localized buckling instability mode is studied using numerical methods and the critical buckling load of the shells is assessed. To estimate the effect of geometric imperfections on the buckling load, four kinds of geometric imperfections are considered including a local dimple shaped and two sinusoidal shaped imperfections. The thin steel cylinders of the present study fail inelastically; this means that local stresses cross the yield stress limit before cylinders reach at their peak moment. In other words, when buckling occurs, the stresses in some regions of the cylinders are more than yield stress limit, and thus strain-hardening models play a critical role. Four types of strain-hardening models are utilized to observe their impact on the bending behavior and imperfection sensitivity of the thin steel cylindrical shells: a bilinear one and three versions of the Ramberg-Osgood model. A shortcoming of the current study which needs to be mentioned is that the shells considered are stress-free and do not account for residual stresses.

To throw new light into the response of wavy cylinders, the response of wavy cylinders under uniform axial compression and bending are explored. First, we focus on thin wavy cylindrical shells under axial compression, similar to the groundbreaking papers by Ning and Pellegrino [66, 67]. The presented work in this study is differentiated from the previous works by the shape of geometric imperfections. The shape of imperfections chosen for this purpose is a local dimple-like, which is more realistic than the first eigenmode. Second, we extend the investigation of wavy cylindrical shells to cylinders under bending, as bending is the primary load in several important applications of thin cylinders, e.g., tall wind turbine towers and gas pipelines. In these applications, for the typical R/t ratio used, the cylinders fail inelastically [1]. The results of Ning and Pellegrino [66, 67] cannot be extrapolated directly to the cylinders under bending and thus a thorough study is needed to evaluate the effectiveness of wavy cylinders under bending considering the inelastic response of the material. So

that wavy cylinders can be used confidently for several important applications where the primary load is bending and the material behavior is not linear elastic. We focus on the effect of imperfections on thin wavy cylinders under bending and the main hypothesis to be tested are they as effective as in the case of elastic axial compression [66, 67] or not? The industrial potential of such a solution could be significant based on the applications of thin cylindrical shells under bending. We choose a typical thin cylindrical shell which represents a section of a tall wind turbine tower studied by the authors in a previous paper [1], and we modify it into a wavy shell. After that, we introduce geometric imperfections in the cylinders and observe their impact. Two types of geometric imperfections are considered: biased sinusoidal shaped [50] and dimple-like imperfections. For the material model, a version of the Ramberg–Osgood strain hardening model is utilized. We are reporting very encouraging results; thin wavy cylinders under bending and in the inelastic range of material are imperfection insensitive especially when the amplitude of imperfection is small ($w_o < 0.3t$). In addition, the effect of wave parameters, e.g., the amplitude and the number of waves, on the bending behavior is explored. We found that wave parameters play a decisive role in making thin wavy cylinders imperfection insensitive.

To fulfill the third objective, the idea of wavy cross-sections is extended to thin tapered cylinders, and their effectiveness is investigated. Further, an important application of tapped cylinders, i.e., wavy tapered wind turbine towers made of wavy tapered cylinders, is explored to assess the practical utility of wavy tapered cylinders. Firstly, we present the response of thin tapered wavy cylinders to imperfections under bending, and show that the tapered wavy cylinders are insensitive to imperfection as compared to tapered circular cylinders. Next, a wavy tapered wind turbine tower is created by modifying a 61 m NORDEX S70/1500 wind turbine tower of 1.5 MW [77] capacity. The S70/1500 wind turbine tower is made by thin tapered circular cylinders

assembled together. These cylinders are designated as thin cylinders in this paper to emphasize that wrinkling and shell-type failure dominate [50, 78] the capacity of cylinders for the range of (R/t) ratios considered in this study. Further, the term thin circular shells is used in past studies [1, 19, 55] to describe wind turbine towers with R/t ratios more than 150. All these cylinders are modified to tapered wavy cylinders and a new wavy tower is made. It has been found that the wavy tower responded significantly better than that of the circular tower. Moreover, the wavy tower bears substantially more load than that of the circular tower. These results are very encouraging and have the potential to change the design of wind turbine towers. The economic benefits of wavy towers are also explored and presented. The scope of this study is to study the imperfection sensitivity of wavy cylindrical shells and the main advantage of these structures which is the significant reduction of sensitivity to geometric imperfections. However, there are other aspects which affect the behavior of these shells such as material nonlinearities and residual stresses which would need to be further studied for a complete picture of the problem at hand. These investigations are beyond the scope of the current study.

To develop a non-destructive technique for the evaluation of thin cylindrical shells buckling capacity, a procedure is proposed to predict the buckling capacity of thin cylinders; this procedure is based on the feedback of probe force-displacement curves of axially loaded cylinders. The proposed procedure is computationally implemented on a thin perfect cylinder ($R/t \approx 286$), and on a single dimple imperfect cylinder with varying imperfection amplitude. Moreover, we study the impact of the location of probing relative to the dimple in the circumferential and axial direction.

1.4 Layout of the dissertation

This dissertation is organized in the following way. Chapter 1 presents introduction, literature review, objective, and scope of the dissertation. Chapter 2 is concerned with the bending behavior of thin steel cylindrical shells that are used in tall wind turbine towers. In chapter 2, first we present localization instability phenomenon of thin steel cylindrical shells under bending. After that, we describe FEA modeling, geometric imperfections, boundary conditions, strain-hardening modeling used in this study. Next, we present the results and findings of the computational analyses, and at the end, we validate the FEA modeling by comparing with past results.

Chapter 3 presents new insights into the response of wavy cylinders under uniform axial compression and bending. In chapter 3, first the geometry of the thin wavy cylinders used in this study is described. Next, in section 2 of chapeter 3, we examine the mechanism behind imperfection insensitivity of wavy cylinders under axial compression assuming linear elastic material behavior. The effects of imperfections, on thin wavy cylinder under bending are discussed in section 4 along with the influence of the wave parameters. In section 5, the comparison is done between thin wavy cylinders and stiffened cylinders under bending to evaluate their effectiveness.

Chapter 4 extends the concept of waviness to tapered cylinders and their application for making wavy wind turbine towers. First, the geometry of thin tapered wavy cylinders is described, and their response to imperfections is presented. Next, the geometry of the 61 m NORDEX S70/1500 wind turbine tower of 1.5 MW is outlined, and its modification to create the wavy tower is discussed in detail. After that, the effects of imperfections on the circular and the wavy towers under bending are explored. Finally, the efficiency of using wavy towers is elaborated and the main findings are discussed.

In chapter 5, a procedure is proposed for the accurate prediction of the axial buckling capacity of thin cylindrical shells without measuring the imperfections and is based on the probing of the axially loaded cylinders. This procedure is implemented computationally on a perfect, and on an imperfect cylinder. Further, the robustness of the proposed procedure is investigated by probing away from the dimple in the circumferential and axial direction.

Chapter 6, the last chapter of the dissertation, concludes the main findings of this study, and suggests the future works.

CHAPTER 2

BENDING OF THIN STEEL CYLINDRICAL SHELLS: BIFURCATION AND LOCALIZATION INSTABILITIES

This chapter investigates the buckling behavior and imperfection sensitivity of thin steel cylindrical shells under pure bending, focusing on a specific range of slenderness, which is commonly found in energy structures such as tall wind turbine towers ($60 < R/t < 120$). The inelastic localized buckling instability is studied using computational methods to assess the critical load of the thin steel cylindrical shells. One of the main goals is to predictively describe the buckling sensitivity of the shells and to provide relationships between the knockdown factor and geometric imperfections. In addition, the impact of steel strain-hardening models on bending behavior is studied using four types of plasticity models: a bilinear and three versions of Ramberg-Osgood plasticity model.

2.1 Localization Instability phenomenon of thin steel cylindrical shells under bending

Before studying the imperfection sensitivity of thin steel cylindrical shells, it is important to understand the bending instability phenomenon. In figure 2.1, a typical example of a moment-curvature diagram and the evolution of ovalization of the cross-section at the middle of the cylinder are shown for a thin steel cylindrical shell under bending having an axisymmetric sinusoidal biased geometric imperfection (biased imperfection has varying amplitude along the longitudinal direction, see section 3.3.4

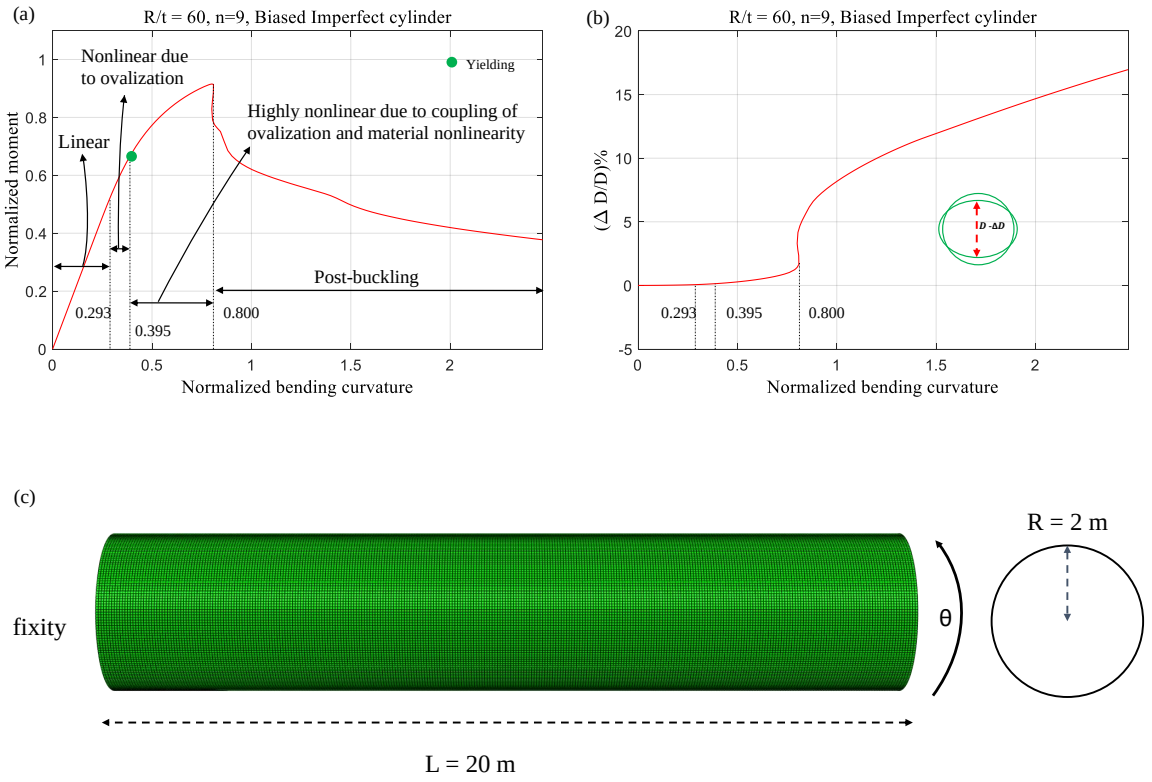

Figure 2.1: (a) Typical moment-curvature diagram and (b) ovalization of thin steel cylindrical shells under bending at the middle of the cylinder. The moment is normalized by $M_{pl} = D_m^2 t\sigma_y$ and the curvature is normalized by $K_l = \frac{t}{D_m^2}$. (c) Dimensions and the boundary conditions of the steel cylindrical shells used in this study.

for detail). One end of the cylinder is fixed and rotation is applied to the other end following a displacement-based FEM analysis. The curvature is found by dividing the end rotation, by the initial length of the cylinder. The moment is normalized by $M_{pl} = D_m t\sigma_y$ and the curvature is normalized by $K_l = \frac{t}{D_m^2}$ following the example of Vasilikis et al. [17]. D_m is the mean diameter of the cylinder (i.e., $D - t$, where D is the outer diameter of the cylinder).

Initially, the moment-curvature diagram (figure 2.1a) is linear, subsequently becomes nonlinear, and finally, buckling takes place. It is of interest to analyze the moment-curvature diagram closely along with the ovalization of the cross-section at the mid-length of the cylinder. Figure 2.1 includes 4 regions on the basis of the re-

lation between the moment and the curvature. The moment-curvature relationship is linear in the first region where the normalized curvature varies from 0.00 to 0.29. This region ends with the appearance of nonlinearity in the moment-curvature relationship. In this region, the ovalization is insignificant as can be seen in figure 2.1b and the stresses, throughout the cylinder, are below the yield stress limit. Local stresses are less than the yield stress limit and the moment is below the yield moment. Thus, the classical moment-curvature relationship ($M = EI\frac{d^2u}{dx^2}$) is valid in the first region as I can be assumed constant. In region two, where the normalized curvature lies between 0.29 to 0.40, ovalization becomes visible (figure 2.1b) and thus moment-curvature relationship becomes nonlinear although the stresses, throughout the cylinder, are still below the yield stress limit. This non-linearity comes from the ovalization and therefore the classical moment-curvature relationship is not valid in this region. At normalized curvature 0.40, the first yielding occurs (i.e., stresses cross the yield stress limit locally, but the moment is less than the yield moment) and material non-linearity starts playing its role. Material non-linearity increases the rate of ovalization (figure 2.1b), which is manifested as a highly nonlinear moment-curvature relationship. At normalized curvature 0.80, shell buckling takes place and the bending moment starts reducing. After the point of buckling, the cross-section changes very rapidly as can be seen in figure 2.1b.

To understand the phenomenon in detail, 10 points are identified in the moment-curvature diagram as shown in figure 2.2. These points represent 10 stages of the applied rotation. The deformation pattern for these 10 stages included in figure 2.2 shows that buckling localizes eventually. At stage 1, no rotation is applied and thus line is in the initial shape. It can be seen that the line is not exactly straight due to the initial geometric imperfection in the form of a sinusoidal wave. At stage 2 and 3, there is not any significant change in the shape of this line although it is rotated due

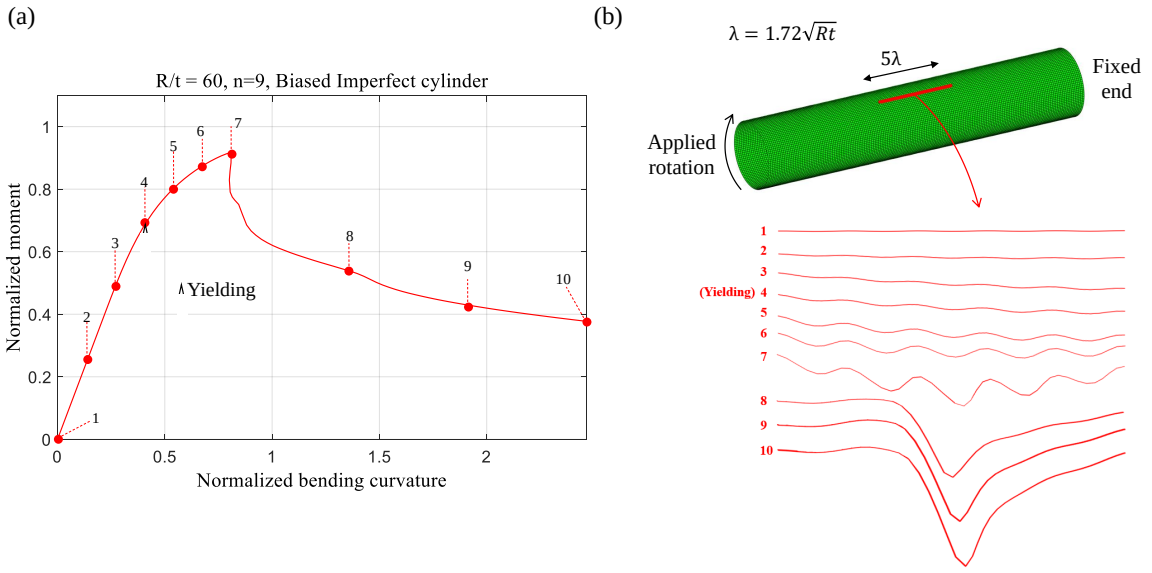

Figure 2.2: (a) Ten stages of applied rotation in moment curvature diagram. Yielding occurs at stage 4. (b) Deformation at a middle line of the cylinder with a length of 5λ at ten stages of applied rotation. Wrinkling can be seen at stages 5, 6 and 7 and the deformation is concentrated only at the center of the line after stage 7 where buckling takes place.

to the bending. At stage 4, first yielding occurs and a small change takes place in the shape of the line. At stage 5, the change in the shape of the line is significant and the sinusoidal pattern can be observed. This is a clear sign of the wrinkling which happens near stage 5. At stage 6, the change in the shape of the line is increased and at stage 7, buckling takes place. After buckling, the deformation is concentrated only at the center of the line as shown in figure 2.2 (stages 8, 9 and 10). It can also be seen that the wrinkling disappears after buckling. Wrinkling takes place in the inelastic range before buckling, and disappears after buckling, as the stresses concentrate in the middle of the cylinder.

To measure the appearance of wrinkling quantitatively, the variation of the amplitude of imperfection against the curvature is studied. The amplitude of the imposed geometric imperfection is $t/10$ and this varies as the rotation is applied. To measure

the amplitude of wrinkling, three nodes (A, B and C) in the middle of the cylinder are selected (figure 2.3). A and B are at the crest and C is at the trough. The displacement of nodes A, B and C are then traced relative to the applied rotation and these displacements are used to find the amplitude of imperfection plus wrinkling. First, the relative displacement vector of node A and B with respect to node C is found, i.e., vectors ν_1 and ν_2 (figure 2.3). Using these vectors, the angle φ is obtained. The amplitude of imperfection plus wrinkling will be half of the projection of vector ν_1 on the line that is normal to the line AB. The expression for w_o can be found using the expressions:

$$\cos\varphi = \frac{\nu_1 \cdot \nu_2}{|\nu_1||\nu_2|} \tag{6}$$

$$2w_o = |\nu_1|\cos\frac{\varphi}{2} \tag{7}$$

$$w_o = \frac{|\nu_1|\cos\frac{\varphi}{2}}{2} \tag{8}$$

This formulation is true only if the nodes A, B, and C are in the plane of bending. The evolution of w_o at every step is obtained using the method described above and w_o is plotted against the applied curvature (figure 2.3). Initially, w_o remains approximately $t/10$, which is expected as the applied rotation is small. It must be noted that $t/10$ is the amplitude of the geometric imperfection and therefore the starting point of the figure. The significant increment in w_o occurs at around 0.50 normalized curvature, which means that wrinkling is happening. Finally, wrinkling in the form of buckling appears at 0.80 normalized curvature. From these observations, it can be observed that the presence of imperfections triggers wrinkling, which finally manifests in the form of buckling.

Although the ovalization in the middle of the cylinder is more pronounced (figure 2.1b), it is interesting to see in further detail the ovalization at different locations

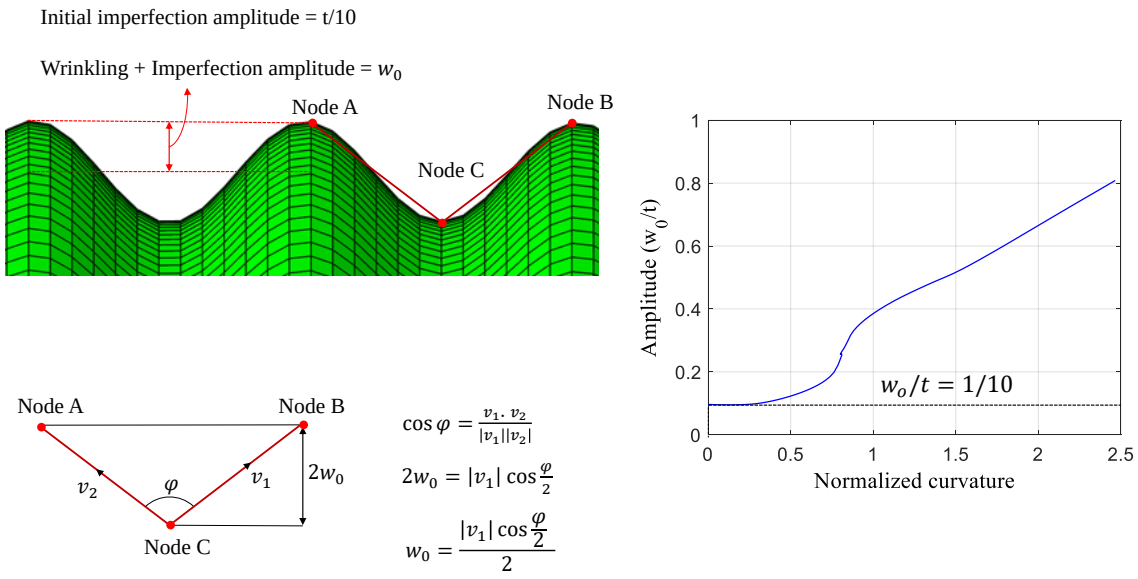

Figure 2.3: Measurement of wrinkling plus imperfection amplitude (w_0) and the variation of ovalization at the middle of the cylinder against the curvature.

of the cylinder. Figure 2.4 presents the ovalization ($\frac{\Delta D}{D}$) for a middle part of the cylinder with a length 5λ (λ here is the half-wavelength of the elastic buckling eigenmode [79]). Initially, the ovalization is small and uniform through the whole 5λ section. But just before buckling (at normalized curvature $0.75 - 0.89$), nonuniform ovalization occurs (figure 2.4), which implies the wrinkling phenomenon. Finally, buckling takes place at 0.80 normalized curvature and the sharp increase can be seen at this curvature in figure 2.4 throughout the section.

The stress distributions at the 10 stages of bending are shown in figure 2.5a. Stage 1 represents the initial no-stress state. At stage 2, some rotation is applied and thus a nonzero stress-distribution can be seen. It can also be seen that the distribution of stresses follows a wavy shape at stage 2. This is happening because the cylinder is imperfect and the shape of imperfection is sinusoidal. The stresses are intensified at stage 3 as the applied rotation is increased. The classical moment-

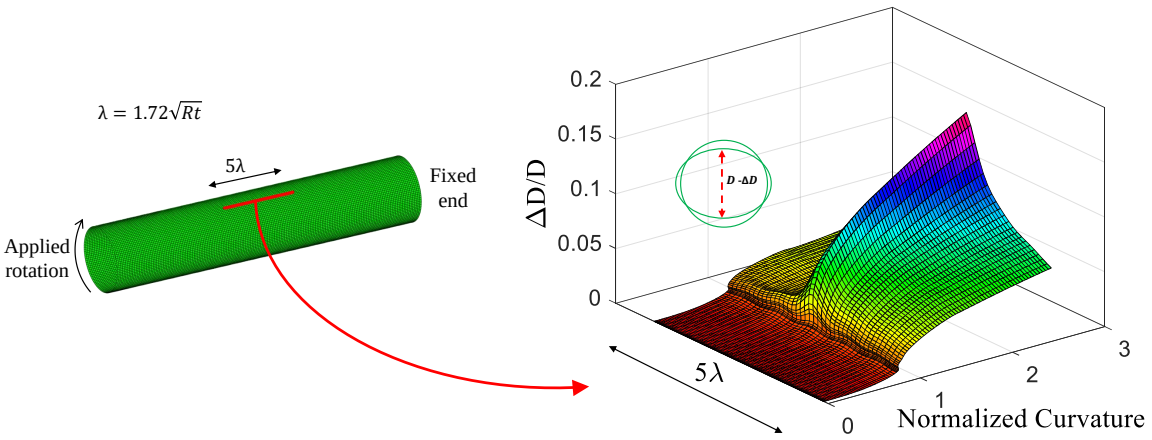

Figure 2.4: Ovalization ($\frac{\Delta D}{D}$) for a middle part of the cylinder with a length of 5λ against the curvature. It is initially uniform with respect to length but becomes nonuniform before buckling. After buckling it is concentrated in the middle of the cylinder.

curvature relationship is valid for stage 2 and 3 because the stresses are less than their yield stress limit and the ovalization is very small. First yielding occurs at stage 4 and the region of plasticity increases at stage 5 and 6. Inelastic localized buckling takes place at stage 7.

After the buckling, the bending moment starts dropping rapidly, which leads to stress redistribution. This redistribution affects the center region and the edge regions of the cylinder differently. In the center region, stresses are almost constant (figure 2.5b), while in edge regions, stresses are reducing rapidly (figure 2.5c) after buckling. These are typical characteristics of a local shell buckling phenomenon. In this case, the cylinder fails due to the shell buckling of the center region, and thus this region follows its post-buckling path. In this region, stresses are not reducing in the post-buckling range. The reduction in the bending moment is compensated by the change of the cross-section, which consequently reduces the moment of inertia. The regions beyond the center do not buckle and they follow an unloading path with the reduction of the bending moment. With this background of bending instability of thin

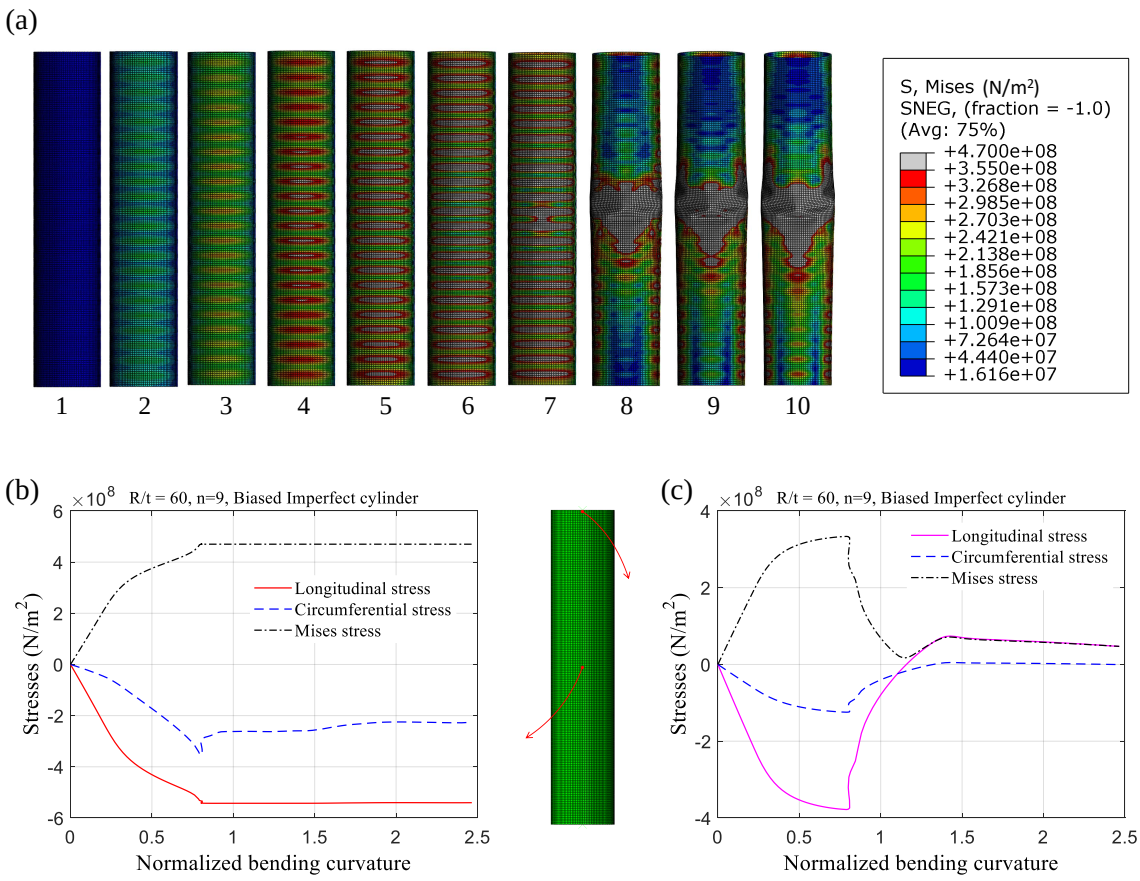

Figure 2.5: (a) Stress distribution at the compressive side of thin steel cylindrical shell at ten stages of loading. (b) Variation of the extreme fiber stresses at the compressive side of the cylinder against the curvature at the center. (c) Variation of the extreme fiber stresses at the compressive side of the cylinder against the curvature at the top.

steel cylindrical shells, the effect of geometric imperfections and material hardening models on the bending behavior of cylindrical shells is further presented.

2.2 Finite Element Modeling

This section describes geometry, boundary conditions, strain-hardening models and Finite Element Modeling of the cylindrical shells used in this study along with the description of geometric imperfections used to make imperfect cylinders.

2.2.1 Geometry of the model

A 20.00 m long steel cylindrical shell with 2.00 m diameter is chosen for the analyses. The thickness t of the cylindrical shells is chosen so that the ratio $\frac{R}{t}$ varies from 60 to 120 with an interval of 20. The reason behind choosing these dimensions is that they cover a section of tall and super-tall wind turbine towers. For the analysis purposes, a displacement method of analysis is used with one end of the cylinder is fixed while the rotation is applied at the other end as shown in figure 2.1. The simulation is performed in ABAQUS [80] utilizing the Riks method and using four-node reduced integration shell ($S4R$) elements. Four integration points are utilized along the thickness of each element. Two rigid body constraints are imposed at the end cross-sections, which make sure that the end cross-sections do not change their shape, i.e, ovalization is prevented during the analysis. These constraints represent the rigid rings, which are used in cylindrical shells at regular intervals to prevent the ovalization [81]. After performing an extensive mesh convergence analysis, it was found that around 20000 elements (each with a dimension of 121.20 $mm \times 121.20$ mm) provide sufficient accuracy for all the R/t ratios and the material-hardening models (see next section for material hardening models). In figure 2.6, the results of mesh convergence analysis are shown for R/t ratios 60, 80, 100 and 120 and material hardening models $n = 9$, $n = 13$ and $n = 30$ (see the next section for the meaning of n). The results are shown in terms of normalized moment capacity and $a/\sqrt{(Rt)}$, where a is the element size (elements are square in shape), t is the thickness of the cylinders and R is the radius. For 20000 elements, the values of $a/\sqrt{(Rt)}$ are 0.43, 0.50, 0.56 and 0.61 for R/t ratios 60, 80, 100 and 120 respectively. These values are quite smaller than the linear bending half-wavelength (i.e., $2.44\sqrt{(Rt)}$) and the classical axisymmetric buckle half-wavelength for cylindrical shells under

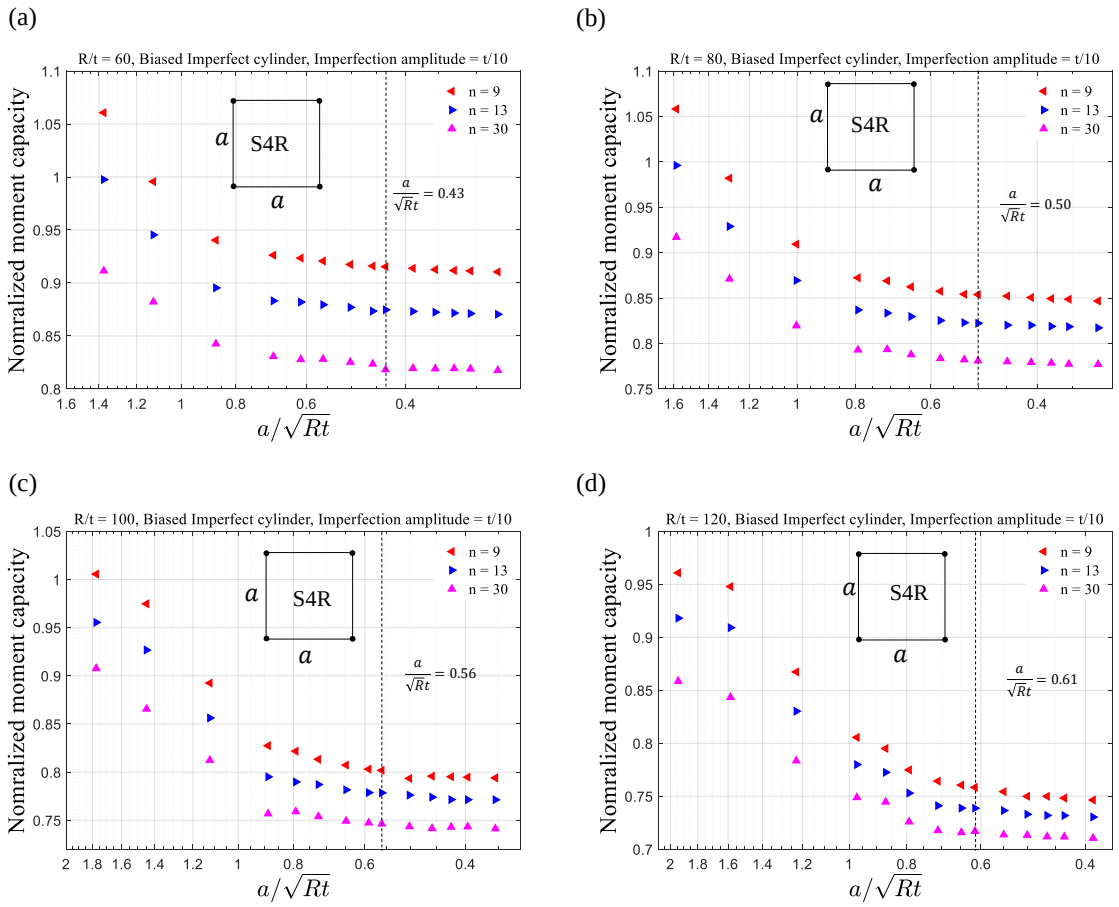

Figure 2.6: Mesh convergence analysis, around 20000 $S4R$ elements give sufficiently accurate results. (a) $R/t = 60$, (b) $R/t = 80$, (c) $R/t = 100$ and (d) $R/t = 120$. The mesh sizes corresponds to 20000 elements are $0.43\sqrt{(Rt)}$, $0.50\sqrt{(Rt)}$, $0.56\sqrt{(Rt)}$ and $0.61\sqrt{(Rt)}$ for $R/t = 60$, $R/t = 80$, $R/t = 100$, and $R/t = 120$ respectively. The element sizes are small than the first mode half-wavelength and thus able to capture the mode of failure.

axial compression [79] and thus the discretization is considered adequate.

2.2.2 Strain-hardening model

Thin steel cylindrical shells in the range $60 < R/t < 120$ are expected to buckle inelastically and therefore the strain-hardening model plays a highly important role in their behavior. To understand the role of strain-hardening models in the bending behavior of thin steel cylindrical shells, four kinds of strain-hardening models−a bi-linear elastic-perfectly plastic and three versions of the Ramberg-Osgood plasticity model−are used, as shown in figure 2.7. The Ramberg-Osgood stress-strain relationship used in this study is (Kyriakides and Corona [78]):

$$\epsilon = \frac{\sigma}{E}\Big[1 + \frac{3}{7}\big(\frac{\sigma}{\sigma_y}\big)^{n-1}\Big] \tag{9}$$

The value for young modulus E is 210.00 Gpa, the Poissons ratio ν is 0.30 and the yield stress σ_y is 355.00 Mpa. Three values of n, i.e. 9, 13 and 30, are considered in this study.

2.2.3 Description of geometric imperfections

To study the effect of geometric imperfections on the bending behavior of thin steel cylindrical shells, four kinds of geometric imperfections are introduced in-turn in the perfect cylinders.

2.2.3.1 Modal shape imperfection

The first geometric imperfection is the first modal shape of the cylindrical shell under bending, which is obtained from the eigenvalue analysis of the perfect cylindrical shell under bending (figure 2.8). Modal shape imperfection cannot be expressed by a simple analytical expression as it is obtained through the Finite Element Analysis.

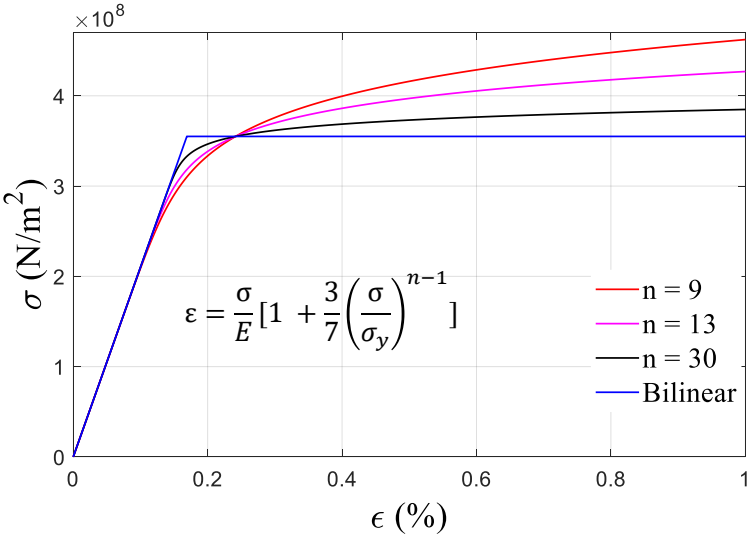

Figure 2.7: Stress-strain diagrams for the bilinear and three versions of Ramberg-Osgood plasticity model.

To create the modal shape imperfect cylinder, a scaled modal shape was introduced to the perfect cylinder having a pre-defined amplitude using the scalar w as shown in figure 2.8.

2.2.3.2 Dimple-like imperfection

The second geometric imperfection used in the analysis is the dimple-like imperfection, which is localized at a particular region. This type of imperfection is considered realistic in thin steel cylindrical shells, when some solid hits the cylindrical shell during transportation or construction (figure 2.9). Different mathematical equations have been proposed to describe these dimples [82, 83]. The present study uses the equation of dimple proposed by Hutchinson [83] for the spherical shell, which is modified to suit the cylindrical shell. The mathematical equation of dimple-like imperfection for the cylindrical shell is:

$$w = -w_o e^{-(\frac{x}{L_1})^2} e^{-(\frac{\theta}{\theta_1})^2} \tag{10}$$

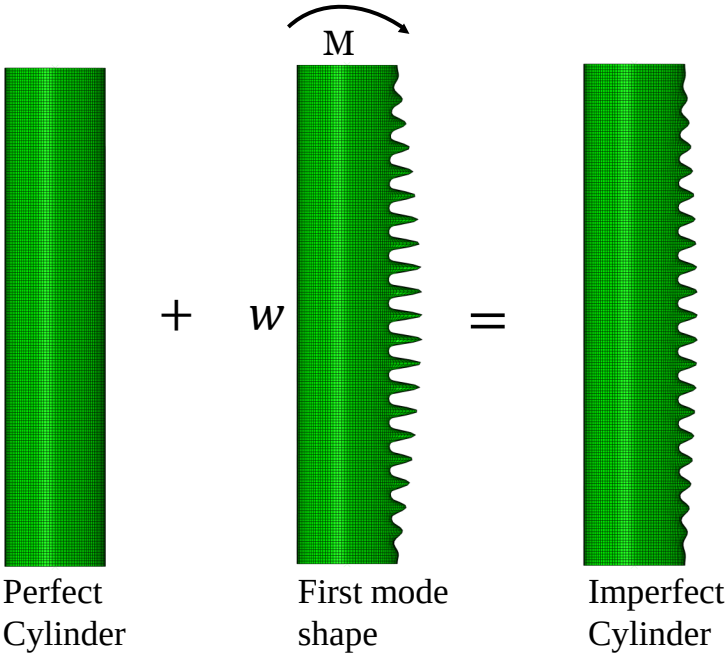

Figure 2.8: Modal shape imperfection under bending.

Where w represents the deviation from the original position in the radial direction and w_o is the amplitude of the imperfection; x and θ are the axial and circumferential coordinates with the origin placed in the middle of the cylinder. L_1 and θ_1 are the parameters which decide the length (in axial direction) and width (in circumferential direction) of the dimple. The values for L_1 and θ_1 are chosen such that the length ($2L_1$) and the width ($2R\theta$) of the dimple are equal to the first mode-shape wavelength of the cylindrical shell under compressive load, i.e. $3.44\sqrt{Rt}$ for $\nu = 0.30$ [79]. The value of half-wavelength of the mode-shape is represented by λ. The value of half-wavelength λ in this study is taken as $1.72\sqrt{Rt}$, which is classical axisymmetric buckle half-wavelength for cylindrical shells under axial compression [79]. This value is less than the linear bending half-wavelength of cylinders under bending ($2.44\sqrt{Rt}$). We calculated the half-wavelength of the first eigenmode for the cylinders (used in this study) under bending and found that they vary from $1.76\sqrt{Rt}$ to $1.96\sqrt{Rt}$. And thus,

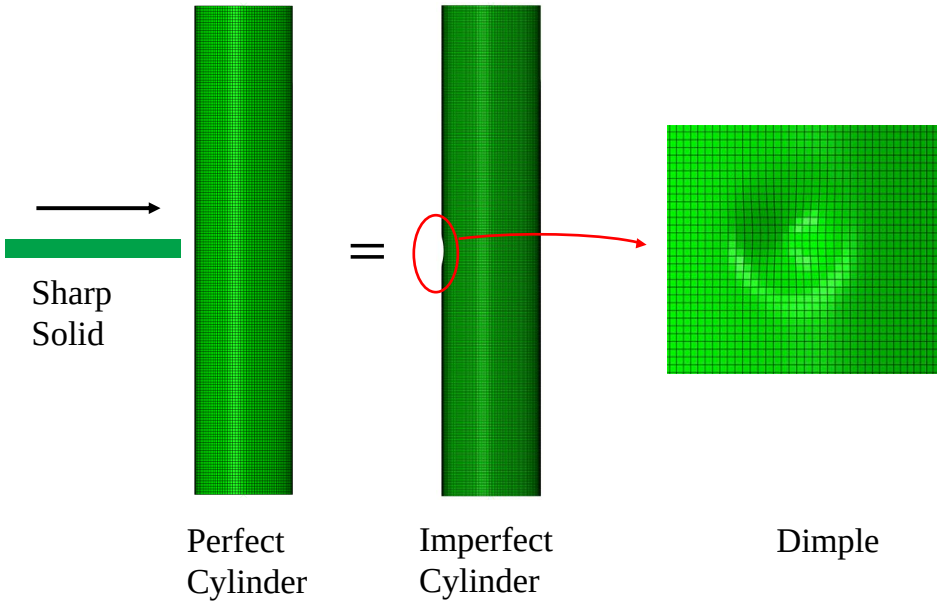

Figure 2.9: The induction of dimple-like geometric imperfection.

we chose a smaller value, i.e. $1.72\sqrt{Rt}$, so that the analysis can capture buckling and post-buckling behavior accurately.

θ_1 and L_1 are:

$$\theta_1 = \frac{1.72\sqrt{Rt}}{R} \tag{11}$$

$$L_1 = 1.72\sqrt{Rt} \tag{12}$$

Figure 2.10 shows the dimple-like imperfection along with its mathematical expression and parameters. The dimple is centered on the meridian with maximum compressive stress at the middle of the cylinder.

2.2.3.3 Unbiased imperfections

The two geometric imperfections mentioned above are non-axisymmetric. The present work also considers two axisymmetric geometric imperfections. The first one is in the shape of the sinusoidal wave whose half-wavelength is λ (where λ is the half-wavelength of the cylindrical shell under compressive load [79] i.e. $1.72\sqrt{Rt}$). In this

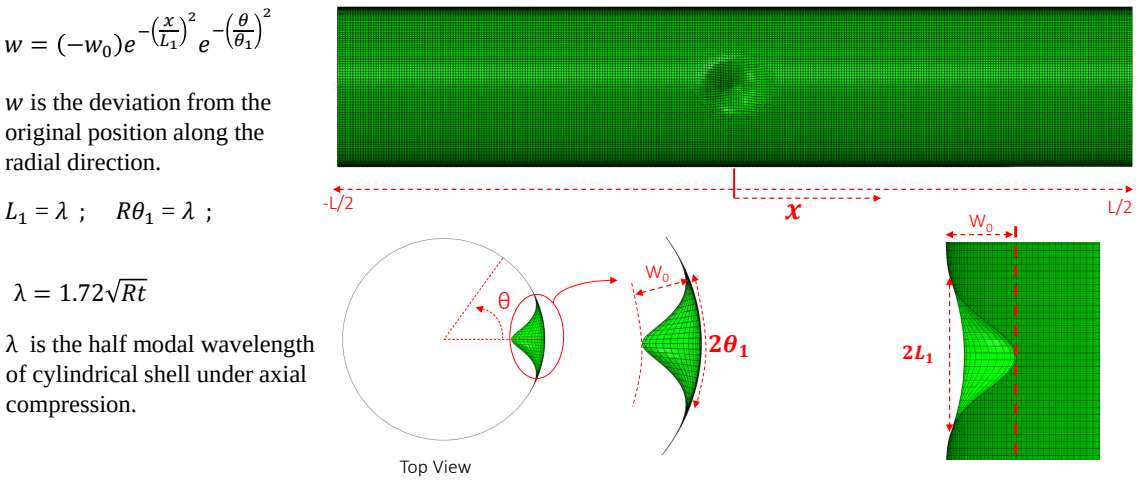

Figure 2.10: Mathematical description of the dimple-like imperfection. The width of dimple (along circumferential directions) and the length (along axial direction) are equal to 2λ.

paper, this imperfection is defined as unbiased imperfection, and mathematically this imperfection can be described as:

$$w = -Ra_{oi} \cos \frac{\pi(x)}{\lambda} \tag{13}$$

Where w represents the deviation from the original position in the radial direction, L is the length of the cylinder, Ra_{oi} is the amplitude of imperfection and x is the axial coordinate with the origin placed in the middle of the cylinder. This equation is generated by modifying the biased imperfection given by Ju and Kyriakides [50]. The perfect and imperfect cylinder are shown in figure 2.11 along with the variation of w along the length.

2.2.3.4 Biased imperfections

This imperfection is similar to the unbiased imperfection with a slight modification. In this case, the amplitude is slightly higher at the center as shown in figure 2.12. This imperfection is defined as biased imperfection as its amplitude is higher at the

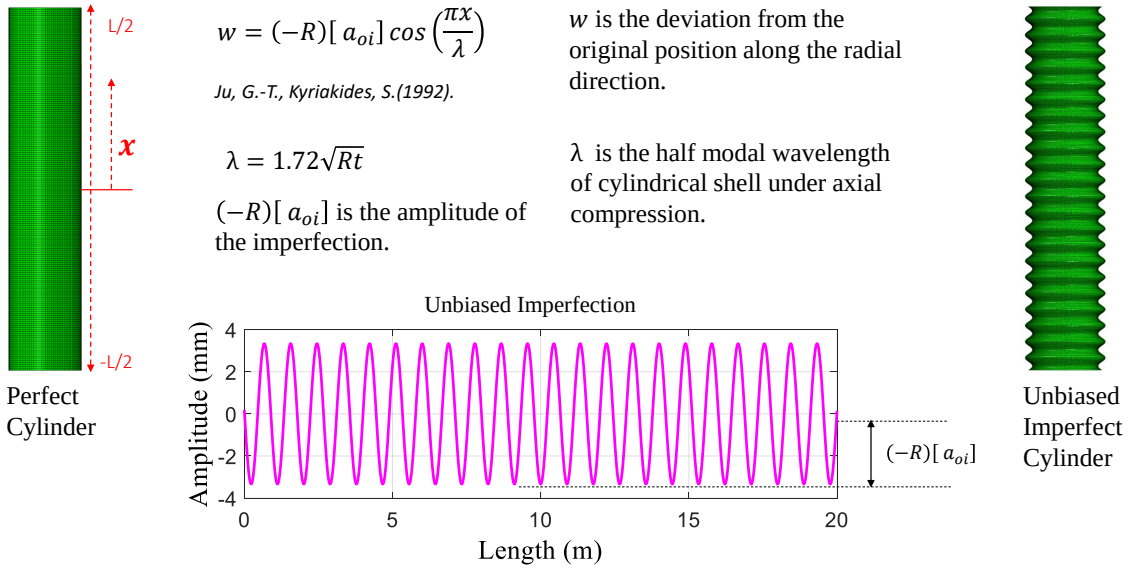

Figure 2.11: Mathematical description of the unbiased imperfection along with a perfect and an unbiased imperfect cylinder. The variation of imperfection amplitude along the length is also shown.

center. its mathematical expression is [50, 78] :

$$w = -R\left(a_{oi} + a_i \cos\frac{\pi x}{N\lambda}\right)\cos\frac{\pi(x)}{\lambda} \tag{14}$$

Where, x is the axial coordinate with the origin placed at center, Ra_{oi} and Ra_i are the unbiased and biased components of amplitude respectively and $N\lambda$ represents the length of the cylinder. In this study, the value of a_{oi} and a_i are chosen such that the ratio $\frac{a_{oi}}{a_i}$ is 5. The variation of the amplitude along the length is depicted in figure 2.12. The rationale behind using biased and unbiased imperfections is that they are generally more deleterious than the dimple-like imperfection and modal shape imperfections. Apart from that, these imperfections (biased and unbiased) are used in past studies of cylindrical shells under bending [50, 78].

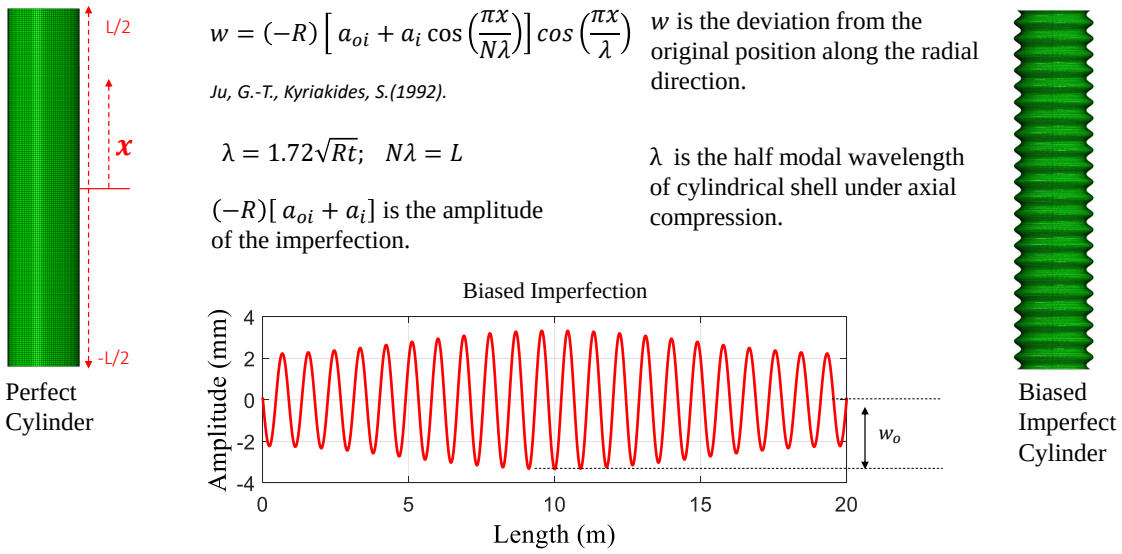

Figure 2.12: Mathematical description of the biased imperfection along with a perfect and a biased imperfect cylinder. The variation of imperfection amplitude along the length is also shown.

2.3 Results form computational analysis

2.3.1 Effect of geometric imperfections

To study the effect of geometric imperfections on the bending behavior of thin steel cylindrical shells, four geometric imperfections are introduced in the perfect cylinders in-turn. The amplitude of imperfections is kept to $t/10$ for all the cases. The first results are presented in figure 2.13 for $R/t = 60$ and Ramberg-Osgood strain-hardening model with $n = 9$. It can be seen that the thin steel cylindrical shells are highly imperfection sensitive under bending in the inelastic range. For the modal shape imperfect cylinder, the reduction in peak moment and collapse curvature are about 14% and 50%, respectively. These reductions are significant compared to the amplitude of imperfection, i.e., $t/10$. Surprisingly, the reduction in the collapse curvature is much higher than the reduction in peak moment. This could be explained by the existence of a highly nonlinear relationship between the moment and curvature

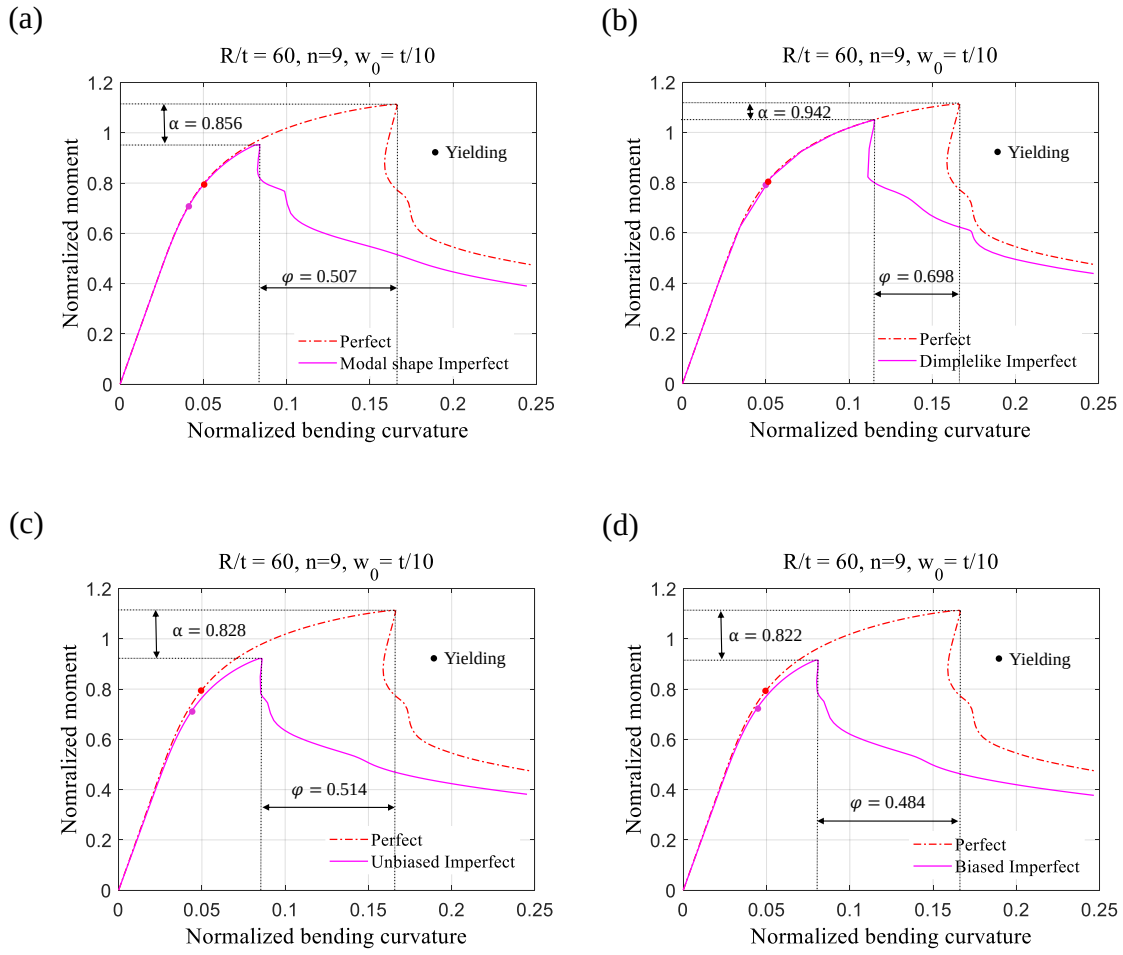

Figure 2.13: Effect of (a) modal shape imperfection, (b) dimple-like imperfection, (c) unbiased imperfection and (d) biased imperfection on the bending behavior of thin steel cylindrical shells. The moment is normalized by $M_{pl} = D_m^2 t \sigma_y$ and the curvature is normalized by $K_l = \frac{t}{D_m^2}$.

before the buckling and thus for a small reduction in the moment, a large reduction in the curvature is required. The large reduction in collapse curvature signifies that the presence of imperfections is more critical when the displacement is the design criteria. The presence of imperfections also changed the location of the first yielding in the moment-curvature space. The first yielding occurs at a lower moment of the imperfect cylinder, which can be attributed to the stress concentration in the imperfect cylinders. The pre-buckling path of perfect and modal shape imperfect cylinders is almost same as shown in figure 2.13a.

The impact of dimple-like imperfection is least deleterious among the four kinds of imperfections considered in the analysis. The reduction in the peak moment and the collapse curvature are approximately 6% and 30%, respectively. Here also, the reduction in the collapse curvature is much more than the reduction in the peak moment. In the case of dimple-like imperfection, the location of first yielding, in moment-curvature space, for the perfect and the imperfect cylinders are almost same (figure 2.13b). The pre-buckling path of the dimple-like imperfect cylinder and the perfect cylinder is approximately the same.

The impact of the biased imperfection is the most severe among the four geometric imperfections considered (figure 2.13c). The reduction in the peak moment and the collapse curvature due to the biased imperfection are, 18% and 51%, respectively. For the unbiased imperfect cylinder, the reduction in the peak moment and collapse curvature are, 17% and 49%, respectively (figure 2.13d). The pre-buckling path of the perfect and the imperfect cylinders are different in the cases of biased and unbiased imperfection in contrast to the modal shape imperfection and the dimple-like imperfection where the pre-buckling path of perfect and imperfect cylinders are almost the same. From these analyses, it can be concluded that thin steel cylindrical shells are very sensitive to the imperfections under inelastic bending ($60 < R/t < 120$).

It is noteworthy to see the impact of shell slenderness (R/t) on the imperfection sensitivity of thin steel cylindrical shells. Figure 2.14 shows the variation of knock-down factor κ and collapse curvature reduction factor ϕ with R/t, respectively. From figure 2.14, it can be seen that the dimple-like imperfection is least catastrophic and the biased imperfection is the most catastrophic among the four geometric imperfection shapes. Another important observation from figure 2.14 is that κ and ϕ do not vary significantly with the R/t, which is expected since the size and the amplitude of imperfections are scaled with R/t (the amplitude is always $t/10$ and for this parametric analysis, $R = 2.00\ m$ and t varies so that $60 < R/t < 120$). The amplitude and the size of imperfections for $R/t = 60$ are higher than for $R/t = 120$, which makes κ and ϕ relatively independent from the R/t ratio.

2.3.2 Effect of imperfections amplitude

In the previous section, the amplitude of imperfections is kept constant, i.e., $t/10$. In reality, the amplitude of imperfections varies significantly depending on manufacturing processes, transportation, and assembly methods (for wind turbine towers). It is interesting to study the role played by the imperfection amplitude on the bending behavior of thin steel cylindrical shells.

For this study, the dimple-like imperfection was selected, as it is more realistically present (created when some solid hits the cylinder during transportation or construction) in the cylinders as compared to other types of imperfections considered in this study. Another realistic and commonly studied imperfection is weld depression [84], but that is not considered in this study as we are not considering the effect of welding, i.e., geometric imperfections and residual stresses. The length and the width of the dimple are the same as in the previous section, i.e. 2λ (figure 2.10), R/t ratio is 60 and the strain-hardening model is Ramberg-Osgood with $n = 9$. The amplitude

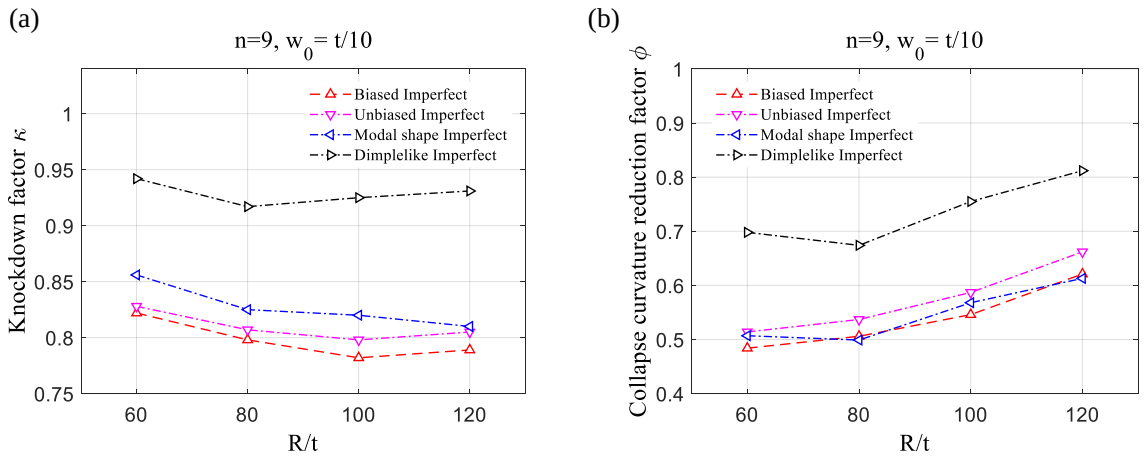

Figure 2.14: Variation of (a) the knockdown factor κ and (b) the collapse curvature reduction factor ϕ with the slenderness ($\frac{R}{t}$).

of dimple w_0 is varied from 0 to $2t$ with an interval of $t/20$ and a perfect and 40 imperfect cylinders have been analyzed. Figure 2.15a shows the bending response of these 41 thin steel cylindrical shells. Many significant observations could be made from figure 2.15a:

1. The load carrying capacity of cylindrical shells reduces with the increase of imperfection amplitude until a certain limit and stabilizes with further increase of the imperfection amplitude. This is shown more clearly in figure 2.15b where the variation of moment capacity is plotted with the amplitude of imperfection. One can observe the existence of a plateau in figure 2.15b, which signifies that the moment capacity of imperfect thin steel cylindrical shells are independent of the amplitude of imperfection once the amplitude crosses a specific limit (in this case for $w_o > 1.30t$). Vasilikis et al. [17] have investigated the effect of imperfection amplitude on the bending capacity of thin cylindrical shells, but they did not increase the imperfection amplitude more than $1.14t$. For that reason, the full length of the plateau was not shown in their moment capacity vs imperfection amplitude plot. This finding is significant to show that thin

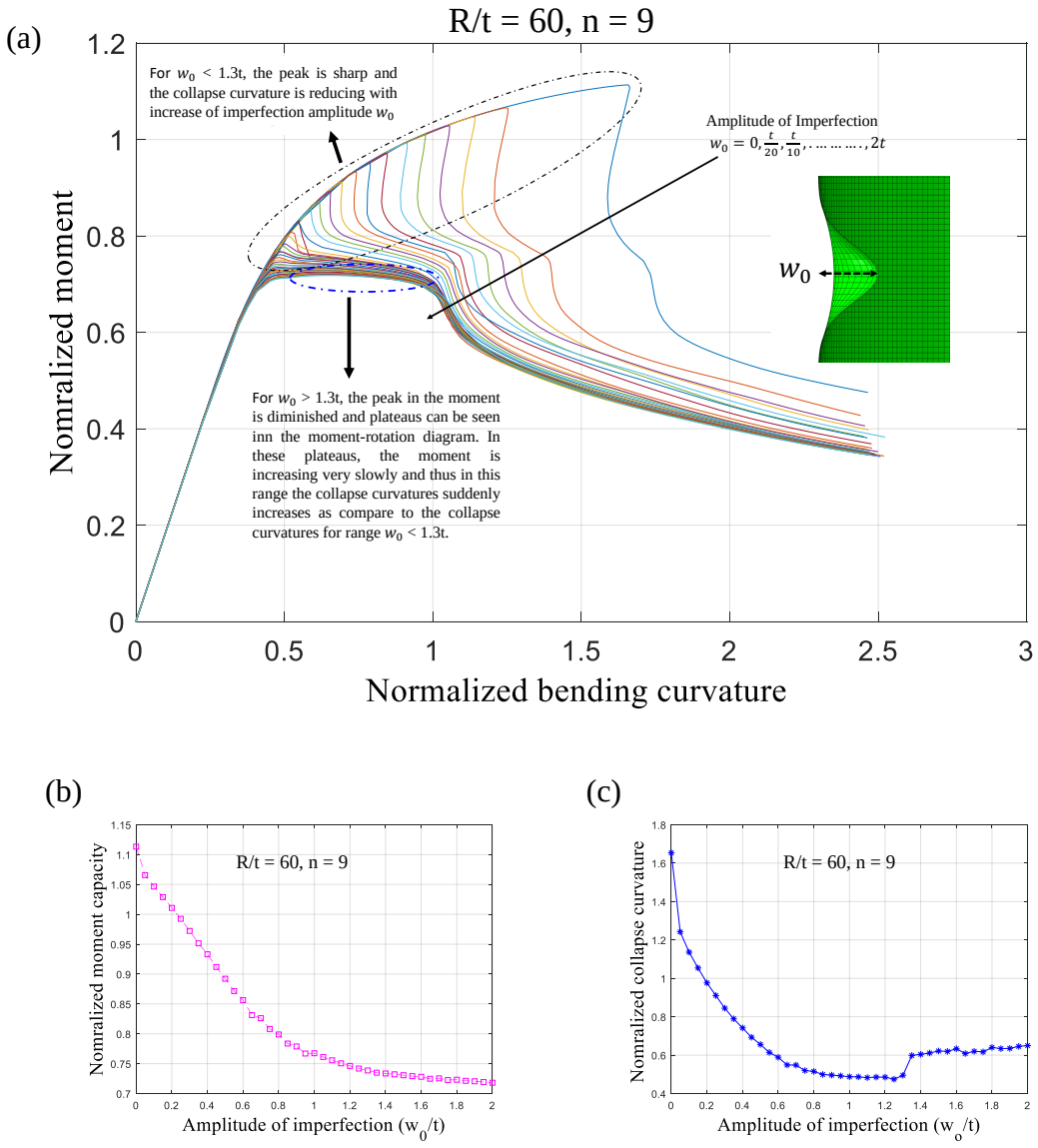

Figure 2.15: (a) Effect of the amplitude of dimple-like imperfection on the bending behavior of thin steel cylindrical shells. (b) Effect of the amplitude of dimple-like imperfection on the moment capacity. (c) Effect of the amplitude of dimple-like imperfection on the collapse curvature.

cylinders possess a minimum capacity irrespective of imperfection amplitudes. It is surprising to compare this finding with the results of Hutchinson [83] and Lee et al. [85] who also found the existence of a plateau but for the spherical shells under uniform external pressure in the elastic range. This unexpected similarity of results between two different structures and loading scenarios, the elastic spherical shells under uniform external pressure and the bending of inelastic thin cylindrical shells, might be attributed to the unifying thin shell characteristics in both cases, i.e., the sensitivity to imperfections.

2. The other important characteristic, which emerges from figure 2.15a, is the diminishing of the peak in the moment-curvature diagram with the increase of the imperfection amplitude. For the high imperfection amplitude ($w_o > 1.30t$), there is no visible sharp peak in the moment. The moment increases with the increase in the curvature and reaches a limiting value (for $w_o > 1.30t$), remaining almost constant at this limiting moment even when the curvature is increasing and finally, collapse takes place. For the small imperfection amplitude ($w_o < 1.30t$), there exists a visible peak moment and collapse takes place at this peak moment. These differences can be explained by the extent of yielding in the two cases. For small imperfection amplitudes ($w_o < 1.30t$), prebuckling stresses cross the yield stress limit in a very small region in the middle of the cylinder. The prebuckling bending stiffness does not reduce significantly and consequently there is no large prebuckling rotation. For high imperfection amplitudes ($w_o > 1.30t$), prebuckling stresses cross the yield stress limit at a large region in the middle of the cylinder. As a result, a significant reduction occurred in the bending stiffness of the cylinder. This leads to large prebuckling rotation. The plateau can be seen in the moment-curvature diagram. This is an important finding, which shows that same imperfection shapes with dif-

ferent amplitude causes different modes of instability. Another observation is that cylinders with higher imperfection amplitude buckle smoothly, while cylinders with small imperfection amplitude fail abruptly. These distinct features of the moment-curvature diagram for the different range of imperfection amplitudes can be compared with the load- deformation curve of Eurocode [15] as given in its figure 8.6. Eurocode [15] also provides a criterion to calculate the load capacity (section 8.7.2.6) for these different load-deformation curves. The moment-curvature diagram for small imperfection amplitude matches the curve which corresponds to the $C2$ criterion (figure 8.6 of Eurocode [15]) and this criterion could be used. For high imperfection amplitudes, the moment-curvature diagram matches the curve which corresponds to the $C3$ criterion (figure 8.6 of Eurocode [15]) and thus this should be used to evaluate the bending capacity.

3. Figure 2.15c shows the variation of collapse curvature with the amplitude of imperfections. Collapse curvature stabilizes at an imperfection amplitude $w_o > 0.60t$ much earlier than the collapse moment, which stabilizes at $w_o > 1.30t$. The important feature of the figure 2.15c is the sudden jump at $w_o = 1.30t$. This can be explained by the fact that for small imperfection amplitude ($w_o < 1.30t$), cylinders do not lose their bending stiffness significantly due to yielding before buckling. As a result, the prebuckling rotation is small. For large imperfection amplitudes ($w_o > 1.30t$), the prebuckling loss of bending stiffness is significant due to yielding and consequently, the rotation is large before buckling. As mentioned in the previous section, for high imperfection amplitudes the failure is smooth, while for low imperfection amplitude the failure is abrupt. Based on this observation, the imperfection amplitude can be classified into these two ranges. The critical imperfection amplitude, when the behavior of cylinders changes, can be obtained from figure 2.15c

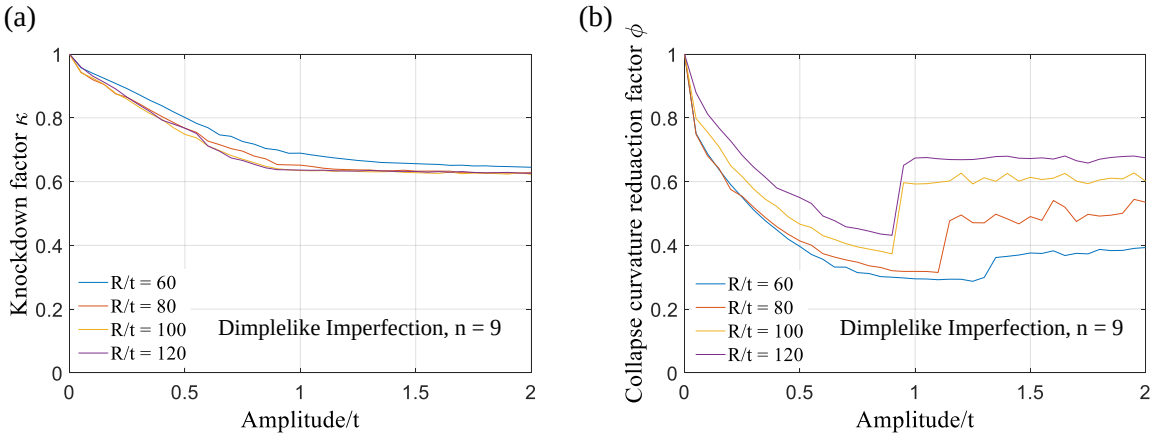

Figure 2.16: Variation of (a) the knockdown factor κ and (b) the collapse curvature reduction factor ϕ, with the amplitude of dimple-like imperfection for four $\frac{R}{t}$ ratios (60, 80, 100 and 120).

To further study the impact of R/t, the knockdown factor κ and collapse curvature reduction factor ϕ are plotted with the amplitude for four R/t ratios, i.e, 60, 80, 100 and 120 in figure 2.16. The independence of κ with R/t comes from the fact that the size and the amplitude of imperfection have been scaled to make it independent [83]. In figure 2.16b, the same jumps appear as described previously. Another significant observation is that for higher R/t, the jumps in ϕ occur at the smaller amplitudes.

2.3.3 Impact of dimple-like imperfection's size

The length and the width of the dimple-like imperfection are taken as 2λ in the previous sections, where λ is classical axisymmetric buckle half-wavelength for cylindrical shells under axial compression [79]. This is done in anticipation that when the dimensions of imperfections are synchronized with eigenmode, they lead to the maximum reduction in load carrying capacity. To verify this assumption, the length and width of the dimple-like imperfection are parametrically changed for the case of $R/t = 60$ and Ramberg-Osgood strain-hardening model $n = 9$. First, the length of

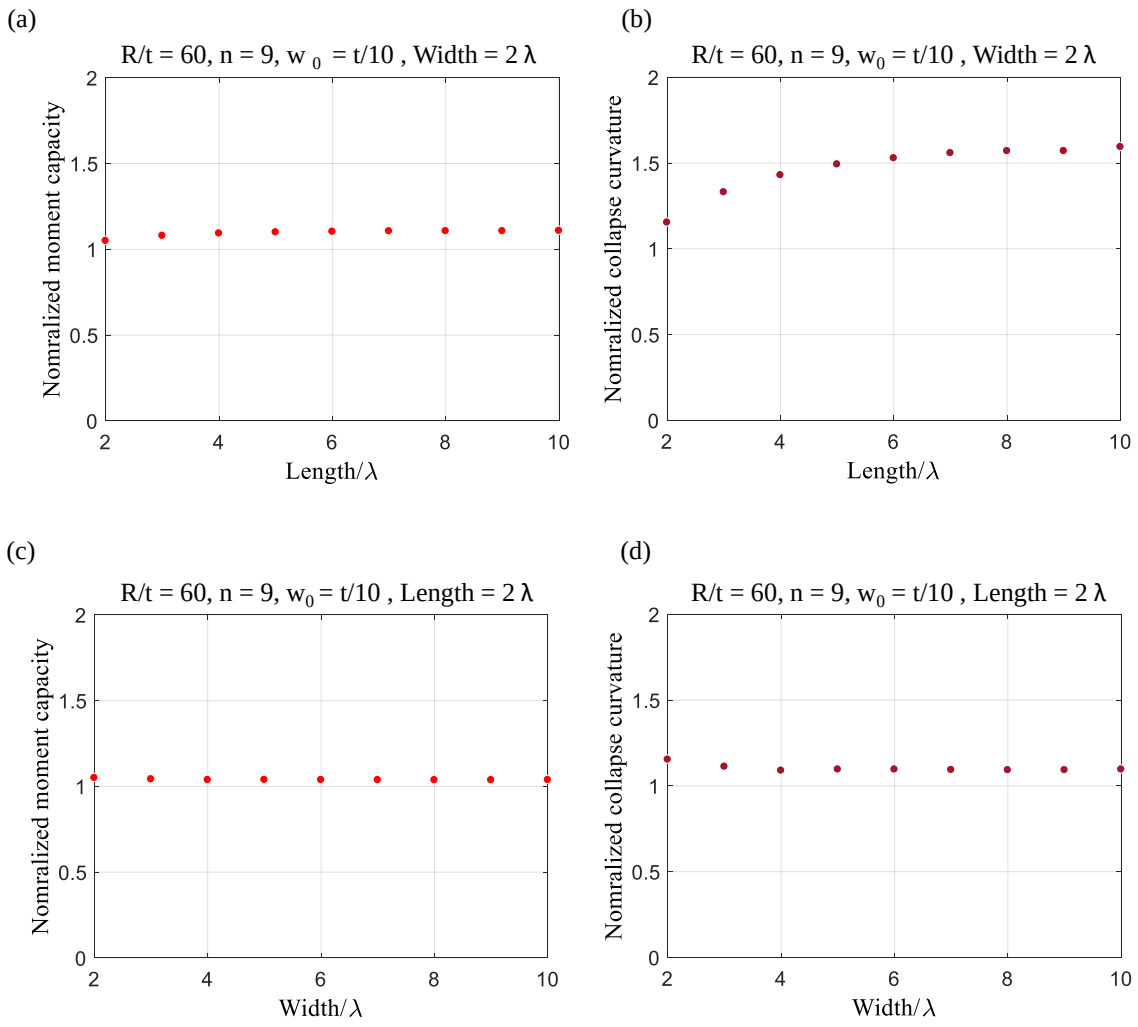

Figure 2.17: (a) The effect dimple length (axial direction) on the moment capacity. (b) The effect dimple length (axial direction) on the collapse curvature. (c) The effect dimple width (circumferential direction) on the moment capacity and (d) The effect dimple width (circumferential direction) on the collapse curvature.

dimple-like imperfection is varied (dimension along the axial direction) from 2λ to 10λ with an interval of λ while the other parameters are kept constant, i.e., the width is 2λ and amplitude is $t/10$. The results of this analysis are shown in figure 2.17. Figure 2.17a shows the moment capacity and figure 2.17b shows the collapse curvature with varying length of the imperfection. It is surprising to see the indifference of moment capacity to the length of the dimple-like imperfection, while the collapse curvature is increasing with the increase of the length. Figure 2.17c and figure 2.17d show the impact of imperfection's width on the moment capacity and collapse curvature. The moment capacity and collapse curvature both are not affected by the width of the dimple-like imperfection. We found similar results for other R/t ratios and strain-hardening models used in these studies, i.e., $R/t = 80, 100, 120$ and $n = 13, 30$. In summary, the moment capacity of thin steel cylindrical shells, which are used in this study, depends primarily on the amplitude of the imperfection and is less dependent on the length and width of the dimple-like imperfection.

2.3.4 Effect of strain-hardening models

Figure 2.18 shows the impact of the different strain-hardening models on the bending behavior for $R/t = 60$. It can be seen that the strain-hardening models affect significantly the peak moment and the collapse curvature. The cylinder has the least capacity when the bilinear model is used and has the maximum capacity for Ramberg-Osgood with $n = 9$. The ratios of the peak moment and the collapse curvature for $n = 9$ and bilinear are 1.23 and 3.00 respectively which demonstrates the significant role played by strain-hardening models. The collapse curvature is reduced by one third by just changing the hardening model from $n = 9$ to bilinear. This is a very crucial finding as sometimes the best fit of a Ramberg-Osgood model is used from the stress-strain tests. This finding suggests that utmost caution should

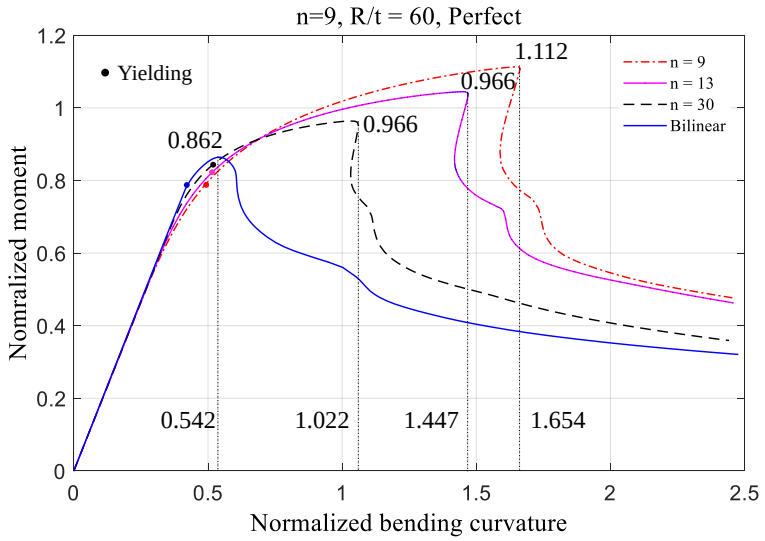

Figure 2.18: Impact of material-hardening models on the bending behavior of thin steel cylindrical shells. The capacity is minimum for bilinear and maximum for $n = 9$.

be taken in choosing the strain-hardening model, as it could heavily overestimate or underestimate the bending capacity of thin steel cylindrical shells. The impact of strain-hardening models is more pronounced on the collapse curvature than the peak moment. The highly nonlinear behavior, due to the coupling of material nonlinearity and ovalization, in the vicinity of buckling is responsible for such a drastic impact of strain-hardening models on the collapse curvature.

The impact of strain-hardening models is not the same for all the R/t ratios. Figure 2.19 shows the moment capacities and collapses curvature for four R/t $(60, 80, 100, 120)$. From figure 2.19, it can be observed that the impact of strain-hardening models are diminishing as R/t is increasing. This is happening because higher R/t reduces the collapse curvature and the peak moment. The nonlinear zone in the vicinity of buckling reduces and consequently the role played by strain-hardening models is also reduced. For much higher values of R/t, thin steel cylinders fail elastically, and strain-hardening models do not play any role in deciding the bending capacity of perfect thin cylinders. However, strain-hardening models affect their post-buckling

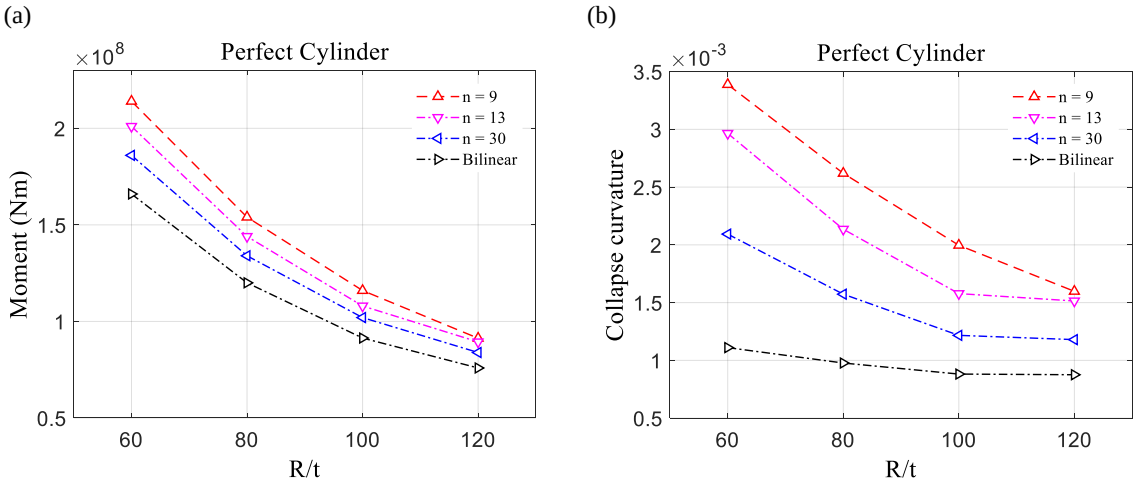

Figure 2.19: Variation of (a) the moment capacity and (b) the collapse curvature with the slenderness ($\frac{R}{t}$).

behavior when large deformation appears. Strain-hardening models may have a role in deciding the capacity of imperfect cylinders with the higher R/t ratios especially if residual stresses are present. But for our range of interest ($60 < R/t < 120$), strain-hardening models do have an important role. Figure 2.20 shows the moment capacities and collapse curvatures for biased and unbiased imperfect cylinders, and figure 2.21 shows the moment capacities and collapse curvatures for modal shape and dimple-like imperfect cylinders. From these figures, it can be concluded that the impact of strain-hardening models on the imperfect cylinders and the perfect cylinder is similar.

2.4 Validation of Finite Element Modeling

To compare our computational results with the past experiments, we collected the experimental data of Guo et al. [19], Sherman [86], Kiymaz [62], Elchalakani et al. [87] and van Es et al. [53]. The dimensions of cylinders, which are used in these experiments, are different from the dimensions of the cylinders used in this study.

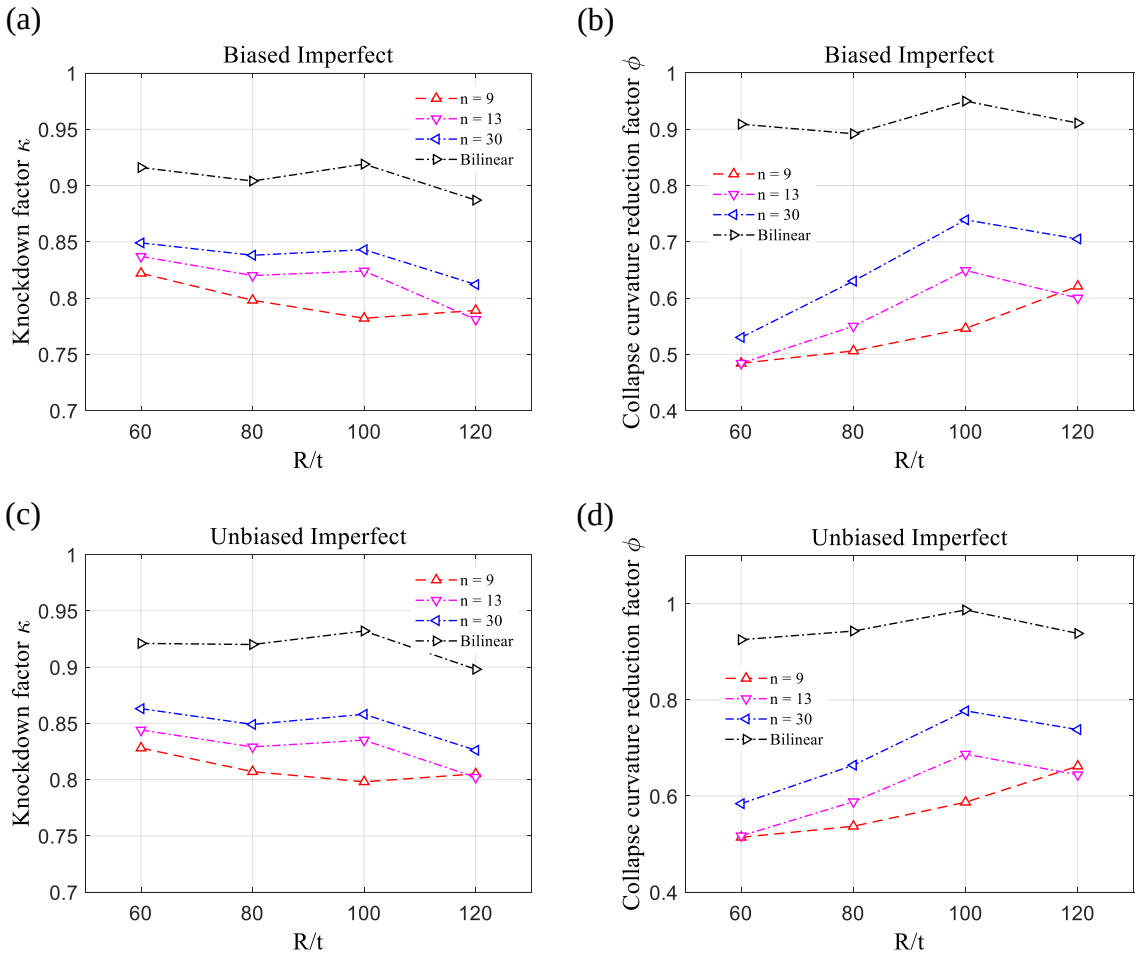

Figure 2.20: Impact of material-hardening models on the knockdown factor κ (a and c) and on the collapse curvature reduction factor ϕ (b and d) for biased and unbiased imperfection.

For this reason, we compare the non-dimensional load parameter M_u/M_p against the generalized section slenderness $\frac{D}{t} \times \frac{f_y}{250}$ as used by Guo et al. [19] and Elchalakani et al. [87]. Here M_u is the bending capacity, M_p is the plastic capacity of the cylinder and f_y is the yield stress in Mpa. Figure 2.22 shows the plot of M_u/M_p against the generalized section slenderness for the experiments and our computational results. For our computational results, we use Ramberg-Osgood strain-hardening model with $n = 9$ and one perfect and four imperfect cylinders: biased, unbiased, dimple-like and Modal all with imperfection amplitude $t/10$. The generalized section slenderness

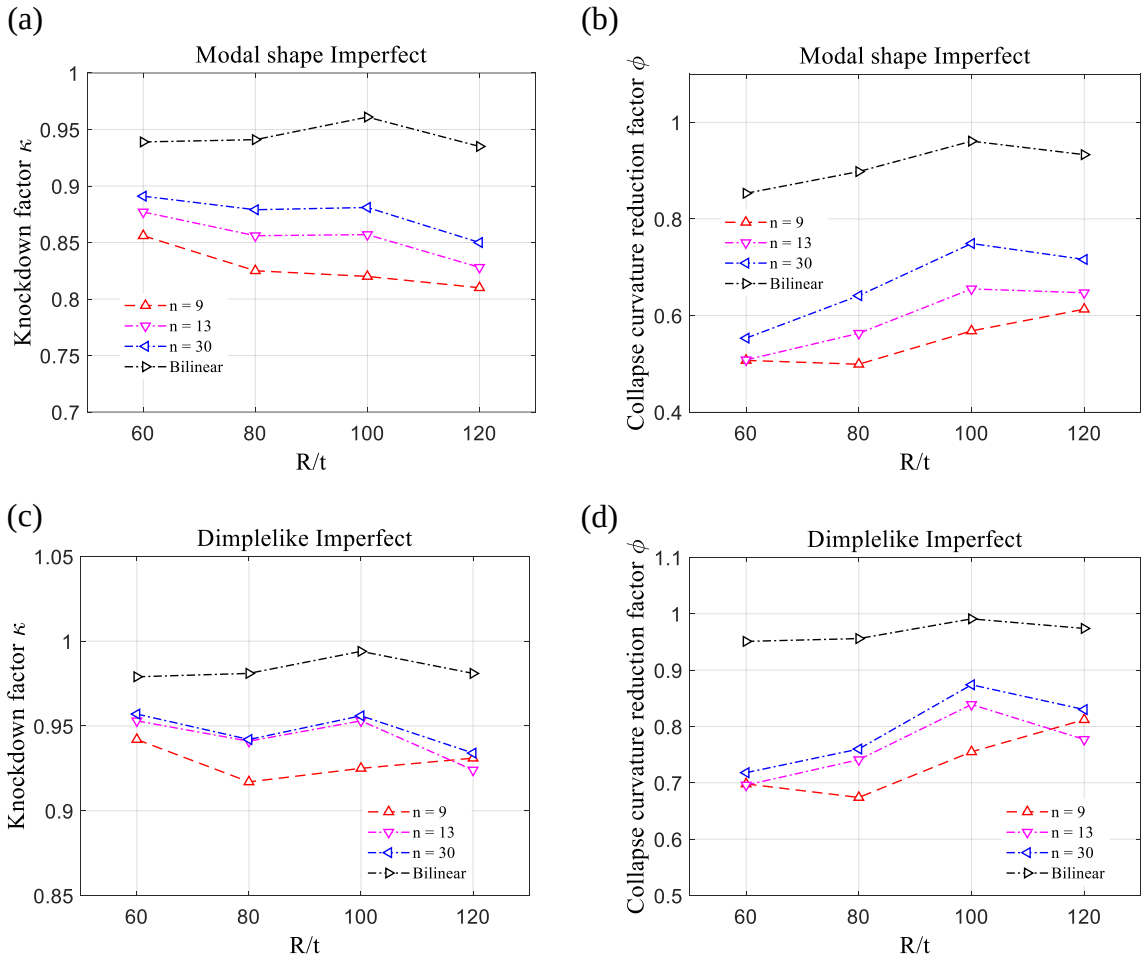

Figure 2.21: Impact of material-hardening models on the knockdown factor κ (a and c) and on the collapse curvature reduction factor ϕ (b and d) for modal shape imperfection and dimple-likes imperfection.

varies from 170.40 to 340.80 for our study and the experiments of Guo et al. [19], van Es et al. [53] and Elchalakani et al. [87] have some samples in this range as shown in figure 2.22. A general trend is followed by our computational study, i.e., a reduction of M_u/M_p ratio with the increase of generalized section slenderness. This trend is also observed by the experimental results as can be seen in figure 2.22.

The recent experiments done by Jay et al.[56] have quite large generalized section slenderness and thus to compare our results with these experiments, we have chosen a different non-dimensional parameter, i.e., knockdown factor κ. The R/t values of

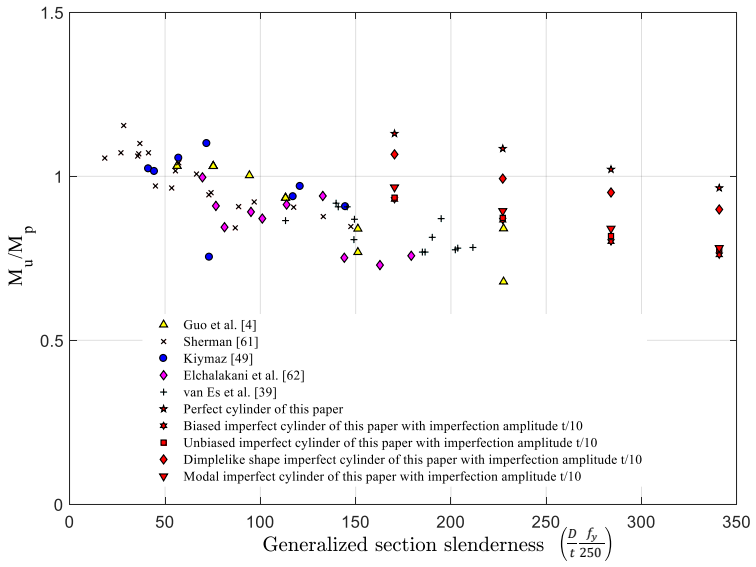

Figure 2.22: Plot of M_u/M_p against the generalized section slenderness $\frac{D}{t} \times \frac{f_y}{250}$ for the past experiments and our computational models.

this experimental sample vary from 137.50 to 160.50, and so we have created computational cylindrical models having R/t ratios equal to these experiments. Mahmoud et al. [18] reported that imperfection amplitude $0.60t$ shows strong agreement with the experiment. For this reason, knockdown factor κ of the computational models are found assuming imperfection amplitude $0.60t$. The results in figure 2.23 show good agreement between the experimental values of κ to the computational values of κ. It should be noted that κ for the experiment is calculated as the ratio of the experimental capacity of the specimen by the capacity predicted by a computational model of the specimen without accounting imperfections (perfect geometry). For dimple-like imperfection, the agreement is quite good, while for biased and unbiased imperfection our κ is lower than the experimental value. This discrepancy shows that dimple-like imperfections are actually the most realistic of all the imperfections accounted in our study. This is evidence to support the recent work undertaken by NASA and others for the update of knockdown factors [88, 89]

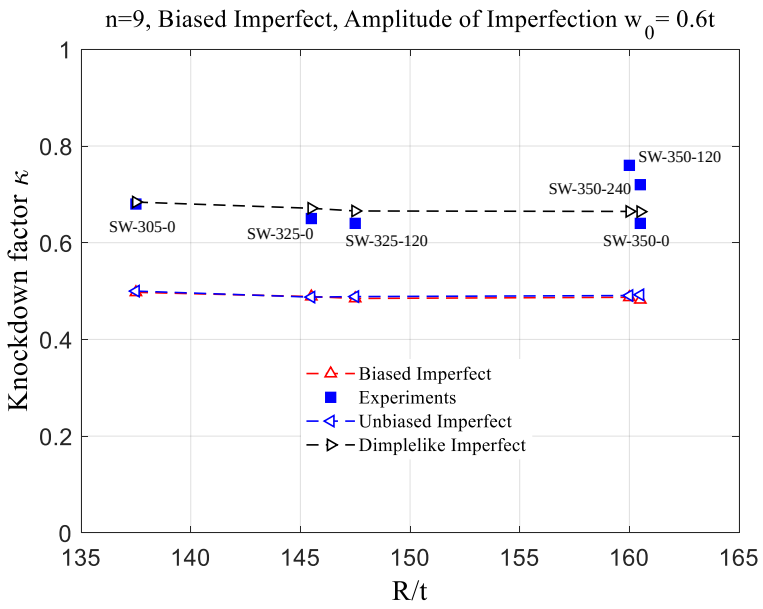

Figure 2.23: Knockdown factor κ for experiments and for finite element modeling with three types of imperfection.

2.5 Discussion

We found that steel cylindrical shells ($60 < R/t < 120$) are highly imperfection sensitive under inelastic bending and that strain-hardening models play a very impactful role on the bending behavior. Four kinds of geometric imperfections, modal shape, dimple-like, unbiased and biased, are applied to make the imperfect cylinders. The presence of imperfections modified many features of the moment-curvature diagram, and reduces the peak moment and the collapse curvature significantly. The reduction in collapse curvature is more pronounced than the reduction in peak moment due to the existence of a highly nonlinear region before buckling. The maximum reduction in load carrying capacity for $R/t = 60$, happens in the case of biased imperfection,i.e. around 18%. The reduction in collapse curvature (51%) is also maximum for biased imperfection for $R/t = 60$. The influence of dimple-like imperfection on the bending behavior is minimum among the four imperfections considered in this study. In this

case, the reduction in load carrying capacity is around 6% and reduction in collapse curvature is around 30% for $R/t = 60$. Similar patterns are observed for other R/t $(80, 100, 120)$. It can be said that the biased imperfection is worst and the dimple-like imperfection is least worst among all the imperfections. The location of first yielding in the moment-curvature space and the pre-bucking path are also affected by the geometric imperfections. The first yielding occurs at lower moments for imperfect cylinders as compared to the perfect cylinders. For the biased and the unbiased imperfect cylinders, the pre-buckling paths are different than the pre-buckling path of perfect cylinder whereas the pre-buckling path of the dimple-like imperfect cylinder and modal shape imperfect cylinder are same as the perfect cylinder.

We also found that the bending behavior of thin steel cylindrical shells highly depends on the strain- hardening models. The moment capacity and the collapse curvature is minimum for the bilinear model and maximum for Ramberg-Osgood model with $n = 9$ among all the models used. The significance of the strain-hardening model can be understood by the fact that the ratio of collapse curvature for $n = 9$ to bilinear is around 3 $(R/t = 60)$, which demonstrates that the same cylinder could collapse at three times less curvature if the strain-hardening model changes. This is a very significant finding and it suggests that the selection of a strain-hardening model is extremely important because it can highly overestimate or underestimate the collapse curvature and bending capacity.

CHAPTER 3

IMPERFECTION INSENSITIVITY OF THIN WAVY CYLINDRICAL SHELLS UNDER AXIAL COMPRESSION OR BENDING

This chapter presents new insights into the response of wavy cylinders under uniform axial compression and bending. The effectiveness of wavy cylinders, to reduce imperfection sensitivity under bending load, is investigated assuming a plastic Ramberg–Osgood material model. The effect of wave parameters, e.g., the amplitude and the number of waves, is also explored. This chapter reveals that wavy thin cylinders are insensitive to imperfections under bending in the inelastic range of the material. It is found that the wave parameters play a decisive role in the response of thin wavy cylinders to imperfections under bending.

3.1 Geometry of thin wavy cylinders and finite element modeling

There are many ways to create a wavy cross-section of a cylinder. We choose a simple way to create wavy cross sections in which a sinusoidal wave is superimposed on the circular cross-section with a specified wavelength and amplitude. Figure 3.1 shows the cross-sections of circular and wavy cylinders along with their analytical equations. The wavy cross-section is created by superimposing a sine wave, with amplitude A_r and number of waves N, on the circumference of the circular (called base circle in [66]) cross-section, whose radius is R.

This wavy cross-section is fully characterized by three parameters: the radius of

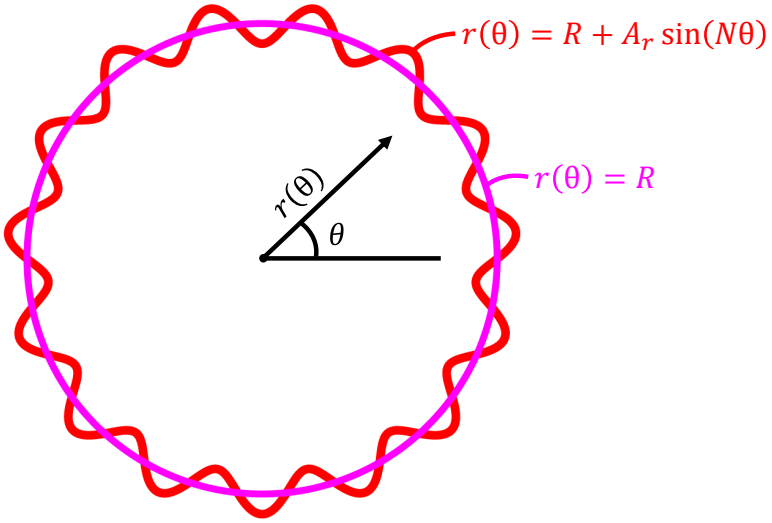

Figure 3.1: The geometry of circular and wavy cylinders. The cross-section of the wavy cylinder is characterized by three parameters: radius of base circle R, the number of waves N along the circumference and the amplitude of the wave A_r.

the base circle R, the wave amplitude A_r and the number of waves N. The analytical equation of the wavy cross-section is [66]:

$$r(\theta) = R + A_r \sin(N\theta) \tag{15}$$

Where θ is the polar coordinate, R is the radius of the base circle, A_r is the amplitude of the wave and N is the number of waves along the circumference.

All the analyses are performed in ABAQUS [80] using the arc-length based Riks method [91]. For meshing, four-node reduced integration shell ($S4R$) elements are created by user-written codes with an element size 121.20 mm, about $0.61\sqrt{Rt}$, in both axial and circumferential directions. Four integration points were utilized along with the thickness of each element. Figure 3.2 demonstrates a representative finite element model. Two nodes are defined at the center of the top and bottom cross-sections of the cylinder; we call them center nodes. Rigid links are created to connect the nodes at the end of the cylinder to the respective center nodes to constrain the

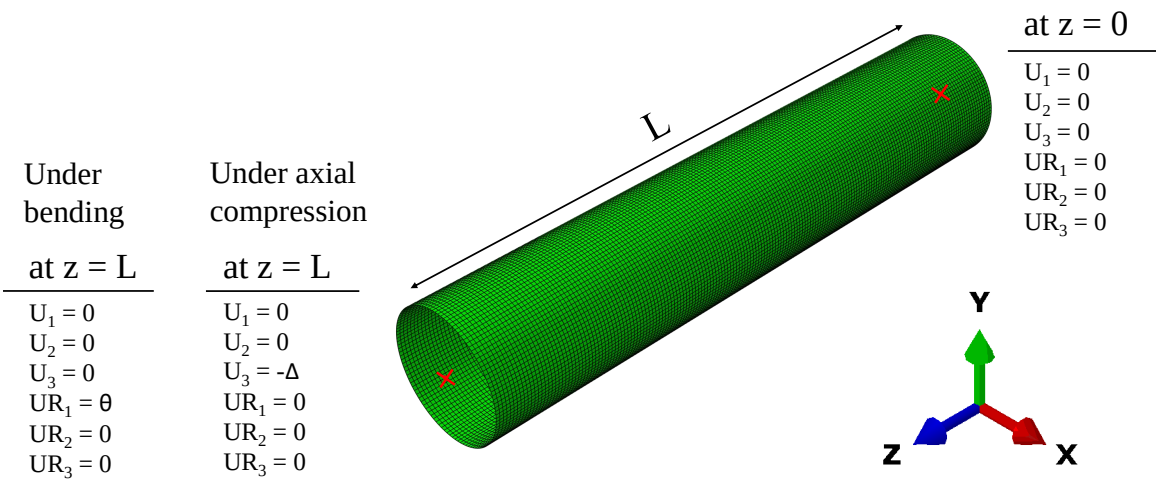

Figure 3.2: Boundary conditions and loading of the model under axial compression and bending.

displacements U_1, U_2, and U_3, and rotations UR_1, UR_1, and UR_1 of the nodes at the end from moving and rotating with respect to the center nodes. Using these constraints one end of the cylinder is clamped by fixing the central node at $z = 0$. At the other end ($z = L$) a clamped boundary condition is enforced, but the end of the cylinder is loaded by applying an axial displacement, $U_3 = -\Delta$, for the cylinder under axial compression and by applying a rotational displacement, $UR_1 = \theta$, for the cylinder under bending. The material properties and the dimensions of the cylinders are described in later sections separately for axial compression (linear elasticity) and bending (plasticity).

3.2 Wavy cylindrical shells under axial compression

In this section, the effect of a dimple-like imperfection is studied to evaluate the effectiveness of wavy cylinders under axial compression. Dimple-like imperfection is a more realistic imperfection because it can be induced easily when thin cylinders are hit by some sharp solid objectsusually during transportation and construction [1, 83, 85,

Table 3.1: Dimensions and material properties of the circular cylinder under axial compression

$E\ (Gpa)$	$R\ (m)$	ν	R/t	L/R
210	2	0.3	120	4

89]. Although previous pioneering studies [66, 67] have observed the response of wavy cylinders to imperfections under axial compression, the imperfections had not been realistic from an application aspect (they are in the shape of the first eigenmode). We also examine the mechanism behind the imperfection insensitivity of wavy cylinders; this is the main objective of this section and thus we assume linear elastic material behavior for simplicity purposes. The dimensions and the material properties of the cylinder, which are used in this section, are given in Table 5.1. These are based on the work of Yadav and Gerasimidis [1] focused on bending of thin cylinders except for the length L. The value of length L is taken as $4R$ based on Gerasimidis et al. [89] work on thin cylinders under axial compression. These dimensions are common in the industry of steel wind turbine towers.

The wave amplitude A_r and the number of waves N of Eq. 1 will be used as variables to explore their effect on imperfection sensitivity.

3.2.1 Sensitivity to dimple-like imperfections

Local dimple-like imperfections are commonly induced in thin cylinders when they are hit by some sharp solid. We apply a single dimple that is placed at the middle of the cylinder. To model dimple-like imperfections, we use what was proposed by Yadav and Gerasimidis [1] and Gerasimidis et al. [89]. The mathematical description of the dimple-like imperfection is:

$$w = -w_o e^{-(\frac{x}{L_1})^2} e^{-(\frac{\theta}{\theta_1})^2} \tag{16}$$

Where w represents the deviation of shell surface from the original position in the radial direction and w_o is the amplitude of the imperfection; x and θ are the axial and circumferential coordinates with the origin placed in the middle of the cylinder. Figure 2.10 shows this dimple-like imperfection, which is placed at the middle of the cylinder, along with the coordinates x and θ. L_1 and θ_1 are the parameters which decide the length (in the axial direction) and width (in the circumferential direction) of the dimple. The values for L_1 and θ_1 are chosen such that the length ($2L_1$) and the width ($2R\theta$) of the dimple are equal to the first eigenmode wavelength of the circular cylinder under axial compression, i.e. $3.44\sqrt{Rt}$ for $\nu = 0.3$ [79]. This is done in anticipation that this length and width of the dimple-like imperfection reduce the capacity the most [1]. We use this dimple-like imperfection in both the circular and wavy cylinders and compute the reduction in their load carrying capacities. For wavy cylinders, the number of waves N is 15 and the wave amplitude A_r is taken as $R/70$ ($1.7t$), $2R/70$ ($3.4t$) and $3R/70$ ($5.1t$). We vary the amplitude of imperfections w_o from 0 to t because for most practical purposes the amplitude of imperfections is not more than the thickness of the cylinder.

Figure 3.3 shows the knockdown factor for the circular and wavy cylinders against imperfection amplitude. The knockdown factors are always higher for wavy cylinders (less reduction) as compared to the circular cylinder and the effectiveness of the wavy cylinders in terms of insensitivity to imperfection increases with the increase of the wave amplitude A_r. This is evidence that the wavy cylinders are not only insensitive to eigenmode imperfections as reported by Ning and Pellegrino [67, 76], but also to dimple-like imperfections.

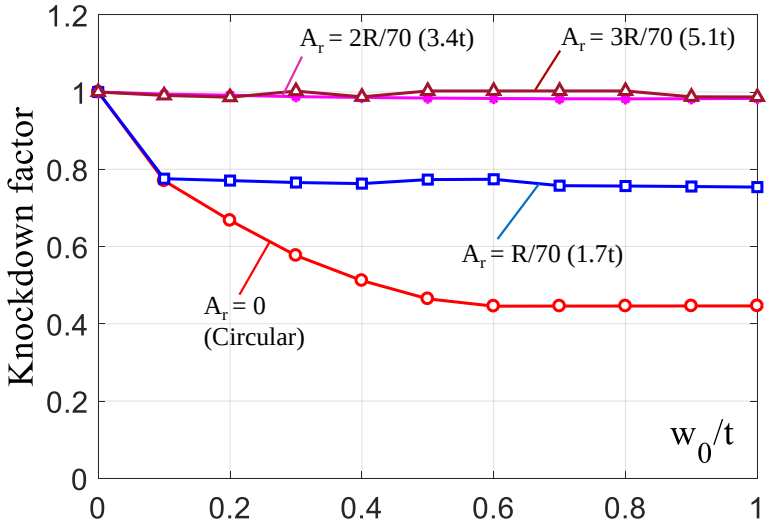

Figure 3.3: Knockdown factor of circular and wavy cylinders; the R/t is 120 for all the cases. The wave amplitude A_r changes the behavior of wavy cylinders drastically.

Many significant observations can be made from figure 3.3. First, the wave amplitude drastically affects the behavior of the cylinders as the knockdown factor in case of $A_r = 2R/70$ $(3.4t)$, and $A_r = 3R/70$ $(5.1t)$ is almost 1. For $A_r = R/70$ $(1.7t)$, the knockdown factor is significantly less than 1 but still more than that of the circular cylinder. Second, knockdown factors stabilize for all the cases at higher imperfection amplitudes and further increase in imperfection amplitude does not further reduce load carrying capacities. Stabilization in knockdown factor is also reported in many past studies [1, 83, 85, 92, 93]. Third, for the wavy cylinders, the plateau occurs at smaller imperfection amplitudes.

The imperfection insensitivity of wavy cylinders is attributed to many factors. The first is the reduction in the local radius of curvature. Due to the waviness, curvatures along the circumference are reduced significantly and thus the effective R/t drops. We know the imperfection sensitivity of shells reduces with the reduction of R/t ratio (figure 1.2). To understand how R/t ratio affects the imperfection sensitivity, we plot the knockdown factor for circular cylindrical shells in figure 3.4a with varying R/t

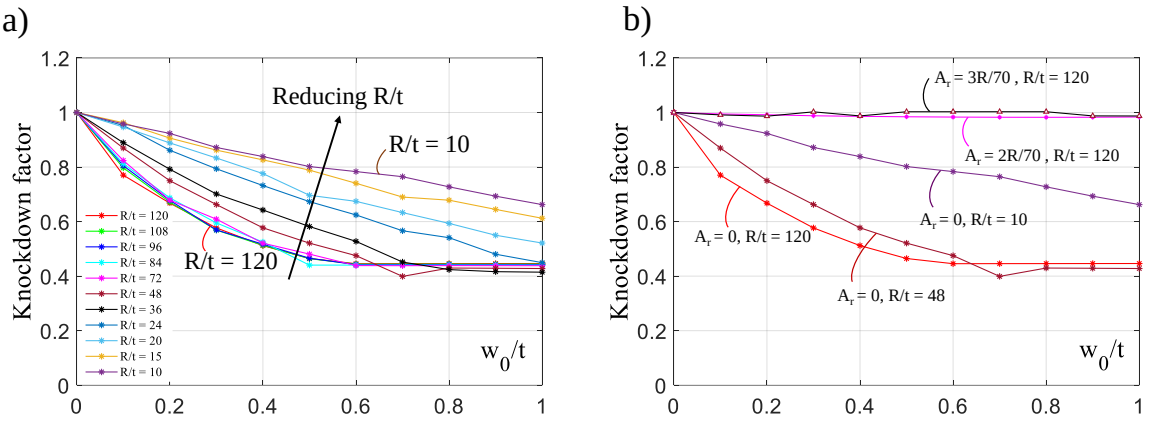

Figure 3.4: (a) Knockdown factor of circular cylinders with varying R/t ratio. The thickness is constant (0.0167 m) for all the cases; the R/t ratio is changed by varying the radius R. The dimple imperfections are also kept the same that means their length, width and amplitude are the same irrespective to R/t ratio. (b) Knockdown factor for selective circular and wavy cylinders. It can be seen that the wavy cylinders with $A_r = 2R/70$ and $3R/70$ are performing even better than the circular cylinder with $R/t = 10$. This shows that the reduction in effective R/t is not only responsible for the imperfection insensitivity of wavy cylinders.

ratio from 120 to 10. The thickness of the cylinder is constant and equal to 2/120 m for all these cylinders; we are varying only radius R to vary the R/t ratio. The local dimple-like imperfections are not scaled; this means that the length and width of the dimple are same for all the cases. It can be observed that the knockdown factor is increasing with the reduction of R/t ratios, keeping imperfection the same (unscaled). Keeping imperfection unscaled is important to see the impact of R/t on knockdown factors otherwise if we scale the imperfection with R/t, knockdown factors will remain unaffected [83]. In figure 3.4b, we plot wavy cylinders with $A_r = R/70$ $(1.7t)$, $2R/70$ $(3.4t)$, and $3R/70$ $(5.1t)$ and the circular cylinder with $R/t = 120, 48$ and 10. For wavy cylinders, the radius of the base circle is 2 m, $N = 15$ and R/t ratio is 120. For wavy cylinders with $A_r = 2R/70$ $(3.4t)$, and $A_r = 3R/70$ $(5.1t)$, the knockdown factors are even higher than the knockdown factor for circular cylinder with $R/t = 10$. In addition, the knockdown factor variation with the imperfection

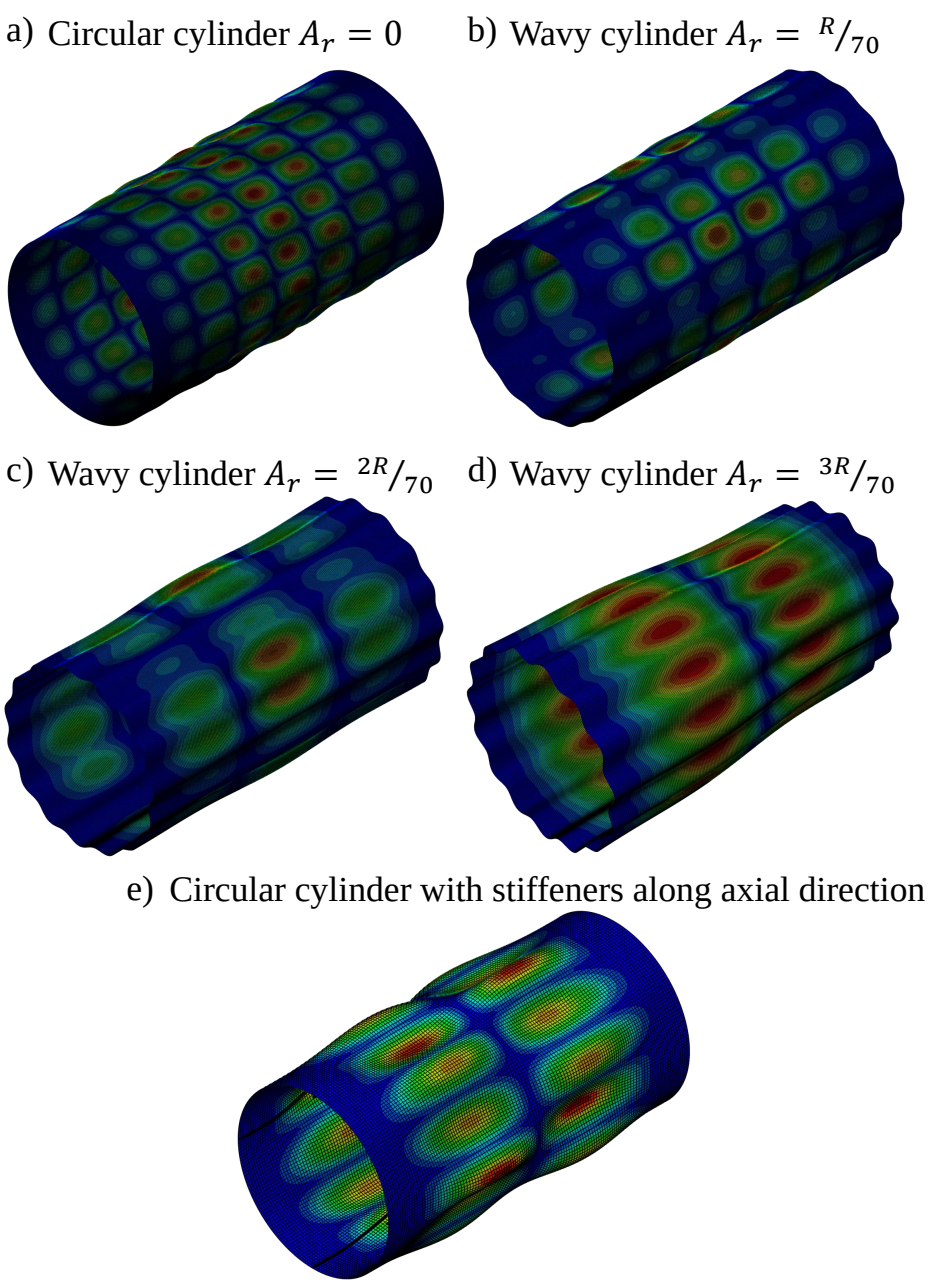

Figure 3.5: First eigenmodes of the circular and wavy cylinders; the value of A_r is 0 (a), $R/70$ (b), $2R/70$ (c), and $3R/70$ (d) for the wavy cylinders. The wavy cylinder with $A_r = R/70$ exhibits similarity to the circular cylinders, while the wavy cylinders with $A_r = 2R/70$ and $3R/70$ exhibit similarity to stiffened cylinders (e). The smaller wave amplitude cylinder (b) is not as insensitive to imperfection as high wave amplitude cylinders (b and c). The waviness acts like stiffeners and thus also contributes to the imperfection insensitivity of wavy cylinders along with the reduction in effective R/t ratio.

amplitude of wavy cylinders is different than that of circular cylinders. For wavy cylinders, the knockdown factor does not vary with imperfection amplitude substantially, whereas, for circular cylinders, the knockdown factor decreases with the imperfection amplitude. The reduction in the R/t ratio reduces the knockdown factor but does not alter the high sensitivity of circular cylinders to imperfections. Therefore, the reduction of the local radius of curvature is not the only reason for the insensitivity of wavy cylinders to imperfections, as given by Ning and Pellegrino [67]; although, this is the primary reason.

The second attribute to the imperfection insensitivity of wavy cylinders is the stiffness developed by the waviness along the axial direction. An important feature of figure 3.4 is the drastic difference in knockdown factors of wavy cylinders by changing the wave amplitude A_r. This is happening because by changing the wave amplitude, the stiffness of the cylinder is changed notably. To understand this more clearly, we show the first eigenmode of circular and wavy cylinders in figure 3.5. It can be seen that for smaller wave amplitude, $A_r = R/70$ $(1.7t)$, the eigenmode of the wavy cylinder is similar to the circular cylinder. This is happening because for small wave amplitude, the stiffening effect of the cylinder is altered only slightly and thus, the increase in imperfection insensitivity, in this case, is not as pronounced as with the other wavy cylinders. For wavy cylinders with $A_r = 2R/70$ $(3.4t)$ and $3R/70$ $(5.1t)$, the first eigenmode is quite different than the circular cylinder and resembles more to the circular cylinder with stiffeners along the axial direction. Consequently, knockdown factors are increased considerably.

3.2.2 Sensitivity to axisymmetric imperfections

We create an axisymmetric imperfection by eliminating the circumferential variation, $e^{-\left(\frac{\theta}{\theta_1}\right)^2}$, from Eq. 16:

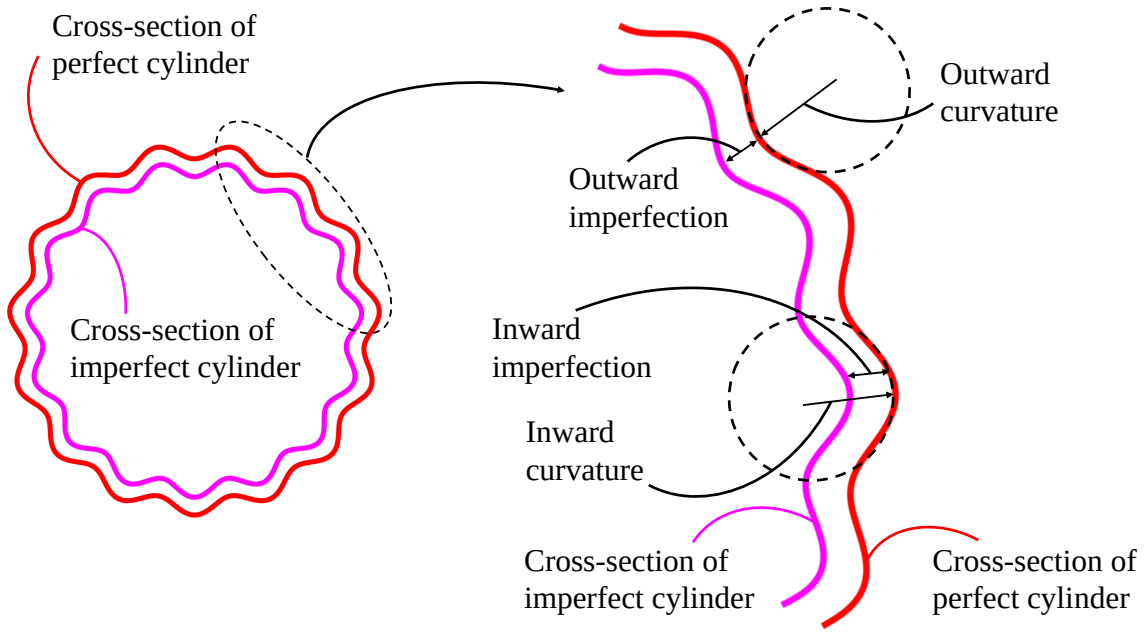

Figure 3.6: Disharmonized axisymmetric imperfections. When the curvature is inward, the imperfection is also considered inward which is the most deleterious case. However, when the curvature of the wavy shell is outward, the imperfection is outward and therefore its effect is not as deleterious as in the first case.

$$w = -w_o e^{-(\frac{x}{L_1})^2} \tag{17}$$

In this equation, the imperfection depends only on the axial coordinate x, and its amplitude is the same along the circumference. All the other parameters of Eq. 17 have the same meaning as in Eq. 16. The direction of the imperfection is always inward (toward the center of the cross-section) while the direction of curvature of the wavy cross-section is changing direction periodically from inward to outward. We know from previous studies on axisymmetric imperfections that inward imperfections are more deleterious than outward imperfections; in the case the imperfection nodes are outside of the perfect cylindrical shell, the reduction in the buckling capacity is less compared to opposite case. In the wavy cylindrical shell with axisymmetric imperfection, this phenomenon appears in both directions as shown in figure 3.6. When

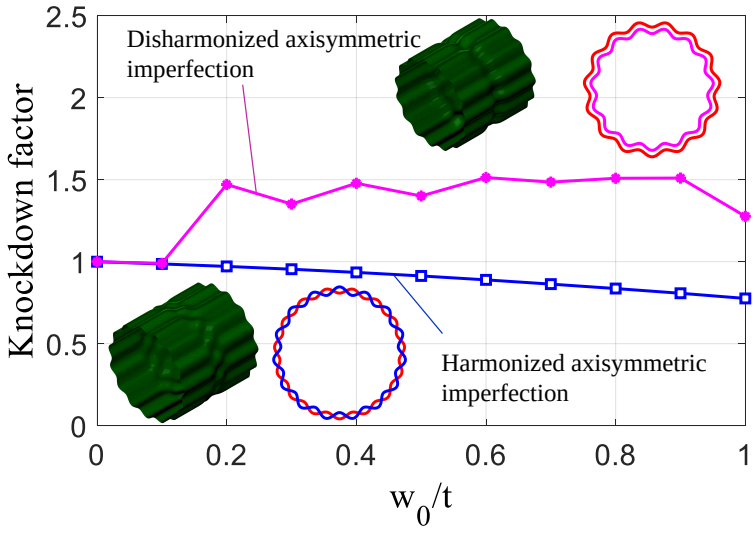

Figure 3.7: Knockdown factor for wavy cylinders with harmonized and disharmonized axisymmetric imperfections. For disharmonized axisymmetric imperfections, the imperfections are surprisingly not reducing but increasing the load carrying capacity, indicating that a two-directional wave could be beneficial for the cylinder.

the curvature is inward, the imperfection is also considered inward which is the most deleterious case. However, when the curvature of the wavy shell is outward, the imperfection is outward and therefore its effect is not as deleterious as in the first case. We call this axisymmetric imperfection as disharmonized as it provides a kind benefit to the buckling of the wavy cylinder. Figure 3.7 illustrates this beneficial effect of wavy cylinder, having $A_r = 3R/70$ $(5.1t)$ and $N = 15$, for disharmonized axisymmetric imperfection. The knockdown factor for disharmonized axisymmetric imperfection is higher than 1 for all the cases, except for imperfection amplitude $0.1t$. Thus, this axisymmetric imperfection is not reducing but increasing the load carrying capacity of the wavy cylinder within the range of imperfection amplitudes considered. This surprising result is an indication that longitudinal waves (here coming from imperfection) could potentially be beneficial for the capacity, if combined with circumferential waves.

To further investigate this issue, we imposed an antisymmetric imperfection in the

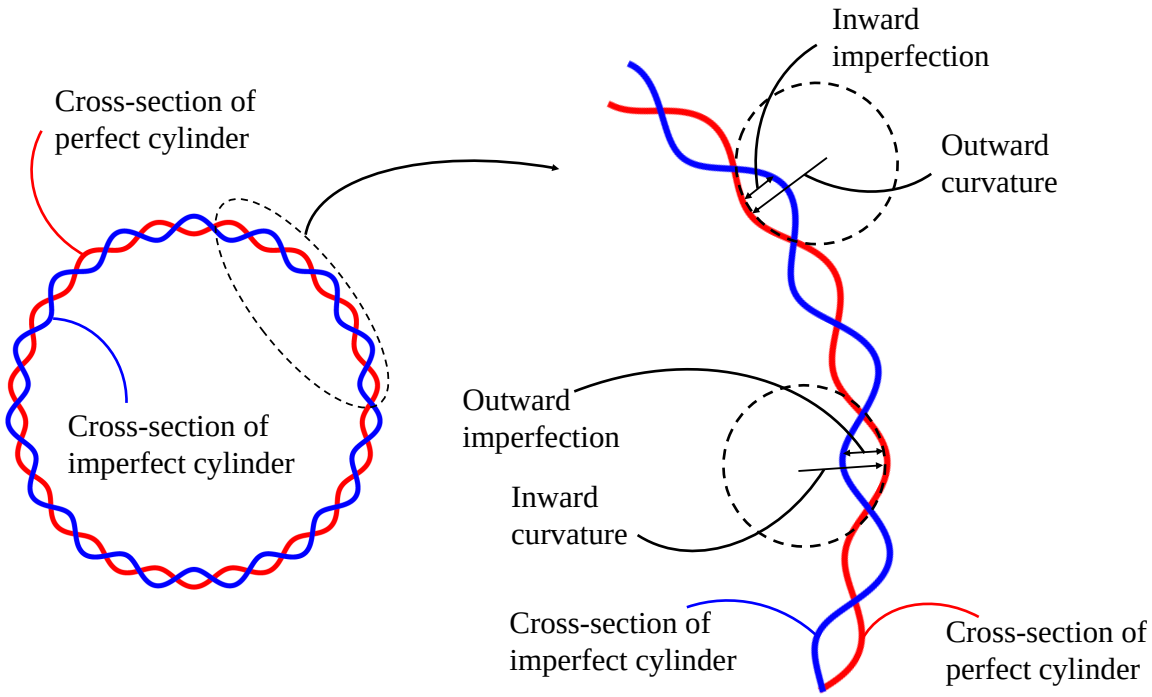

Figure 3.8: Harmonized axisymmetric imperfections. When the curvature is inward, the imperfection is outward and, when the curvature of the wavy shell is outward, then the imperfection is inward.

wavy cylinder, which is aligned with the curvature direction of the wavy cross-section; i.e. if the direction of the curvature is inward then the imperfection is outward and if the direction of the curvature is outward then the imperfection is inward (figure 3.8). To create such an imperfection pattern, we modified Eq. 16 by adding a $\sin(N\theta)$ term in the equation. The value of N is kept 15 as for the wavy cross-section. We call this imperfection as harmonized. The mathematical equation of this imperfection is:

$$w = -w_o e^{-(\frac{x}{L_1})^2} \sin(N\theta) \tag{18}$$

Figure 3.7 shows the harmonized imperfect wavy cylinder along with the cross-sections at the middle of the perfect and imperfect wavy cylinders. Again, we have scaled up the imperfection amplitude in this figure for visual clarity. The knockdown

factor is also shown in figure 3.7. The knockdown factor, for harmonized imperfection, is reducing with increasing imperfection amplitude, which is a contrast to the response of the wavy cylinder to the disharmonized imperfection. This is happening because there is no resistance to radial displacement in this case and thus the behavior is as expected, i.e., the knockdown factor reduces with the increase of imperfection amplitude w_o. However, the wavy cylinder is still rather insensitive to imperfection. Harmonized imperfection is quite artificial as the direction of imperfection is inward or outward. Thus, we have another benefit of using wavy cylinders, which further makes them insensitive to imperfection.

In summary, the mechanism behind the imperfection insensitivity of wavy cylinders can be described by the following observations:

1. The first observation, the most significant one, is that the reduction in effective radius of curvature, which consequently reduces the effective R/t ratio renders wavy cylinders less sensitive to imperfections.

2. Second is the stiffness developed by the waviness of wavy cylinders. Waviness also works as a stiffener, which can be seen by the change of the first eigenmode with the increase in the wave amplitude (figure 3.5).

3. The third is the periodic change in the direction of the curvature of wavy cylinders: the direction of curvature changing from inward to upward. Often, the direction of a real imperfection is inward or outward but not in both directions. Thus, there is disharmony between the curvature direction and the direction of the imperfection. This provides a kind benefit, which makes wavy cylinders further insensitive to the imperfections.

These three factors work simultaneously and make wavy cylinders insensitive to imperfections.

3.2.3 Verification of computational findings

To verify our numerical analysis and the key finding, i.e., the insensitivity of wavy cylinders to imperfections, we compared our numerical results with experimental data of Ning and Pellegrino [67] as these are the only experiments on the imperfection sensitivity of wavy cylinders. The dimensions and the material properties used in the experiments are different from the dimensions and the material properties used in this study. For this reason, we modified the dimensions and the material properties of our analyses and compared the results of our computational analysis with the experimental data. The length L, radius R, and the wave amplitude A_r of the three experimental samples are 70 mm, 35 mm, and 1.5 mm respectively. The nominal shell thickness t of the samples is around 180 μm, and the measured thickness of the three samples are 166 ± 16 μm, 166 ± 22 μm, and 165 ± 19 μm. The experimental samples are composites; interested readers are referred to Ning and Pellegrino [67] for the ABD matrix and other details. The measured amplitudes of the mid-surface imperfections of the three samples are $2.08t$, $2.53t$, and $2.98t$. The cross-section of the samples is a mirror-symmetric with a NURBS interpolation having 16 control points along the circumference [66, 67]. To model the samples, we use the sinusoidal cross-section (Eq. 1) with $N = 22$ and $A_r = 1.5$ mm as these values resemble the closest the optimized mirror-symmetric cross-section of the experimental sample [66]. The thickness is considered as 166 μm, and the material properties are taken from Ning and Pellegrino [67]. To introduce the imperfections, we use the first eigenmode shape with amplitude $2.08t$, $2.53t$, and $2.98t$ for samples 1, 2, and 3 respectively. The results of our computational analysis and the failure loads from the experiment are given in Table 4.2.

The buckling loads values from our computational analysis are in accordance to

Table 3.2: Computational results from current analysis compared to the experimental failure loads from [67]. Sample 1 has an imperfection with an amplitude of $2.08t$, sample 2 with an amplitude of $2.53t$ and sample 3 with $2.98t$. The computational results are in accordance to the experimental findings of [67] and both reveal an insensitivity of the wavy cylinders to imperfection amplitude.

	Computational results of current study(kN)	Experimental failure loads from [67](kN)
Sample 1	10.9411	11.48 ± 0.03
Sample 2	10.9403	11.68 ± 0.03
Sample 3	10.9394	11.30 ± 0.03

the experimental failure loads. The small differences between the predicted and experimental data can be attributed mainly to three factors. First, the cross-sections of the experimental samples and the computational models are not exactly the same: sinusoidal wavy cross-section is used for the computational analysis, while the sample's cross-section is a mirror-symmetric with a NURBS interpolation. Second, the shapes of imperfection in the samples and the modeling are not the same: the first eigenmode is used in the modeling, while the samples have complicated shape imperfections [67]. And third, the experimental failure loads correspond to the entire failure of the sample including material failure, while the predicted values are based on buckling loads considering elastic material properties. However, a pattern is clear from both the predicted values and experiment data, and that is they do not vary significantly with the imperfection amplitude (sample 1, 2, and 3 have imperfection amplitudes $2.08t$, $2.53t$, and $2.98t$ respectively). The application of our analysis method on the experimental samples of [67] predicts accurate results.

In all the discussions in section 3, the primary load is axial compression and the material is assumed linear elastic. For many important applications, the primary load is bending (wind turbine towers, gas pipelines, etc.) and extrapolation of the above

Table 3.3: Dimensions and material properties of the circular cylinder under bending

$E\ (Gpa)$	$\sigma_y\ (Mpa)$	$R\ (m)$	ν	R/t	L/R	n
210	355	2	0.3	120	10	9

results is not possible without further investigation. In the next section, we explore the sensitivity of wavy cylinders under bending.

3.3 Wavy cylinders under bending

To study the imperfection sensitivity of wavy cylinders under bending, we choose the dimensions and material properties as taken by Yadav and Gerasimidis [1] and given in Table 4.3. One end of the cylinder is fixed and rotation is applied at the other end (see Section 3.1 for details). For the stress-strain relationship, a version of the Ramberg-Osgood stress-strain relationship is used [1]:

$$\epsilon = \frac{\sigma}{E}\Big[1 + \frac{3}{7}\big(\frac{\sigma}{\sigma_y}\big)^{n-1}\Big] \tag{19}$$

Two rigid body constraints are imposed at the end cross-sections, which make sure that the end cross-sections do not change their shape, i.e, ovalization is prevented during the analysis. We chose these dimensions, and material properties because they are typical sections of tall and super-tall wind turbine towers and for these cylinders, the stresses cross the yield stress limit before buckling [1].

3.3.1 Axisymmetric disharmonized imperfections

To study the response of thin wavy cylindrical shells under bending to imperfections, a sinusoidal axisymmetric disharmonized geometric imperfection is used first. The amplitude of this imperfection is higher at the center of the cylinder, and this

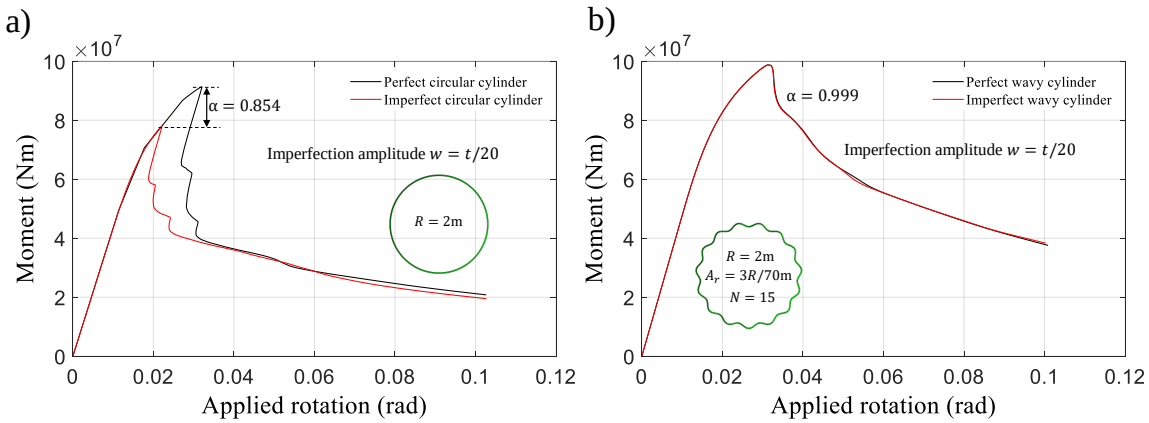

Figure 3.9: (a) Moment-rotation diagram of the perfect and the imperfect circular cylinders. (b) Moment-rotation diagram of the perfect and the imperfect wavy cylinders. The amplitude of imperfection is $t/10$ for both circular and wavy cylinders. The reduction in the case of the circular cylinder is around 15%, while the reduction in the case of the wavy cylinder is almost negligible.

imperfection is defined as biased imperfection. We consider this imperfection as the most deleterious compared to the other geometric imperfections: local dimple imperfection, eigenmode imperfection and unbiased sinusoidal axisymmetric imperfection for which the amplitude is constant along the length [1]. The mathematical expression of the biased imperfection is [1, 50, 78]:

$$w = -R\left(a_{oi} + a_i \cos\frac{\pi x}{N_x \lambda}\right)\cos\frac{\pi(x)}{\lambda} \tag{20}$$

Where, x is the axial coordinate with the origin placed at the center, R is the radius of the cylinder, a_{oi} and a_i are the relative value of unbiased and biased components of the amplitude respectively ($R \times a_{oi}$ and $R \times a_{oi}$ are the absolute values of the unbiased and biased components), and $N_x \times \lambda$ represents the length of the cylinder. The λ represents the first eigenmode half wavelength of the circular cylinder under axial compression, i.e. $1.72\sqrt{Rt}$ for $\nu = 0.30$ [79]. In this study, the value of a_{oi} and a_i are chosen such that the bias of the imperfection defined by the ratio $\frac{a_{oi}}{a_i}$ is 5

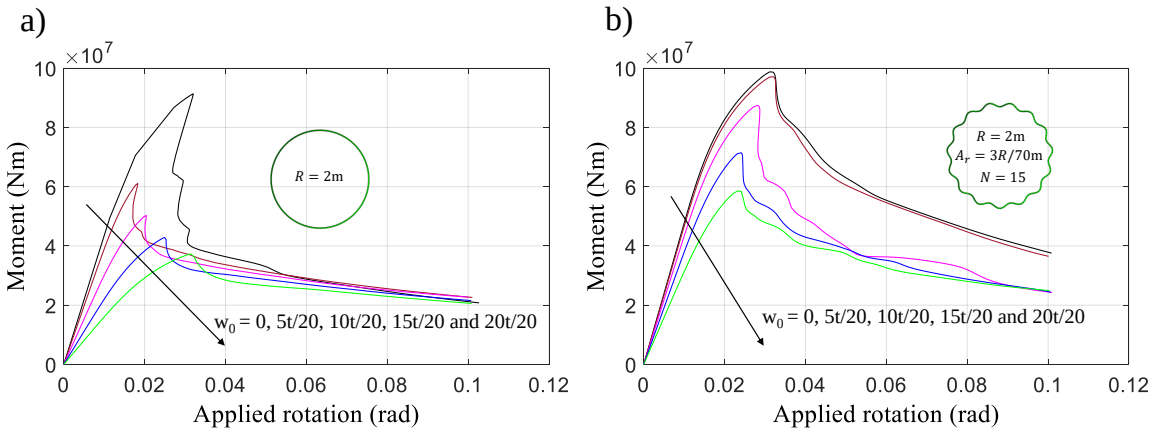

Figure 3.10: Moment-rotation diagram of perfect and imperfect circular and wavy cylinders. The reduction due to imperfection is always low for the wavy cylinders as compare to circular cylinders.

[1, 50, 78]. We induce this biased geometric imperfection in both circular cylinders and wavy cylinders having $A_r = 3R/70$ m and $N = 15$. We find again that the wavy cylinder is insensitive to imperfection as in the case of axial compression.

Figure 3.9a shows the moment-rotation diagrams of the perfect and imperfect circular cylinder, while figure 3.9b shows the moment-rotation diagrams of wavy cylinders. The amplitude of imperfection is $t/10$ in both cases, where t is the thickness of cylinders (0.0167m). The presence of imperfection reduces the load carrying capacity of the circular cylinder significantly (around 15%), whereas the presence of imperfection does not reduce the capacity of wavy cylinder: the moment-rotation diagram of perfect and imperfect wavy cylinders are almost same. It is astonishing that the shape and the amplitude of the imperfection are the same in both cases, but the response of circular and wavy cylinders are entirely different. In figure 3.10, the moment-rotation diagrams are shown for perfect and imperfect cylinders (circular and wavy) with higher amplitudes of imperfection, i.e., $5t/20$, $10t/20$, $15t/20$ and $20t/20$. The reduction in load carrying capacity is always more in case of circular cylinders, however, significant reduction also occurs for wavy cylinders with higher

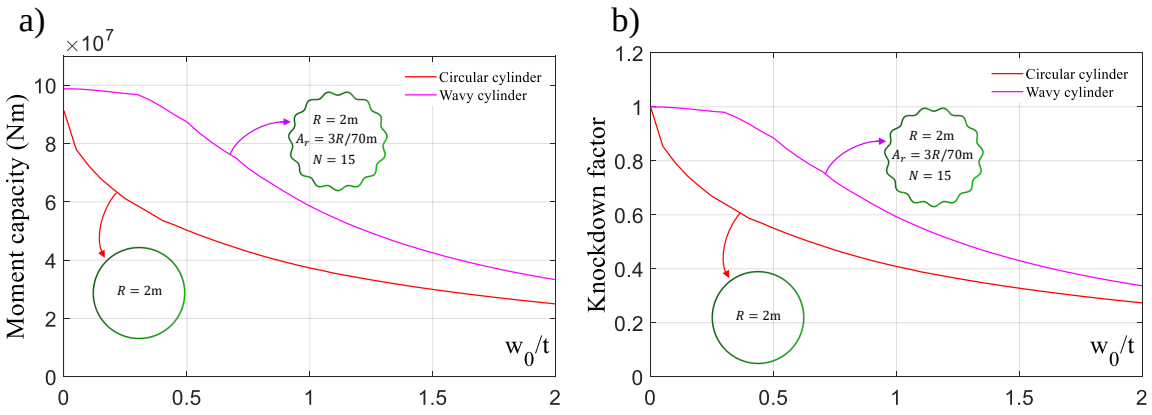

Figure 3.11: (a) Moment capacities of the circular and the wavy cylinders against the imperfection amplitude. (b) Knockdown factor for the circular and the wavy cylinders against the imperfection amplitude. The moment capacity and knockdown factor of the wavy cylinders are always more than the moment capacity and knockdown factor of circular cylinders. In case of wavy cylinders, the knockdown factor is almost 1 (insensitive to imperfections) for imperfection amplitude $w_o < 0.30t$.

imperfection amplitude. This result is quite encouraging as the loading scenario, material properties and the dimensions of the cylinder are different to the cylinders in the Section 3.2 and in the study of Ning and Pellegrino [67] showing constancy in the imperfection insensitivity.

In figure 3.11a, the moment capacity of imperfect circular and wavy cylinders is plotted against the normalized imperfection amplitude and in figure 3.11b, the knockdown factor is plotted against the normalized imperfection amplitude. For small imperfection amplitude ($w_0 < 0.3t$), the knockdown factor is almost unchanged for wavy cylinders, whereas, for circular cylinders, it is reducing rapidly with increase in imperfection amplitude. The reduction in case of circular cylinders is around 35% for $w_0 = 0.3t$, whereas, for wavy cylinder, it is almost negligible. For higher imperfection amplitude ($w_0 > 0.3t$), significant reduction is taking place for the wavy cylinders, but their knockdown factor is always higher than the knockdown factor of circular cylinders. Increasing the imperfection amplitude, the difference between knockdown

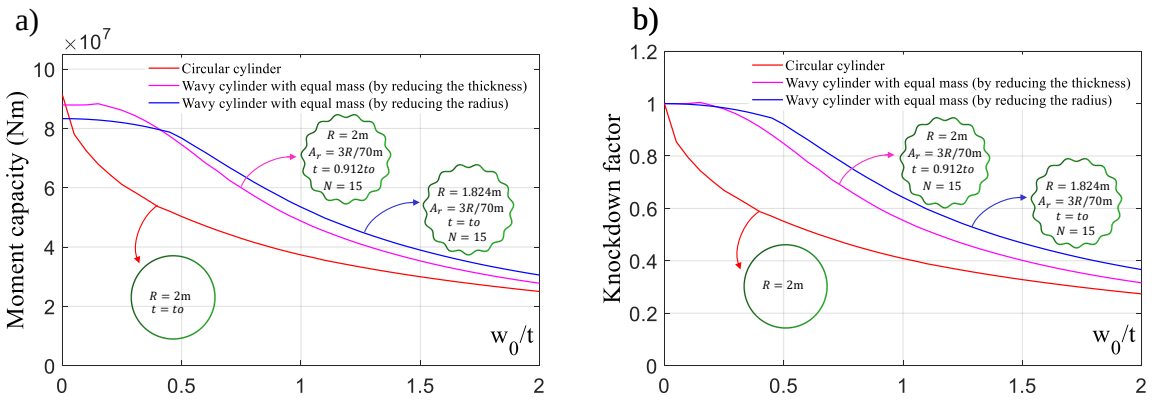

Figure 3.12: (a) Moment capacities and (b) knockdown factor of the circular and the two wavy cylinders. The material volume of the wavy cylinders is the same as the circular cylinder and is achieved by reducing the thickness for one case and by reducing the radius for the second case. The performance of wavy cylinders is still better than the circular cylinder.

factors for circular and wavy cylinders is reducing (figure 3.11b) and it is anticipated that for further increase in imperfection amplitude ($w_0 > 2t$), the difference will be diminished. A first conclusion from these results is that wavy cylindrical shells are the most beneficial for small imperfection amplitudes which could be the case of new advanced manufacturing process. For higher imperfection amplitudes, the usefulness of using wavy cylinders diminishes, but the imperfections rarely reach that limit for all practical applications. Apart from higher knockdown factor, the wavy cylinders also have higher moment capacities (figure 3.11a). This is happening because the moment inertia of the wavy cross-sections is higher than the moment of inertial of circular cross-sections and also due to the stiffening effect of waviness.

It could be argued that the wavy cylinders require more material than the circular cylinders and this could reduce the associated benefits, i.e., imperfection insensitivity. To investigate this issue, we reduce the material volume required in the wavy cylinders, which can be done in two ways: first by reducing the thickness and keeping the base radius constant, and second by reducing radius keeping the thickness constant.

Figure 3.12a and figure 3.12b shows the moment capacities and knockdown factors respectively of the circular cylinder, and the wavy cylinders whose material volume is the same as the circular cylinder. For perfect cylinders, the capacity of the circular cylinder is higher than the capacity of both wavy cylinders (figure 3.12a, moment corresponding to 0 imperfection amplitude). However, for all the cases of imperfect cylinders, the capacities of both wavy cylinders are higher than the circular cylinders. The knockdown factor of wavy cylinders, even after reducing its thickness or radius to make their volume equal to the circular cylinder, are much higher than the circular one. Therefore, wavy cylinders are still preferable because their imperfection insensitivity surpasses the burden of extra material requirement. An interesting result emerges from figure 3.12a: reducing thickness is a more beneficial choice than reducing the base radius for small imperfection amplitude, but for higher imperfection amplitude, reducing the base radius is preferable.

3.3.2 Effect of wave parameters on knockdown factors

In the previous section, a particular wavy cross-section with $A_r = 3R/70$m and $N = 15$ is used to demonstrate the benefits associated with wavy cylinders. To further explore the imperfection insensitivity of wavy cylinders, we created a total 25 wavy cross-sections. These 25 wavy cross-sections are created using five wave amplitudes and five numbers of waves. The values of A_r are $R/70$ ($1.7t$), $2R/70$ ($3.4t$), $3R/70$ ($5.1t$), $4R/70$ ($6.9t$), and $5R/70$ ($8.6t$); and the values of N are 3, 5, 15, 20 and 25. All 25 cross-sections of the wavy cylinders are shown in figure 3.13. For imperfections, we are imposing the biased axisymmetric imperfection as given by Eq. 20.

First, we will discuss the effect of wave amplitude. The knockdown factor for the five cylinders with $N = 15$ and varying A_r are plotted against the normalized imperfection amplitude in figure 3.14. The knockdown factors are increasing with

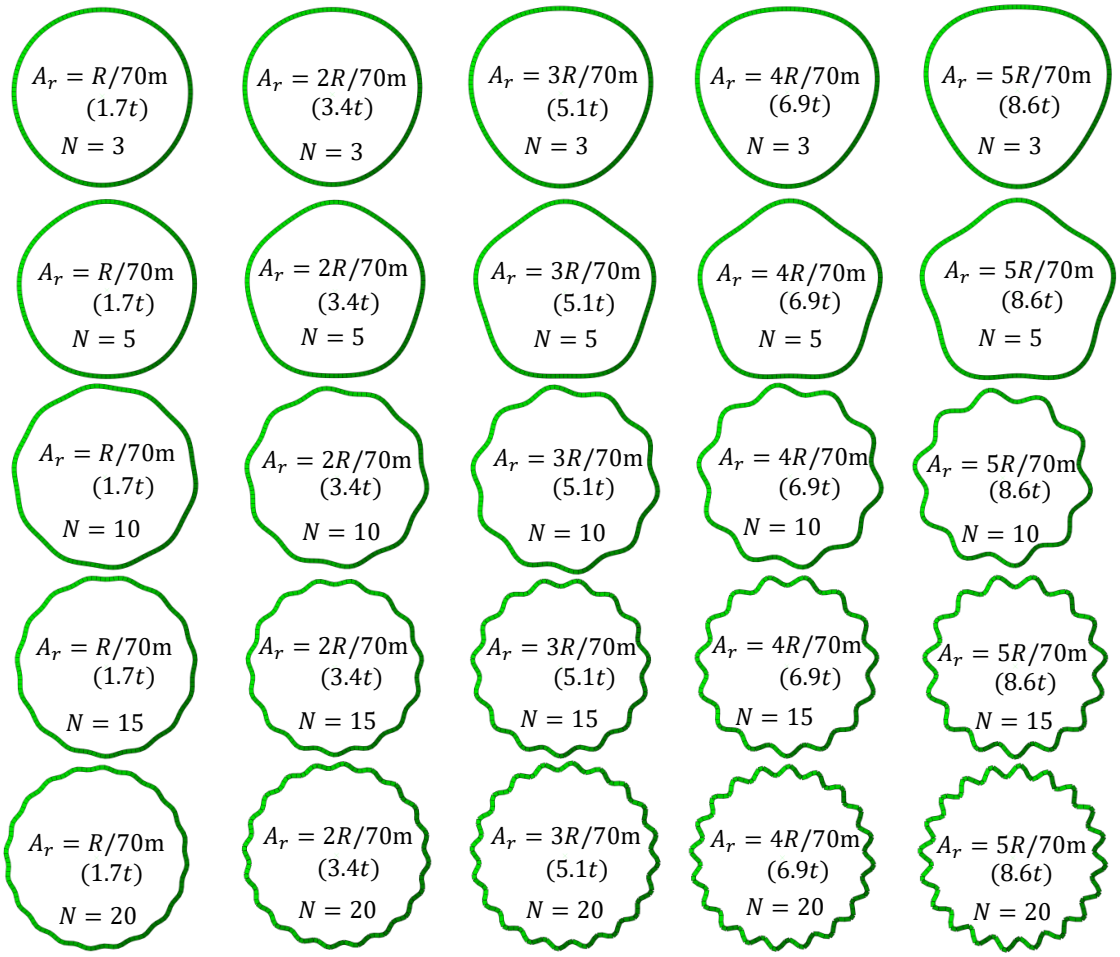

Figure 3.13: The cross-sections of wavy cylinders used in this study. In total five wave amplitudes $A_r = R/70\text{m}$ $(1.7t)$, $2R/70\text{m}$ $(3.4t)$, $3R/70\text{m}$ $(5.1t)$, $4R/70\text{m}$ $(6.9t)$, $5R/70\text{m}$ $(8.6t)$ and five numbers of waves $N = 3, 5, 15, 20, 25$ are used to create the wavy cylinders. The radius of base circle $R = 2\text{m}$ and the radius to thickness ratio $R/t = 120$ applies for all cylinders.

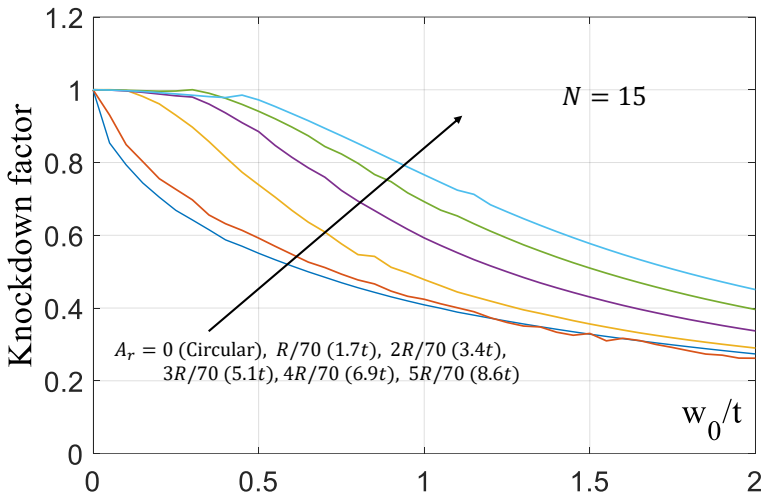

Figure 3.14: Knockdown factor for wavy cylinders with the varying wave amplitude of A_r. The number of waves N is constant and is 15. The effectiveness of wavy cylinder is increasing with the increase of A_r.

increase in wave amplitude A_r, i.e., for a given imperfection amplitude the value of knockdown factor is higher for the cylinder having higher wave amplitude. These trends suggest that higher wave amplitudes improve the performance of wavy cylinders; they become less and less sensitive to imperfections. The difference among knockdown factors is more pronounced for small imperfection amplitudes, while for higher imperfection amplitudes, the difference among knockdown factors is reducing. These results signify the benefits of using wavy cylinders. Similar patterns, the increment in knockdown factor with the increment in A_r, are observed for other the number of waves, e.g., $N = 3$, 5, 20 and 25. Figure 3.15 shows the effect of wave amplitude A_r on the knockdown factor for $N = 20$ and $N = 25$. From these results, it can be concluded that the performance (insensitivity to imperfections) of wavy cylinders improves with the increase in the wave amplitude A_r.

To show the effect of the number of waves N, we keep $A_r = 2R/70$ (3.4t) and vary N from 0 to 25. The knockdown factors for these six cylinders are plotted against the normalized imperfection amplitude in figure 3.16. The effectiveness of wavy cylinders

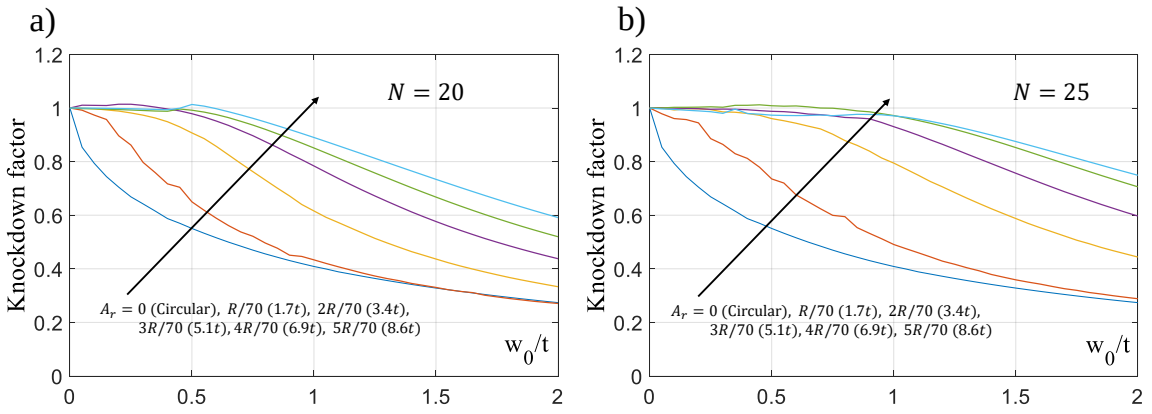

Figure 3.15: (a) Knockdown factor for wavy cylinder with $N = 20$. (b) Knockdown factor for wavy cylinder with $N = 25$. The effectiveness of wavy cylinder is increasing with the increase of A_r as in the case of $N = 15$.

improves with an increase in the number of waves N along the circumference, i.e., wavy cylinders become less and less sensitive to imperfection as N increases. The number of waves plays a significant role on the performance of wavy cylinders, e.g., the reduction in load carrying capacity is 4% for $N = 25$ and 44% for $N = 3$, for imperfection amplitude $0.5t$. A similar pattern is obtained for the other wave amplitudes as shown in figure 3.17 for $A_r = R/70$ $(1.7t)$ and $A_r = 5R/70$ $(8.6t)$. There is not much difference between the response of circular cylinder and wavy cylinder with $N = 3$. But, the difference between circular and wavy cylinders becomes visible with higher numbers of waves, i.e., $N = 5, 15, 20, 25$. There are three notable characteristics coming out of figure 3.16: 1) the higher number of waves means better performance of wavy cylinders, 2) the differences among knockdown factors are more pronounced for small imperfection amplitude and diminishes with increase in imperfection amplitude, and 3) for small imperfection amplitude ($w_0 < 0.4t$), the reduction in load carrying capacity is almost negligible for $N = 20$ and $N = 25$.

From the above parametric analysis, we have demonstrated that the wave parameters, A_r and N play a crucial role in the response of wavy cylinders to imperfections.

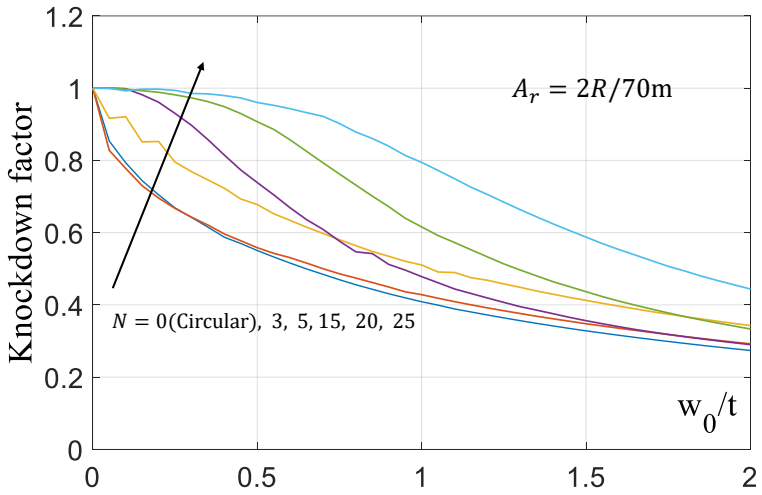

Figure 3.16: Knockdown factor for wavy cylinders with the varying number of waves N. The wave amplitude number A_r is constant and is $2R/70$m. The effectiveness of wavy cylinder is increasing with the increase of N.

Higher values of A_r and N lead to lower sensitivity to imperfections, with values of wave parameters that improve the knockdown factor substantially found around $A_r = 2R/70$ $(5.1t)$ and $N = 15$.

3.3.3 Effect of orientation of imperfections and waves

So far, the orientation of both the wave and the imperfection are concave at the meridian with maximum compressive stress at the middle of the cylinder under bending (case A of figure 3.18a and figure 3.18b) in anticipation that the maximum reduction in the moment capacity due to the imperfection will occur with this combination. But, the wave and the imperfection can have any orientation; figure 3.18 shows 3 orientations of both the wave and the imperfection (biased imperfection), which results in total 9 core combinations of the wave and the imperfection. We analyzed the effect of imperfections in these 9 combinations to investigate the importance of the orientation of the imperfection and the wave. The orientation is not an issue for axial compression as loading is symmetric but for bending, it might have some

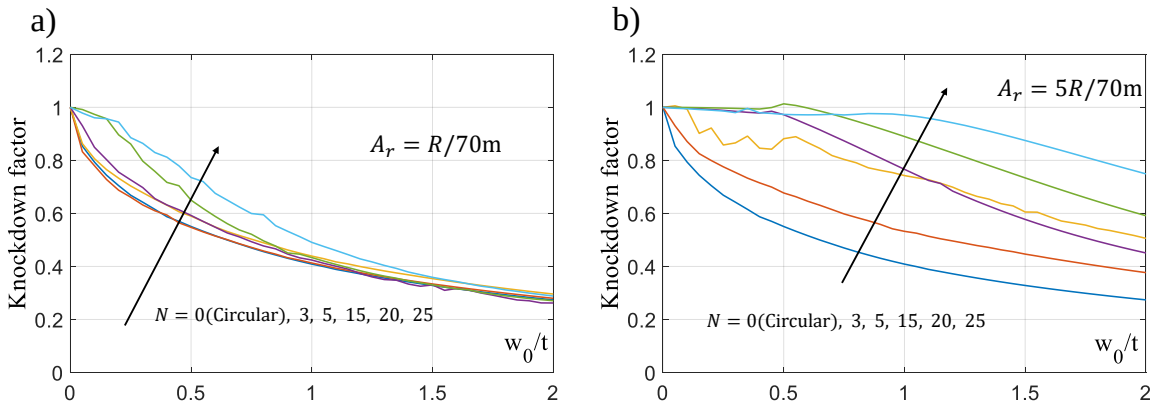

Figure 3.17: (a) Knockdown factor for wavy cylinder with $A_r = R/70$m. (b) Knockdown factor for wavy cylinder with $A_r = 5R/70$m. The effectiveness of wavy cylinder is increasing with the increase of N as in the case of $A_r = 2R/70$m.

effect as the bending is asymmetric by nature. We use the wavy cylinder with $A_r = 3R/70$ and $N = 15$ for this investigation. Figure 3.19 shows the knockdown factors for the 9 combinations of the wave and the imperfection. Surprisingly, the orientation of the wave and the imperfection does not affect the knockdown factor significantly, as the 9 curves in figure 3.19 are almost identical. This is significant, and shows that wavy cylinders are indifferent to the orientation of the imperfection. This property is not available with conventionally stiffened cylinders, where if the stiffeners are not located in the middle of the compressive side, they would not be as effective under bending.

3.3.4 Local dimple imperfections

In all the previous subsections for the cylinders under bending, we have applied the biased geometric imperfection (Eq. 20) as the most deleterious imperfection. To illustrate this, we use the dimple-like (Eq. 16) imperfection, and compare the response of wavy cylinders to these two imperfections: dimple-like, and biased imperfection. The dimple-like imperfection is introduced on the meridian with maximum compressive

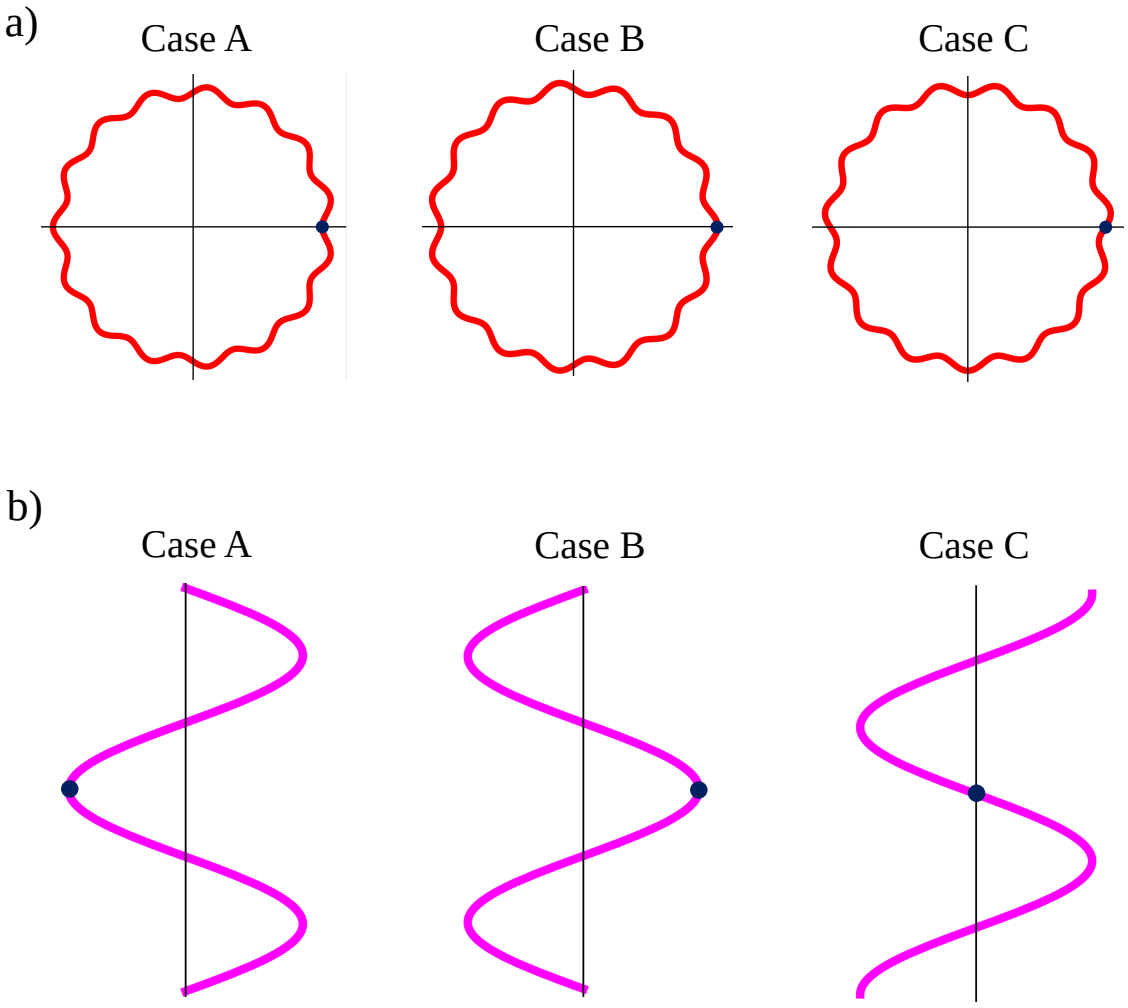

Figure 3.18: Three core possible orientation of the wave (a) and the imperfection (b) at the meridian with maximum compressive stress at the middle of the cylinder. In total nine possible combinations exist of the wave and the imperfection.

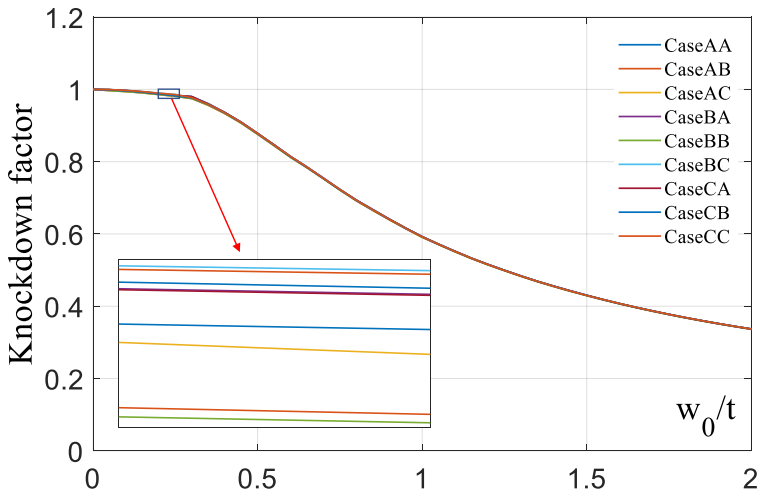

Figure 3.19: The effect of orientation of waves and imperfections on knockdown factor. Knockdown factor is unaffected by the orientation of waves and imperfections.

stress at the middle of the cylinder under bending. Figure 3.20, shows the knockdown factor of wavy cylinders corresponding to biased axisymmetric and local dimple-like imperfections. For small imperfection amplitude ($w_0 < 0.4t$), both imperfections reduce the moment capacities almost equally, but for higher imperfection amplitudes ($w_0 > 0.4t$) the reduction due to the biased imperfection is more than the dimple like imperfection and the difference between knockdown factor is increasing with imperfection amplitude. Wavy cylinders are therefore more effective when the imperfection is local in nature, which is a more realistic imperfection.

3.3.5 Mass efficiency and comparison with stiffened cylinders

Stiffeners are generally used to increase the load carrying capacity of thin cylindrical shells and to reduce their sensitivity to imperfections [66]. The wavy cylinders can also be assumed as a kind of stiffened cylinders. It is of interest to compare the imperfection sensitivity of conventionally stiffened cylinders and wavy cylinders. For this purpose, one circular, one wavy (with $A_r = 3R/70$ and $N = 15$) and four stiff-

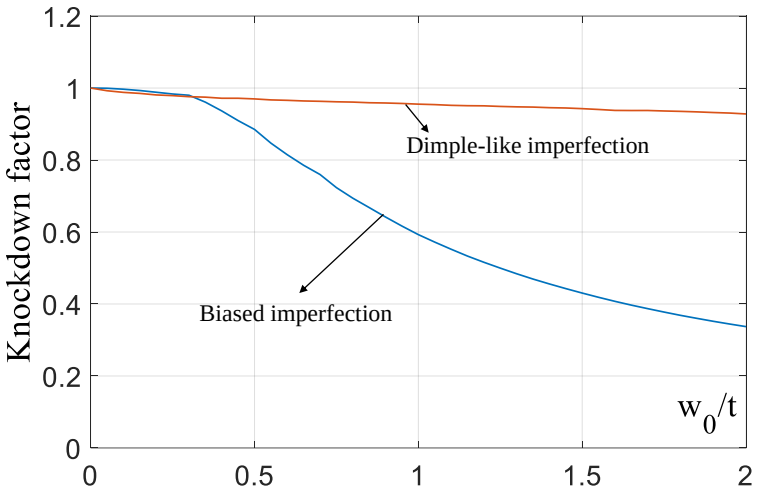

Figure 3.20: The effect of the local dimple-like imperfection on knockdown factor. For small imperfection amplitude ($w_o < 0.4t$) both the dimple-like and the biased axisymmetric imperfections reduce knockdown factor similarly but for higher imperfection amplitude, the biased axisymmetric imperfection is more catastrophic.

ened cylinders are created as shown in figure 3.21. 4 longitudinal stiffeners along the circumference are used for stiffened cylinders 1 and 2, and 16 longitudinal stiffeners along the circumference are used for stiffened cylinders 3 and 4. For stiffened cylinder 1, the width (circumferential direction) of stiffeners is $5t$ and the depth (radial direction) of stiffeners is $32t$, while for stiffened cylinder 2, the width of stiffeners is $5t$ and the depth of stiffeners is $72t$, where t is the thickness of cylinders. Similarly, for stiffened cylinder 3 the width of stiffeners is $5t$ and the depth of stiffeners is $2t$, while for stiffened cylinder 4, the width of stiffeners is $5t$ and the depth of stiffeners is $4t$. The volume of material required for the circular, wavy, stiffened 1, stiffened 2, stiffened 3 and stiffened 4 cylinders are V_0, $1.1V_0$, $1.2V_0$, $1.4V_0$, $1.2V_0$ and $1.4V_0$ respectively, where $V0$ represents the volume of the circular cylinder.

To study the effect of imperfections, we used the biased imperfection (Eq. 20). The moment capacities and knockdown factors of these six cylinders are shown in figure 3.22a and figure 3.22b respectively. Stiffeners not only increase the bending

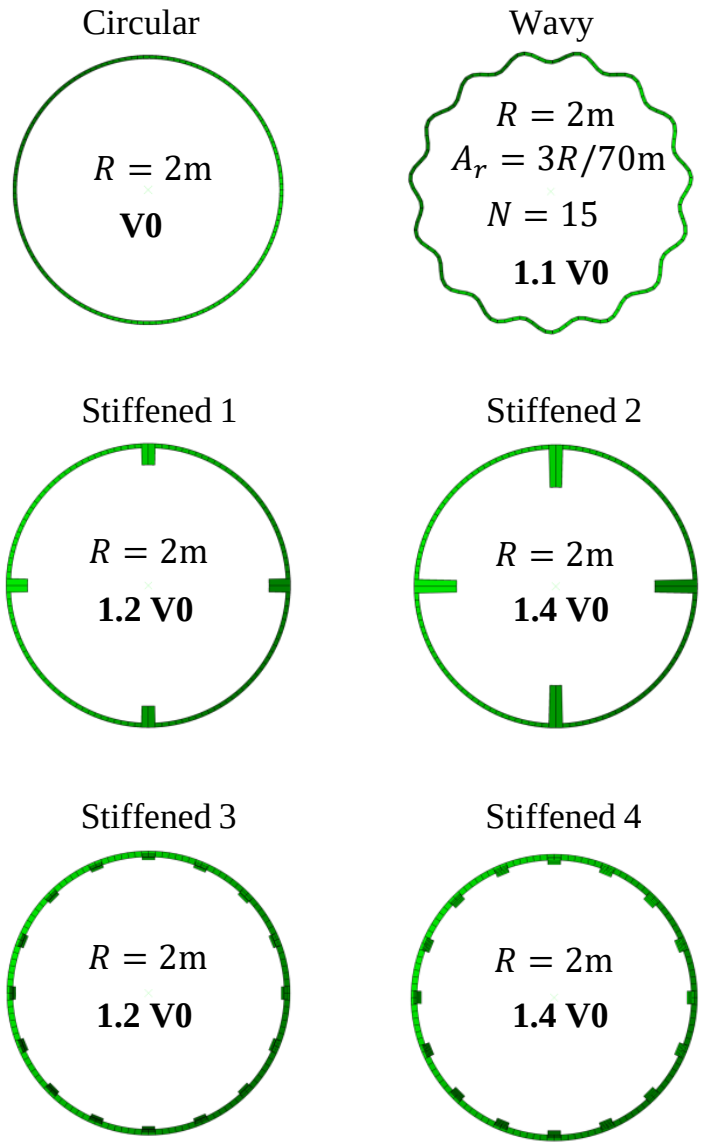

Figure 3.21: Circular, wavy and four stiffened cylinders along with their cross-section and material volume. The material volume of circular, wavy, stiffened 1, stiffened 2, stiffened 3 and stiffened 4 cylinders are V_0, $1.1V_0$, $1.2V_0$, $1.4V_0$, $1.2V_0$ and $1.4V_0$.

capacity of the circular cylinder, but also reduce the sensitivity of the circular cylinders to imperfections. When compared to wavy cylinders, the knockdown factors for the wavy cylinder are higher than the four stiffened cylinders for imperfection amplitude $w_o < 0.75t$. Although the capacity of the perfect stiffened cylinders is more than the perfect wavy cylinder, for imperfect cylinders, the capacity of the wavy cylinder is more than the stiffened cylinder 1 for $0.05t < w_o < 0.75t$ and more than stiffened cylinders 2 and 3 for $0.2t < w_o < 0.55t$. Stiffened cylinder 4 always has more capacity than the wavy cylinder. An important feature of the wavy cylinder is the imperfection insensitivity for imperfection amplitude for $w_o < 0.4t$ (i.e., knockdown factor is almost 1), when compared to all the alternatives in this analysis. This reduces the uncertainties associated with all practical (imperfect) cylinders which does not apply for the stiffened cylinders. In addition, the material required for the wavy cylinder is 10% more than the circular cylinder, while the material required for the stiffened 1, stiffened 2, stiffened 3 and stiffened 4 cylinders are 20%, 40%, 20% and 40% more than the circular cylinder, respectively. Wavy cylinders are not only performing better than the stiffened cylinders considered in this study, in terms of imperfection insensitivity for small imperfection amplitude ($w_o < 0.75t$), but are also more economical in terms of required material. An interesting finding is that the many small distributed stiffeners are more beneficial in terms of bending capacity (figure 3.22a) but are not very effective in terms of imperfection sensitivity (figure 3.22b).

In addition, it is expected that the wavy cylinders will perform better than the stiffened cylinders if the imperfections are local in geometry—dimple-like imperfection (Eq. 16). Dimple-like imperfections could be located anywhere in the shell. Consequently, stiffeners will be ineffective to reduce imperfection sensitivity if dimple-like imperfections are located away from the stiffeners. This is not the case with wavy cylinders as waviness is present across the circumference. In other words, waviness

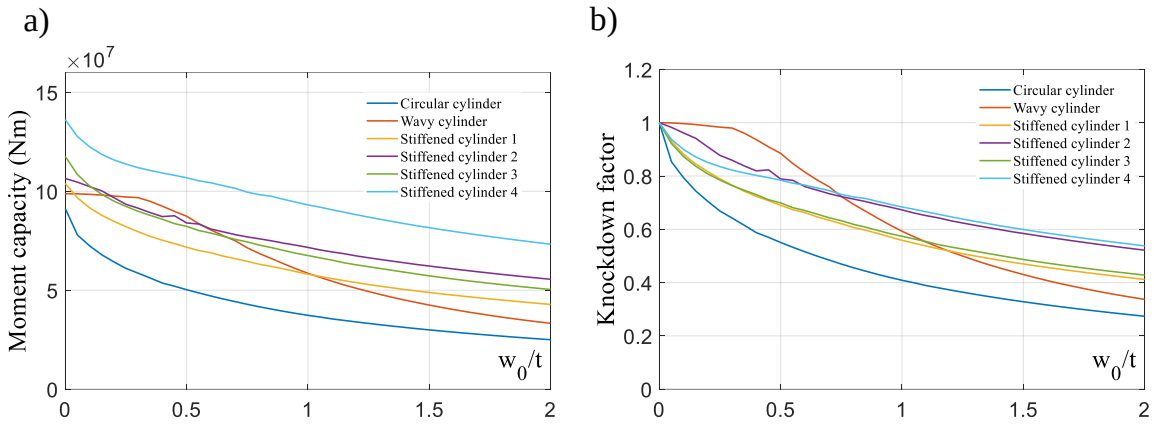

Figure 3.22: (a) Moment capacity and (b) knockdown factor of circular, wavy and four stiffened cylinders against the imperfection amplitude. Biased axisymmetric imperfection is used to create the imperfect cylinders for all the cases. The wavy cylinder is the least imperfection sensitive for $w_o < 0.75t$.

acts as a stiffener but distributed uniformly across the circumference.

3.4 Discussion

Many factors are responsible for making wavy cylinders insensitive to imperfections: 1) reduction in effective radius of curvature [66], 2) stiffness introduced by waviness, and 3) periodic change in the direction of curvature that creates disharmony with imperfection and consequently, reducing the impact of imperfections. These factors are engaged simultaneously to achieve the imperfection insensitivity. We did not delve further in evaluating separate contributions of these three factors, but instead we studied the effectiveness of wavy cylinders under bending—an important loading scenario for many applications of thin cylinders, considering inelastic behavior.

For the wavy cylinders under bending, we found that wavy cylindrical shells are insensitive to the imperfections and the presence of imperfections does not reduce the load carrying capacity significantly. Previous studies [66, 67] have revealed similar conclusions for thin cylindrical shells under axial compression. Based on the compar-

isons between the knockdown factors of the wavy cylinders and the circular cylinders we report that for small amplitudes of imperfection ($w_o < 0.3t$) the reduction in bending capacities is high for the circular cylinders compared to the insignificant reduction for the wavy cylinders. Apart from this, we also found that the bending capacities of wavy cylinders are higher than the bending capacities of the circular cylinders. The wave parameters, i.e., the wave amplitude A_r and the number of waves N, play a crucial role to impact the knockdown factor. The effectiveness of the wavy cylinders increases as the number of waves and the wave amplitude increase. For the higher wave amplitudes and higher number of waves, wavy cylinders are less sensitive to imperfections, and their bending capacities are high. Further, this study reveals that wavy cylinders perform better than the stiffened cylinders in terms of imperfection sensitivity and the volume of the material required.

These results are very promising as the imperfection sensitivity of thin cylindrical shells has been a big obstacle for their economic applications for a long time. This study shows that if wavy cross-sectional cylindrical shells are used, the inherent drawback (high imperfection sensitivity) of thin circular cylindrical shells can be circumvented and material can be used optimally.

CHAPTER 4

IMPERFECTION INSENSITIVE THIN CYLINDRICL SHELLS FOR NEXT GENERATION WIND TURBINE TOWERS

This chapter proposes wavy wind turbine towers to avoid the imperfection sensitivity of conventional wind turbine towers. Wavy wind turbine towers are made by wavy cross-sectional thin tapered cylinders. The waviness of the cross-section reduces the slenderness (R/t) of the towers significantly; consequently, the sensitivity of the towers to imperfections is reduced drastically. Besides, the waviness of the cross-sections works as stiffeners, which further results in the reduction of imperfection sensitivity. In this chapter, the sensitivity of the proposed wavy wind turbine towers to imperfections is assessed, and it is found that the sensitivity of the wavy towers is exceptionally small compared to that of the circular towers.

4.1 The geometry of thin tapered wavy cylinders, their finite element modeling, and the effect of imperfections

Yadav and Gerasimidis [2, 68] have shown that thin straight wavy cylinders (i.e., the radius of the cylinders is constant along the length) under bending are insensitive to imperfections. However, no attempt has been made to understand the imperfection sensitivity of tapered wavy cylinders—an important variation of thin cylinders whose radius is varied linearly along the length. In this section, this area is explored by computationally studying the geometry. Firstly, the geometry is described for wavy straight and wavy tapered cylinders; and then, their finite element modeling

is explained. Finally, the effect of imperfections on the wavy straight and wavy tapered cylinders is presented and compared with that of circular straight and circular tapered cylinders.

4.1.1 The geometry of wavy tapered cylinders

There are many ways to create a wavy cross-section of a cylinder; for this study, a simple method is chosen in which sinusoidal waves are superimposed on the circular cross-section with a specific wavelength and amplitude. Figure 3.1 shows the circular and wavy cross-sections along with their analytical equations. To create the wavy cross-section, a sine wave with amplitude A_r and the number of waves N is superimposed on the circumference of the circular (called base circle [66]) cross-section whose radius is R. Three parameters are needed to fully characterize this wavy cross-section: the radius of the base circle R, the wave amplitude A_r and the number of waves N. The analytical equation of the wavy cross-section is [66]:

$$r(\theta) = R + A_r \sin(N\theta) \tag{21}$$

Where θ is the angle from the x axis.

For straight wavy cylinders, the radius of the base circle R is constant, while for tapered wavy cylinders, the radius of the base circle R is varying linearly along the length. Figure 4.1 shows two wavy and two cylinders: figure 4.1(a) straight circular, figure 4.1(b) straight wavy, figure 4.1(c) tapered circular, and figure 4.1(d) tapered wavy cylinders.

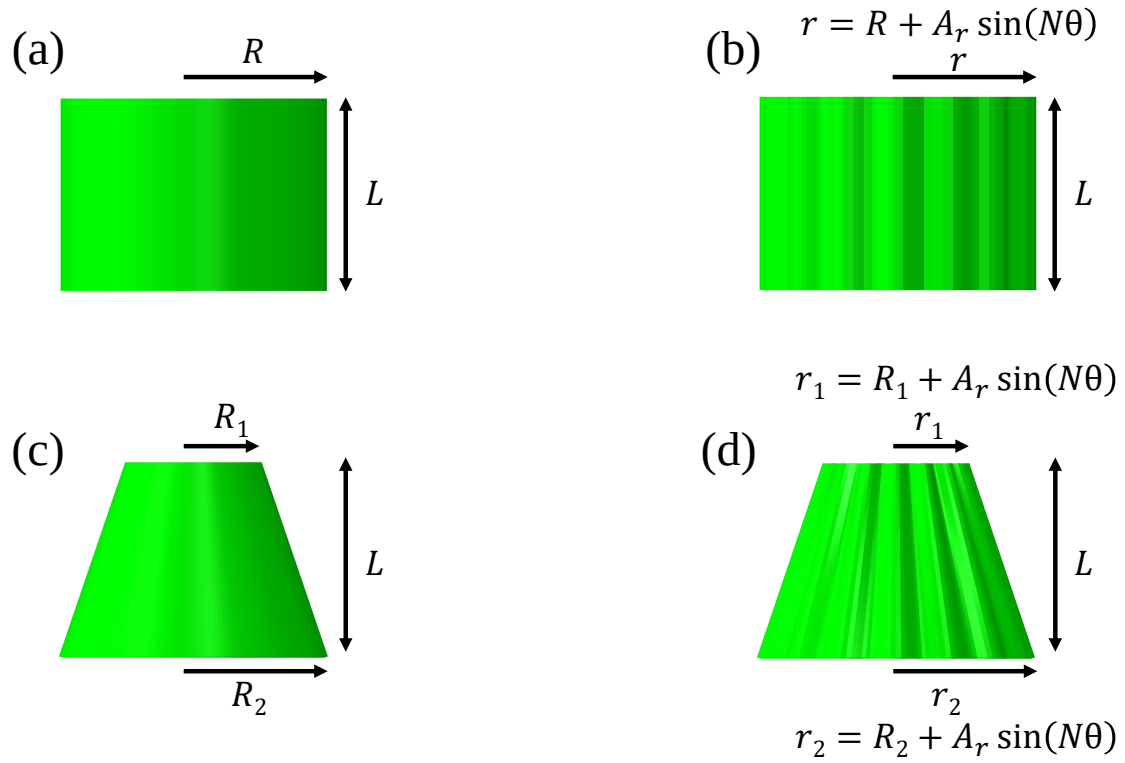

Figure 4.1: The straight circular (a), straight wavy (b), tapered circular (c), and tapered wavy (e) cylinders.

4.1.2 Dimensions of the cylinders

To investigate the effect of imperfections on the tapered wavy cylinders, first, a circular tapered cylinder is selected; this cylinder is used in the 61 m NORDEXS70/1500 wind turbine tower of 1.5 MW [77]. The dimensions of the tapered wavy cylinder are given in table 5.1. R_2 and R_1 are the radii (the radius) of the cross-sections at the two ends of the tapered cylinder, and L is the length of the cylinders. The difference between R_1 and R_2 is very small. This is typical dimensions of a tapered cylinder used in wind turbine towers; they usually have very small tapering. Next, this circular tapered cylinder is modified using equation21 to create a tapered wavy cylinder. The value of R in equation21 is varying linearly from R_1 to R_2 along the length, and the wave parameters A_r and N are $3R_2/70$ and 15 respectively following Yadav and

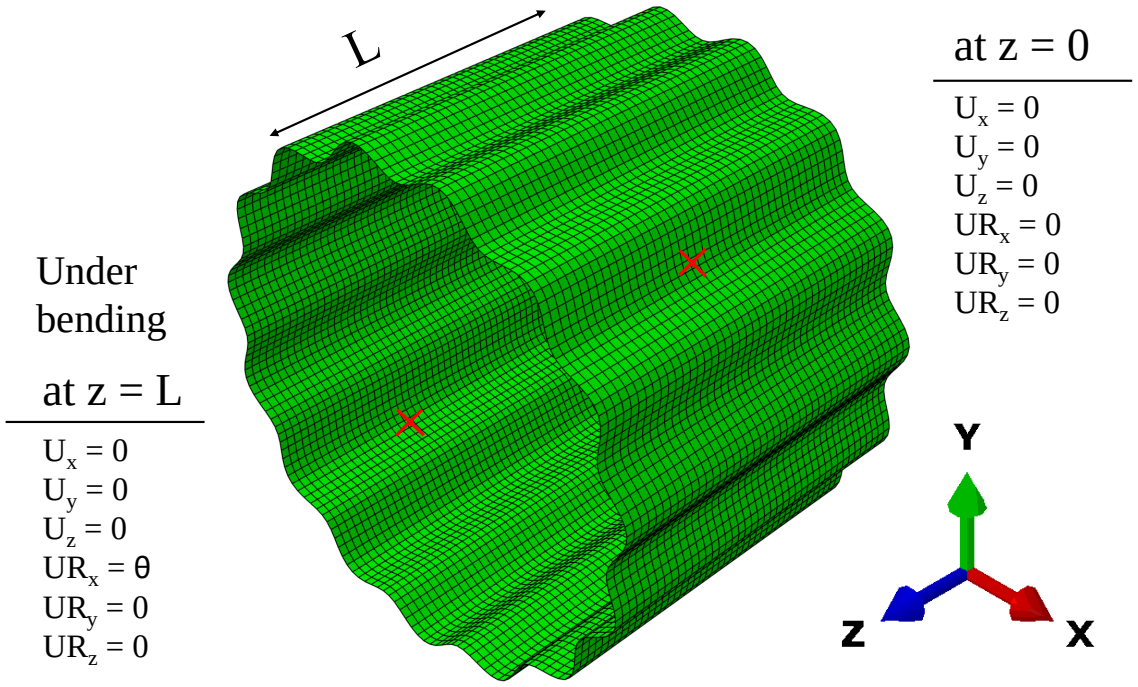

Figure 4.2: Boundary conditions of the model. One end of the cylinder is fixed ($Z = 0$) while the rotation is applied at the other end ($Z = L$).

Gerasimidis [2, 68]. For the sake of completeness, a straight circular, and a straight wavy cylinders are also created by keeping the radius R constant and equal to R_2.

font=12pt

Table 4.1: Dimensions of the cylinders

$L(mm)$	$R_1(mm)$	$R_2(mm)$	$t(mm)$	$A_r(mm)$	N
2940.0000	2000.5714	2000.6427	13.0000	$3R_2/70(85.7418)$	15

4.1.3 Finite element modeling

All the analyses are performed in the commercial FEA package ABAQUS [80] using the arc-length based Riks method [91]. For the meshing, four-node reduced integration shell ($S4R$) elements are used with an element size $74.81mm \times 68.37mm$ in the circumferential and the axial directions respectively. This element size is quite smaller

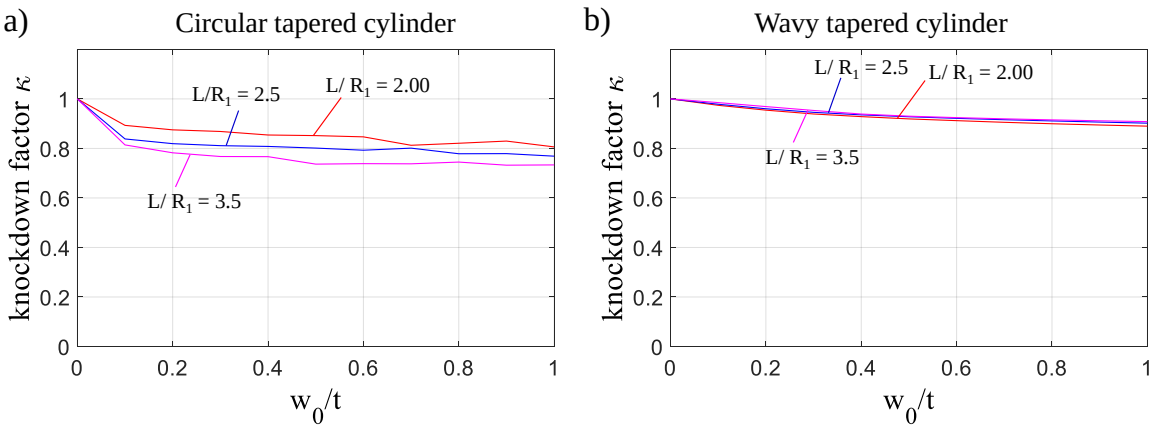

Figure 4.3: Knockdown factor κ for the circular (a) and wavy (b) cylinders for three L/R_1 ratios. L is the length and R_1 is base radius of the top cross-section of the cylinders. For the circular tapered cylinders, κ is reducing as L/R_1 is increasing, whereas for the wavy tapered cylinders, κ is almost independent of L/R_1 ratio. This means that the wavy cylinders are highly beneficial even for higher imperfection amplitude for high L/R_1 ratio.

the classical axisymmetric buckle half-wavelength (i.e., $2.44\sqrt{R_1 t} \approx 345.11mm$) for cylindrical shells under axial compression [79], and thus the discretization is considered adequate. Four integration points were utilized along with the thickness of each element. Figure 4.2 demonstrates a representative finite element model of the wavy tapered cylinders. Two nodes, called center nodes, are defined at the center of the end cross-sections of the cylinder. Rigid links are created to connect the edge nodes at the ends of the cylinder to their respective center nodes. These connections constrain the displacements U_x, U_y, and U_z, and rotations UR_x, UR_y, and UR_z of the edge nodes from moving and rotating with respect to the center nodes. Using these constraints one end of the cylinder is clamped by fixing the central node at $z = 0$. At the other end ($z = L$), a clamped boundary condition is enforced, but the end of the cylinder is loaded by applying a rotational displacement $UR_x = \theta$.

The material properties of the cylinders are given in table 4.2 following Yadav and Gerasimidis [1, 2]. Wind turbine towers are often made by steel, and these values are

commonly used in tall and super tall wind turbine towers [1, 55], and and steel tubes [17, 53]. For the stress-strain relationship, a version of Ramberg-Osgood stress-strain relationship is employed [1, 2, 50, 78] that is represented by equation 22. This model is chosen because Ramberg-Osgood is the most commonly used relationship to represent structural metal stress-strain responses [50, 78]. Moreover, a nonlinear stress-strain response is generally required for the numerical analyses as Eurocode [15] recommends GMNIA (Geometric and Material Nonlinear Analysis with Imperfections) for the strength assessment based on nonlinear shell finite element models.
font=12pt

Table 4.2: Material properties of the cylinders

$E\ (Gpa)$	$\sigma_y\ (Mpa)$	ν	n
210	355	0.30	9

$$\epsilon = \frac{\sigma}{E}\Big[1 + \frac{3}{7}\big(\frac{\sigma}{\sigma_y}\big)^{n-1}\Big] \tag{22}$$

4.1.4 Effect of imperfections

The first eigen modes of the cylinders under bending are utilized to create the imperfect cylinders by following three steps: a) the first eigen mode is found out, b) it is scaled with a specific factor (imperfection amplitude), and c) the scaled eigen mode is superimposed on the perfect cylinders. These three steps are applied on all the four cylinders: 1) straight circular, 2) tapered circular, 3) straight wavy, and 4) tapered wavy cylinders. Three different imperfection amplitudes (scaling factor), $0.1t$, $0.5t$ and $1.0t$, are considered in this section; t is the thickness of the cylinders. These values are quite realistic as imperfection amplitudes are rarely more than the thickness of the cylinders. $0.1t$ imperfection amplitude represents the class A (Excellent quality), and $0.5t$ imperfection amplitude represents the class B (High quality) of Eurocode

[15]. $1.0t$ imperfection amplitude does not represent the class C (Normal quality, i.e., less than $0.91t$) of the code, but this value is chosen to observe the effect of higher imperfection amplitude on the strength of the cylinders.

The reductions in the bending capacities, due to the presence of the eigen mode imperfections, are given in Table 4.3 in terms of knockdown factor κ, which is defined as the ratio of the imperfect capacity to the perfect capacity. The knockdown factor κ for the straight circular cylinder is less than the κ for the straight wavy cylinder: the values of κ are 0.88 and 0.96 for the straight circular and the straight wavy cylinders respectively, for the imperfection amplitude $w_0 = 0.1t$. For the imperfection amplitude $w_0 = 1.0t$, the values of κ are 0.84 and 0.86 for the circular and wavy cylinders respectively—again the reduction in the wavy cylinder is less than that of the circular. A similar pattern is observed for the imperfection amplitude $w_0 = 0.5t$. The tapered wavy cylinder performs better against imperfections than the tapered circular cylinder for all the considered imperfection amplitudes. For the imperfection amplitude $w_0 = 0.1t$, the values of κ are 0.88 and 0.96 for the tapered circular and tapered wavy cylinders.

The benefit of using wavy cylinders, both straight and tapered, is more pronounced for small imperfection amplitude. As an illustration, for the imperfection amplitude $w_0 = 0.1t$, the reductions are 12% for both straight and tapered circular cylinders, while the reductions are just 4% for both straight and tapered wavy cylinders—a significant gain of 8% if wavy cylinders are used. In comparison, for the imperfection amplitude $w_0 = 1.0t$, the reductions are 16% and 15% for straight and tapered circular cylinders respectively, while the reductions are 14% for both straight and tapered wavy cylinders— a marginal gain around 2% if wavy cylinders are used.

However, it should be noted that the length to radius ratio of the cylinders is very small, and thus the rigidity of the end is affecting the imperfection sensitivity.

This is the reason that for larger imperfection amplitudes the benefit of the wavy tapered cylinder is marginal. For practical applications, the length to radius ratios are much higher, and the benefit of the wavy tapered cylinder will be significant even for higher imperfection amplitude. To explore this issue, three tapered circular and tapered wavy cylinders with length to radius L/R_1 ratios 2.00, 2.5, and 3.5 are used. The tapering (i.e., $(R_2 - R_1) \div L$) for these cylinders are kept same as for the cylinders of Table 5.1; this is achieved by keeping R_1 constant ($2000.5714mm$) and varying R_2. The knockdown factor κ of these cylinders is shown in figure 4.3. For the circular tapered cylinders, κ is reducing as L/R_1 is increasing, whereas for the wavy tapered cylinders, κ is almost independent of L/R_1 ratio. This means that the wavy cylinders are highly beneficial even for higher imperfection amplitude for high L/R_1 ratios.

To verify our numerical analysis and the key findings, i.e., the insensitivity of wavy cylinders to imperfections, the results of the tapered wavy cylinder are compared with the findings of Ning and Pellegrino [66] and Yadav and Gerasimidis [2] in table 4.4. In both these studies, wavy cylinders are used with $N = 15$, and $A_r = 3R/70$. For the imperfection amplitude $w_0 = t$, the knockdown factors are 0.86, 0.79, and 0.59 for the current study, Ref. [66], and Ref. [2] respectively. The difference between the current study and Ref. [66] is attributed to the loading scenario as the cylinder is under the axial compression in Ref. [66] while in the current study, the loading is bending. The small difference in the values, moreover, is further validation of this technique as the knockdown factors are similar between bending and axial compression for this range of R/t. The difference between the current study and Ref. [2] is due to the shape of imperfections and the L/R ratio. A sinusoidal biased imperfection is used in Ref. [2] while eigen mode imperfection is used in the current study, and the value of the L/R ratio is 10 in Ref. [2], while its value is 1.47 in the current study. For the

validation purpose, an analysis is done on the tapered cylinder having $L/R = 10$, and sinusoidal biased imperfection. It is found that the knockdown factor is 0.58; quite close to the 0.59 the finding of Ref. [2]. More importantly, a clear pattern emerged from the current, and both referred studies that are wavy cylinders are less sensitive to imperfection compared to the circular cylinders.

These results show that not only straight wavy cylinders under bending are insensitive to imperfections as found by Yadav and Gerasimidis [1], but also tapered wavy cylinders are insensitive to imperfections especially when the imperfection amplitudes are small.

The behavior of individual tapered wavy cylinders under bending, i.e., less sensitivity to imperfections, might not propagate to a system, e.g., wind turbine towers and gas pipelines which are made of several tapered cylinders. And thus, the findings of this section cannot be extrapolated for a system made of several tapered cylindrical shells. A thorough investigation at the system level is needed. Firstly, the next section describes a wind turbine tower made by tapered circular cylinders (circular tower) and a wavy wind turbine tower made by modifying the circular tower to a wavy tower. Subsequently, the effect of imperfections on these towers will be presented and compared.

font=12pt

Table 4.3: The reduction in the bending capacity of the cylinders due to first eigen mode geometric imperfection with varying imperfection amplitude (w_0)

Case	$w_0 = 0.1t$	$w_0 = 0.5t$	$w_0 = 1.0t$
Straight circular cylinder	0.88	0.84	0.84
Straight wavy cylinder	0.96	0.89	0.86
Tapered circular cylinder	0.88	0.86	0.85
Tapered wavy cylinder	0.96	0.89	0.86

font=12pt

Table 4.4: The knockdown factors comparison of straight wavy cylinders from current analysis to the results of Ref. [66] and Ref. [2]

Current study	Result of Ref. [66]	Result of Ref. [2]
0.86	0.79	0.59

4.2 The geometry and finite element modeling of the circular and the wavy wind turbine towers

To demonstrate the benefits of using wavy tapered cylinders at a system level, a 61 m NORDEX S70/1500 wind turbine tower of 1.5 MW capacity is consider, this tower is used in the past studies Sadowski et al. [77]. This tower is used because the required data are publicly available[77]; any other wind turbine tower made of tapered circular cylinders can also be utilized for this purpose. Firstly, this section describes the geometry of the circular and the wavy towers; subsequently, elaborates finite element modeling of the towers.

4.2.1 The geometry of the circular tower

The circular wind turbine tower that is used by Sadowski et al. [77] is reproduced in figure 4.4. The height of the tower is 61 m, and it is made by joining 22 thin tapered (conic) circular cylinders. Three stiffeners, two at the middle and one at the top, are applied in the form of solid rings; the stiffeners are shown by F and T in figure 4.4. The length L, the outer diameter d_o, and the thickness t of the two middle stiffeners F are 220 mm, 4012 mm and 133.5 mm respectively. While the length L, the outer diameter d_0, and the thickness t of the top stiffener T are 80 mm, 2955 mm and 96.5 mm respectively. The first middle stiffener F is placed between the fourth

and the fifth cylinders and the second middle stiffener F is placed between the twelfth

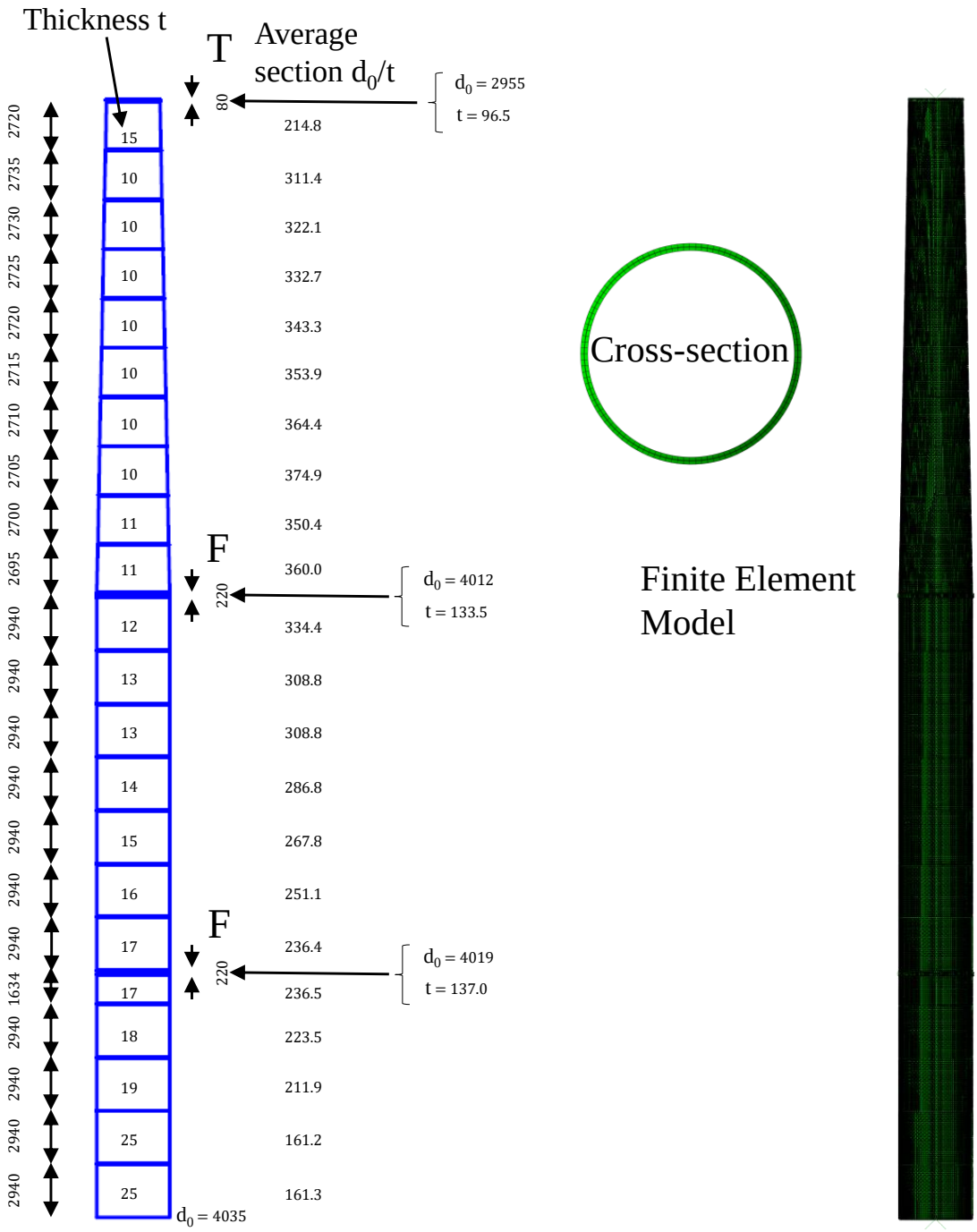

Figure 4.4: Schematic of a 61 m NORDEX *S*70/1500 wind turbine tower of 1.5 MW capacity; adopted from Sadowski et al. [77]. The dimensions of the tower are in mm.

and the thirteenth cylinders. The top stiffener T is located at the top to support the turbine. The thickness t of the cylinders is shown in the middle of the tower in figure 4.4; their values are increasing from 25 mm for the bottom cylinder to 10 mm for the second top cylinder. The thickness of the top cylinder is 15 mm, which is higher than the second top cylinder as it is supporting the turbine. The length of each of the cylinders are shown at the left of the tower in figure 4.4; the length varies from a maximum of 2940 mm to a minimum of 2695 mm. The ratio of the average outer diameter d_{ave} to the thickness of t of cylinders is shown at the right of the tower in figure 4.4; the ratio d_{ave}/t varies from a maximum of 161.2 mm near the bottom to a minimum of 374.9 mm near the top. In the actual tower, there is a door opening at the bottom [77], but that is not considered in this study to simplify the analyses.

4.2.2 The geometry of the wavy tower

To create a wavy wind turbine tower that is made by wavy tapered cylinders, the circular tapered tower is modified. The cross-sections of all the 22 tapered cylinders along with the 3 stiffeners of the circular tower are altered from circular to wavy using equation 21. The values of wave parameters N and A_r of equation 21 are taken as 15 and $3R_{min}/70$ respectively, where R_{min} is the minimum radius among all the cylinders of the circular tower. The values of A_r and N are constant for all the cylinders and the stiffeners; this maintains the continuity of the cross-sections along with the height of the tower. these values are chosen because they were used in the past studies [2, 68], and were found that they reduce the imperfection sensitivity substantially. All the other parameters, i.e., thickness t, length, and d_{ave}/t ratio, are the same as that of the circular tower. Although the wavy tower requires more material because of the waviness of the circumference. Figure 4.5 shows the wavy tower along with the values of the parameters, and d_0 represents the outer diameter of the base circle of the wavy

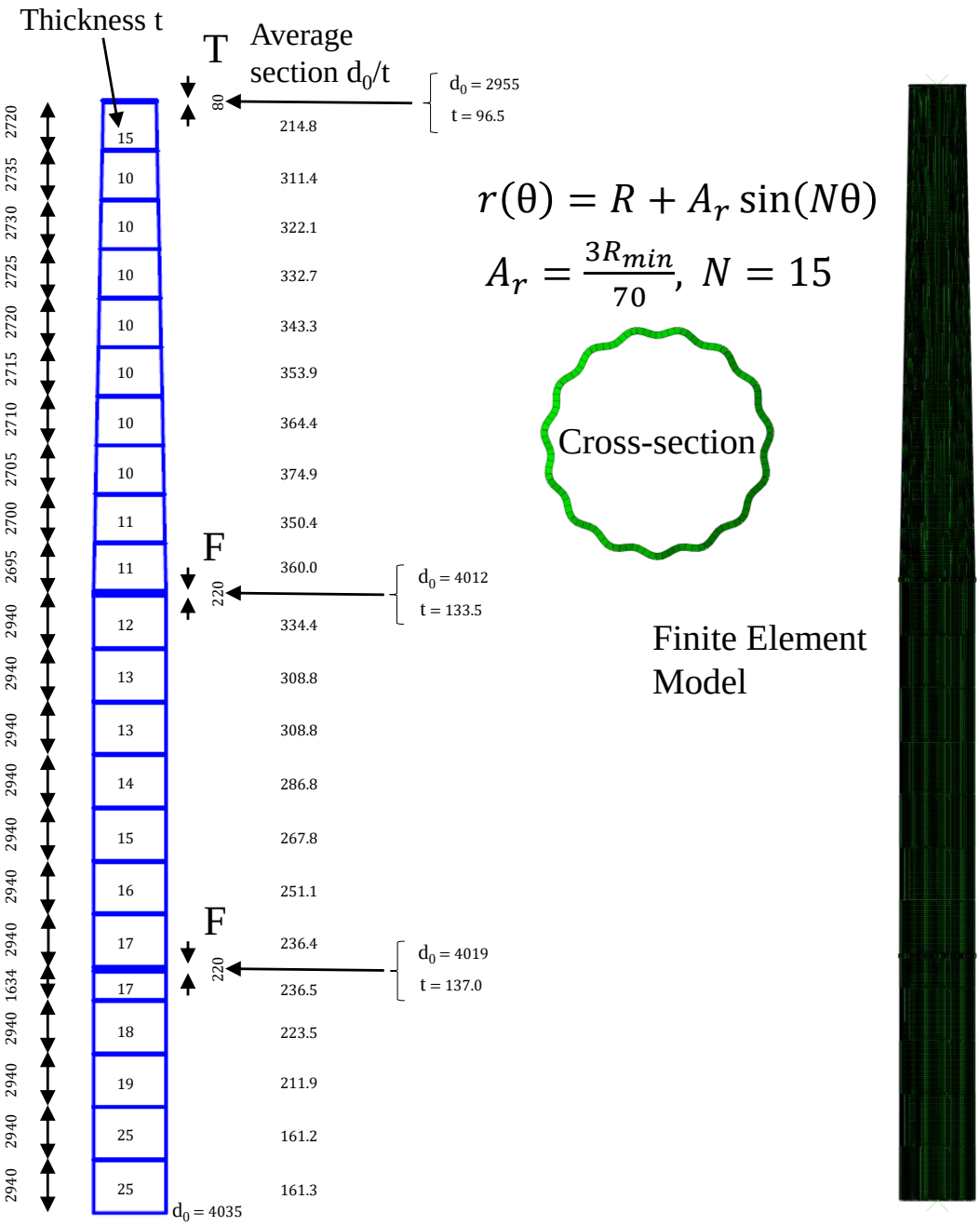

Figure 4.5: Schematic of the wavy wind turbine tower made by modifying the NORDEX $S70/1500$ circular tower. The dimensions of the tower are in mm.

cylinders.

4.2.3 Finite element modeling

To investigate the effect of imperfections on the circular and the wavy towers, all the analyses are performed in ABAQUS [80]. The arch-length based Riks method [91] is applied for GMNIA (Geometric and Material Nonlinear Analysis with Imperfections) to assess the bending strength of the towers using $S4R$ elements that have four integration points along with the thickness (similar to the finite element modeling in section 2). 20000 $S4R$ elements are utilized after the mesh convergence analyses of both circular and wavy towers. The mesh convergence analyses have been performed for the bending capacities of the towers (both perfect and imperfect) using GMNIA method. The FEM models of the circular and the wavy towers are shown at the right side of figure 4.4 and figure 4.5 respectively along with the cross-sections. Similar to section 2, two nodes (center nodes) are defined at the center of the top and the bottom of the towers and rigid links are created to connect the center nodes with the top and bottom edge nodes of the towers. These rigid links constrain the displacements U_x, U_y, and U_z, and rotations UR_x, UR_y, and UR_z of the edge nodes at the top and the bottom from moving and rotating with respect to the center nodes. Using the constraints, the bottom of the towers is clamped by fixing the central nodes of the towers at the bottom. At the top of the towers, a clamped boundary condition is enforced, but the top of the towers is loaded by applying a rotational displacement of $UR_x = \theta$ on the center nodes. The material properties of the towers are given in table 4.2. For the stress-strain relationship, a version of the Ramberg-Osgood stress-strain relationship as shown in equation 2 is employed [1].

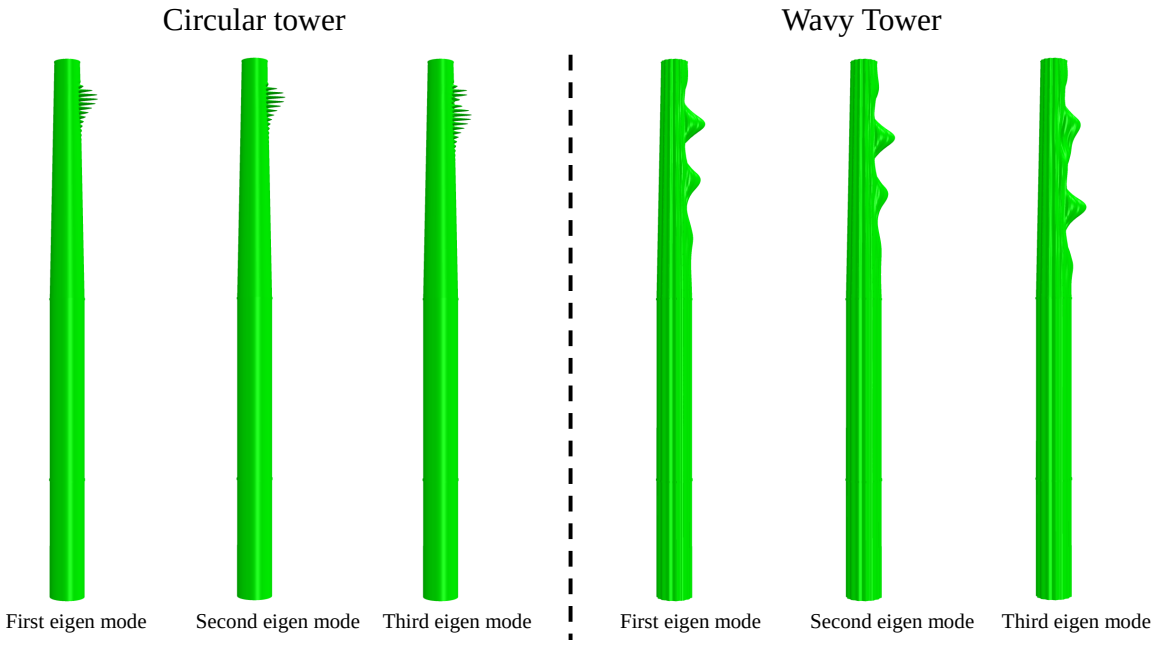

Figure 4.6: First three eigen modes of the circular and wavy towers.

4.3 The effect of imperfections on the bending capacities of the wind turbine towers

Wind turbine towers are primarily subjected to bending [1, 18, 54–57], and thus only bending load is considered to investigate the effect of imperfections. Firstly, the individual eigen modes of the tower is considered (under bending) as the shape of imperfection, for they are expected to significantly reduce the load-carrying capacities; secondly, a dimple-like imperfection is considered as the shape of imperfection, for it is more realistic.

4.3.1 The effect of individual eigen mode shape imperfections

The first three eigen modes of the circular and the wavy towers are induced—with specific imperfection amplitude w_0—in the respective perfect towers to create imperfect towers. The first three eigen modes of the circular and wavy towers are

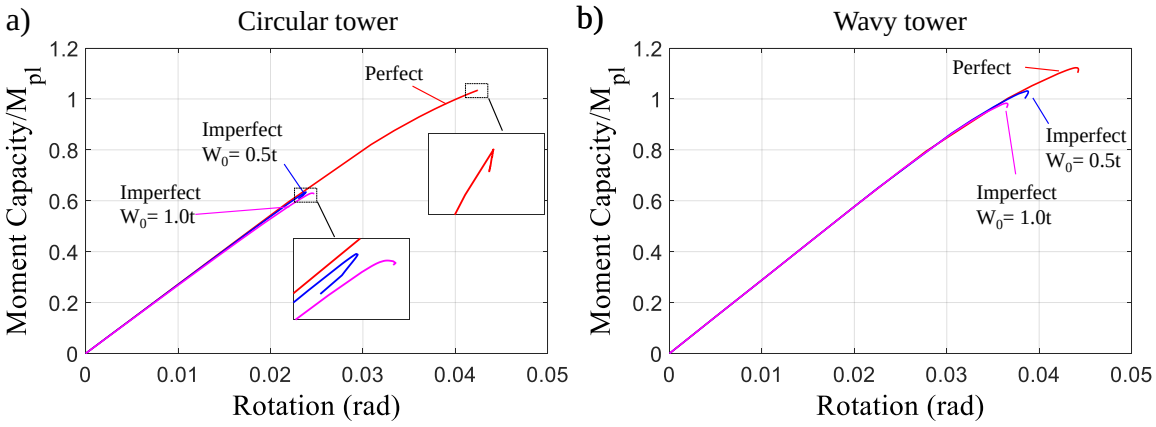

Figure 4.7: The moment-rotation diagrams for geometrically perfect and imperfect (first eigen mode shape) circular towers (a) and wavy towers (b). The moment is normalized by a constant M_{pl} whose value is $d_{min}^2 \sigma_y t_{min}$, where d_{min} is the minimum diameter among all the tapered cylinders used for making the towers, and σ_y is the yield stress of the material. The presence of imperfections affects the capacity of circular tower substantial, while the capacity of wavy tower is affected slightly. For imperfection amplitude $0.5t$ and $1.0t$, the reductions are 38.0%, and 38.0% for the circular tower, while the reductions are 9.0%, and 13.0% for the wavy towers.

shown in figure 4.6. The imperfection amplitude w_0 is varied from 0 to t_m, where t_m is the minimum thickness among all the tapered cylinders used in the towers. The thicknesses of the cylinders are the same for the wavy and the circular tower; consequently, the value of t_m is also equal for the both towers.

In figure 4.7, the relationship between moment and rotation is shown for the perfect and first eigen mode imperfect towers for both circular and wavy. The moment is normalized by a constant M_{pl} whose value is $d_{min}^2 \sigma_y t_{min}$ (3.0706 $E7$ Nm), where d_{min} is the minimum diameter among all the tapered cylinders used for making the towers, and σ_y is the yield stress of the material. The capacities is normalized by M_{pl} because it has a physical meaning (i.e., the plastic moment of a cylinder with diameter d_{min} and thickness t) and was used in the past studies [1, 17, 53]. In all the cases, the first limit load is taken as the moment capacity of the towers. From figure 4.7, it is not clear that the limit load (bifurcation point) is reached for all the cases, but

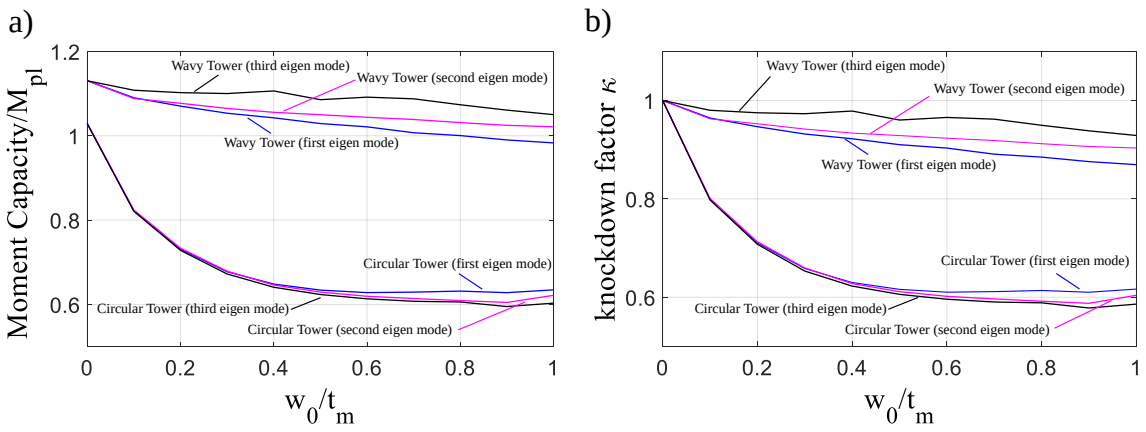

Figure 4.8: Moment capacities (a) of the circular and the wavy towers against the imperfection amplitude. Moment capacities are normalized by $M_{pl} = d_{min}^2 \sigma_y t_{min}$, where d_{min} is the minimum diameter among all the tapered cylinders used for making the circular tower, and σ_y is the yield stress of the material. Knockdown factor κ (b) for the circular and the wavy towers against imperfection amplitude. The moment capacity and κ of the wavy tower are always more than the moment capacity and κ of the circular tower.

by observing moment capacities data it is clear that limit load has been reached as their value starts reducing at the end. For clarity, two subfigures are added in figure figure 4.7a to show the bifurcation points. For certain fully symmetric geometries it is not possible to go deeply to the post-peak behavior using the Riks method. However, this is not a problem for this analysis as the peak capacity is the measure of interest and not the post-buckling behavior. From figure 4.7a and figure 4.7b, it is clear that the presence of imperfections affects the capacity of circular tower substantial, while the capacity of wavy tower is affected slightly. For imperfection amplitude $0.5t$ and $1.0t$, the reductions are 39.0%, and 39.0% for the circular tower, while the reductions are 9.0%, and 13.0% for the wavy towers.

The bending capacities of the imperfect circular and wavy towers are shown against the imperfection amplitude w_0 in figure 4.8a. The imperfection amplitude w_0 is normalized by t_m, and the bending capacities are normalized by M_{pl}. Figure 4.8a shows that the bending capacities of the wavy tower are always more than

that of the circular tower. The wavy tower has higher capacities than that of the circular tower because of two reasons: first, the wavy cross-section has a higher moment of inertia, and more importantly, the wavy tower is much less sensitive to the imperfection.

In figure 4.8b the knockdown factor κ, i.e., the ratio of the capacity of imperfect towers to the capacity of perfect tower $M_{Imperfect}/M_{Perfect}$, of the circular and the wavy towers are shown. These figures show that the sensitivity of the wavy tower to imperfections is less than that of the circular tower for all three eigen mode shape imperfections.

For the first eigen mode shape imperfect wavy tower, the reductions in the load bending capacities are 3.6%, 9.0%, and 13.0%, for the imperfection amplitudes $0.1t$, $0.5t$, and $1.0t$ respectively. In contrast, for the first eigen mode imperfect circular tower, the reductions in the load bending capacities are 20.0%, 39.0%, and 39.0%, for the imperfection amplitudes $0.1t$, $0.5t$, and $1.0t$ respectively—substantially higher reductions than that of the wavy tower.

Although the circular tower is equally sensitive to second and third eigen mode shape imperfections, the wavy one is always much less and it is even more insensitive to higher modes. Indicatively, for imperfection amplitude $0.5t$ the wavy tower loses only 7.0% and 4.0% of its capacity for second and third eigen mode shape imperfections, while the circular one loses 39.0%. This is a striking difference demonstrating the potential of the wavy shape.

The reductions due to first, second and third eigen modes imperfections are not the same; nevertheless, figure 4.8b paints a very clear pattern that the wavy tower is remarkably less sensitive to imperfections compared to that of the circular tower. This means that not only tapered wavy cylinders but also wavy towers are insensitive to imperfections, and the imperfection insensitivity is propagated from a unit level

(tapered cylinders) to a system level (wavy towers). Imperfections insensitivity of wavy tower is encouraging, and to the knowledge of authors, this is the first time that a structural system made by wavy cylinders is investigated.

4.3.2 The effect of a local dimple-like realistic imperfection

The eigen mode imperfections that have been used in the previous sections are considered among the most deleterious shapes, but are far from being realistic. They were used in the anticipation that the maximum reduction in load carrying capacities occur when the imperfections are in the shape of eigen modes. Usually, imperfections are commonly induced in thin cylinders when they are hit by some sharp solid during transportation or construction, and thus the imperfections are local in nature and dimple-like in shape. These dimple-like imperfections are induced when some solid hits the cylinders that are used for making towers during construction or transportation. To model dimple-like imperfections, we follow what was proposed by Gerasimidis et al. [89] and Yadav and Gerasimidis [1]. The mathematical description of the dimple-like imperfection for a cylindrical shell under bending is:

$$w = -w_o e^{-(\frac{x}{L_1})^2} e^{-(\frac{\theta}{\theta_1})^2} \tag{23}$$

Where w represents the deviation from the original position in the radial direction, w_o is the amplitude of the imperfection. x and θ are the axial and circumferential coordinates with the origin placed at the middle of the cylinder such that the dimple is centered on the meridian with maximum compressive stress. L_1, and θ_1 are the parameters that dictate the length (in the axial direction) and the width (in the circumferential direction) of the dimple. The values for L_1 and θ_1 are chosen such that the length ($2L_1$) and the width ($2R\theta$) of the dimple are equal to the first eigenmode

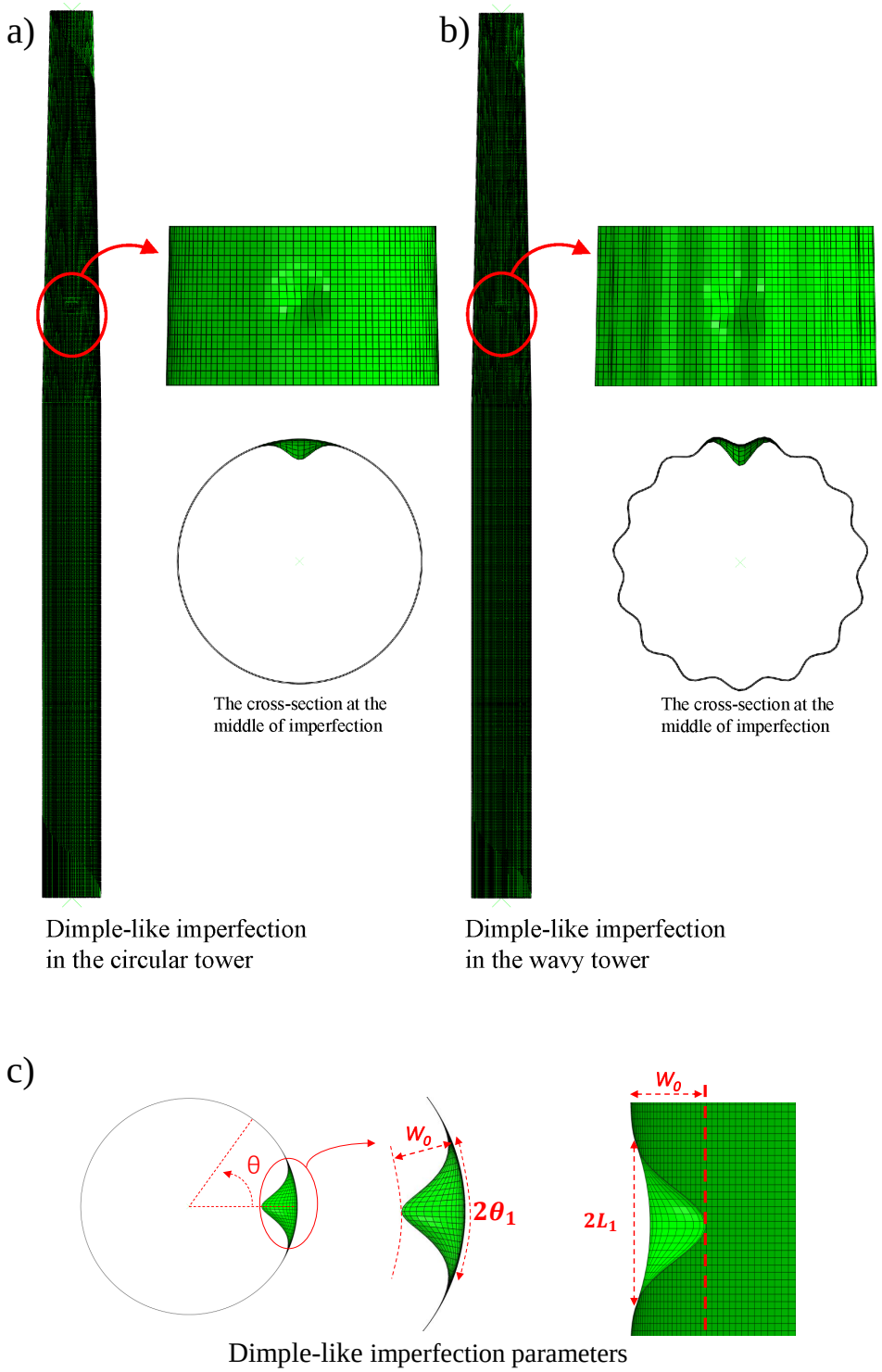

Figure 4.9: Dimple-like imperfect circular tower (a) and wavy tower (b). The parameters L_1, and θ_1 (c) dictate the length (in the axial direction) and the width (in the circumferential direction) of the dimple.

half-wavelength of the cylinder under axial compression, i.e. $3.44\sqrt{Rt}$ for $\nu = 0.3$ [79]. This is done in the anticipation that these parameters reduce the capacity the most [1].

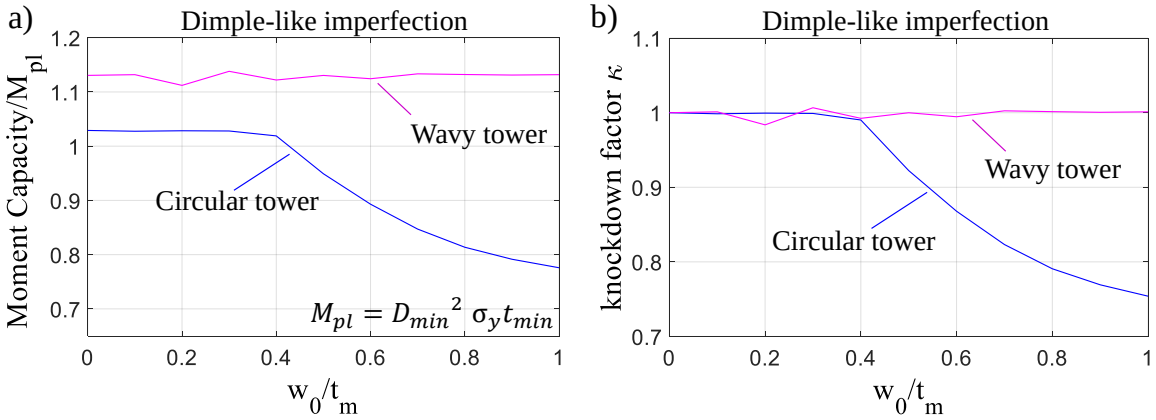

Figure 4.10: (a) Moment capacities of the circular and the wavy towers against the imperfection amplitude. Moment capacities are normalized by $M_{pl} = d_{min}^2 \sigma_y t_{min}$, where d_{min} is the minimum diameter among all the tapered cylinders used for making the circular tower, and σ_y is the yield stress of the material. (b) Knockdown factor κ for the circular and the wavy towers against imperfection amplitude.

This dimple-like imperfection is applied in both the circular and the wavy towers. For doing that a dimple is introduced in the middle of that cylinder for which radius to thickness ratio (R/t) is maximum and thus more imperfection sensitive. The values of $2L_1$ and $2\theta_1$ are taken as $3.44\sqrt{R_m t_m}$ and $3.44\sqrt{R_m t_m}/R_m$ respectively; where, R_m and t_m are the average radius (as the cylinder is tapered) and the thickness of the cylinder having maximum R/t. The dimple-like imperfect towers are shown in figure 4.9; the dimple is centered on the compressive side of the towers.

Figure 4.10a shows the normalized moment capacity of the circular and the wavy towers against the imperfection amplitude. The capacities of the wavy tower are unaffected by the presence of the imperfection for the range of imperfection amplitude considered $(0 < w_0 < 1.0t)$; in caparison, the capacity of the circular tower is reducing for $w_0 > 0.4t$ and unaffected for $w_0 < 0.4t$. Figure 4.10b shows the knockdown factor

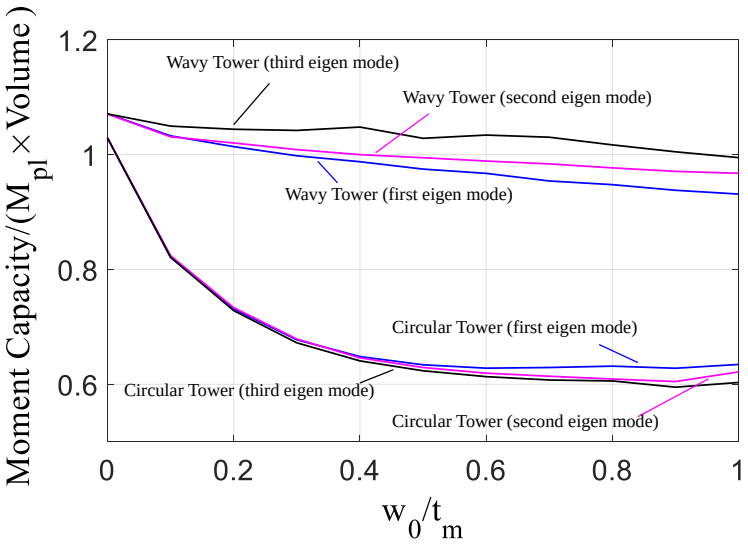

Figure 4.11: Moment capacities of the circular and the wavy towers against the imperfection amplitude. Moment capacities are normalized by $M_{pl} \times V$, where $M_{pl} = d_{min}^2 \sigma_y t_{min}$, d_{min} is the minimum diameter among all the tapered cylinders used for making the circular tower, σ_y is the yield stress of the material and V is the material volume whose value is V_0, $1.1V_0$ for the circular and the wavy towers.

κ of the circular and the wavy towers against the imperfection amplitude; it can be seen that the benefit of using wavy cylinders for $w_0 > 0.4t$ is remarkable.

The imperfection insensitivity of the circular tower for $w_0 < 0.4t$ is in contrast to the behavior of circular cylinders, where small-amplitude dimple-like imperfections also reduce the capacity significantly [1]. The reason for this contrast might be that the dimple is not at the most deteriorating location. In the case of circular cylinders, due to the symmetry, the most deteriorating location of the dimple is the meridian with maximum compressive stress in the middle of the cylinder. In contrast, for the circular tower—due to asymmetry—the most deteriorating location of the dimple is not obvious. A significant reduction might be observed if the dimple is at the most deteriorating location, but we did not pursue in that direction. However, for eigen mode imperfections, significant reduction is occurring even for small imperfection amplitude because the eigen modes are the inherent property of the tower. It is

noteworthy that there might be some other local imperfection shapes that might reduce the bending capacity more than the dimple-like imperfections; however, wavy cylinders would be less sensitive to other kind of geometric imperfections too as in the case of eigen mode imperfections. The dimple-like imperfections are chosen because they are more likely present in the towers and were used in the past studies [83, 85, 88, 89].

4.4 Mass efficiency of the wavy tower

It is clear from the previous sections that the wavy tower has more capacity and less sensitivity to imperfections than that of the circular tower. However, more material is required to make the wavy tower than to make the circular cylinder. To investigate this issue, the bending capacities of the wavy and the circular towers is normalized by their respective material volume.

If the volume of material required for making the circular tower is V_0; it is found that the volume of material required for making the wavy tower is $1.10V_0$. The calculation of the material volume for these complex towers has been performed using ABAQUS [80] and its functionality to calculate the mass of the model if density is specified. To calculate the material volume of the towers, this ABAQUS [80] functionality is utilized by specifying the mass density 1. The moment capacities of the wavy and the circular towers against the imperfection amplitude are shown in figure 4.8a; these capacities are normalized by a constant factor $M_{pl} = d_{min}^2 \sigma_y t_{min}$ and respective material volumes. This means that the capacities of the wavy tower are normalized by $M_{pl} \times 1.10V_0$, and the capacities of the circular tower are normalized by $M_{pl} \times 1.00V_0$. These normalized bending capacities are shown in figure 4.11 for eigen mode one, two, and three shapes imperfection. For all the cases, the normalized bending capacities of the wavy tower are more than that of the circular tower. The

difference between the normalized capacity of the wavy and the circular towers are marginal for the perfect tower, i.e, $w_0 = 0.00t$. However, the capacity of the wavy tower is substantially high than that of the circular tower for imperfect towers, i.e, $w_0 > 0.00$. All real structures contain imperfections, and thus using the wavy tower is beneficial even if it requires more material than the circular tower. However, ultimately the efficiency of the wavy tower must include all cost components such as fabrication and erection costs. Since this paper is focused on the sensitivity of wind turbine tower shells to geometric imperfections the efficiency of the mass of steel used for the tower is only taken into account. A complete study on the efficiency would need many different aspects which are not studied here.

4.5 Discussion

The study investigates the effectiveness of the waviness on reducing the imperfection sensitivity of a 61 m NORDEX S70/1500 wind turbine tower of 1.5 MW capacity, subjected to bending. Firstly, the response of tapered wavy cylinders to imperfections is looked. For this purpose, a circular tapered cylinder which is used in the 61 m NORDEX S70/1500 wind turbine tower is selected, and modified into a wavy tapered cylinder. It is found that the tapered wavy cylinder is insensitive to imperfections especially for small imperfection amplitude, while the tapered circular cylinder is highly sensitive to imperfections. For imperfection amplitude $w_0 = 0.1t$, the reduction in the tapered wavy cylinder is 4.0% while the reduction in the tapered circular cylinder is 12%. This means that not only straight wavy cylinders but also tapered wavy cylinders are insensitive to imperfections. Encouraged by this finding, the effect of imperfection on the wavy wind turbine tower made by tapered cylinders is explored.

The NORDEX S70/1500 wind turbine tower is converted into a wavy tower by

using sinusoidal waves along the circumference. This study reveals that the reduction due to imperfections in the bending capacity of the wavy turbine tower is insignificant compared to the reduction in the circular tower. For imperfection amplitude, $w_0 = 0.1t$ and first eigen mode imperfection, the reduction in the wavy tower is 4.0%, while the reduction in the circular tower is 20%. A similar pattern is found for all the other imperfections and imperfection amplitudes. This means imperfection insensitivity of individual tapered wavy cylinders is transferred to the wind turbine tower made by tapered wavy cylinders. Moreover, the wavy tower can bear substantially more load than the circular towers, and the wavy tower is more economical in terms of the volume of material required. Besides, the effect of a realistic dimple-like imperfection on the bending capacity of the towers is explored, and it found again that the wavy tower performed better than the circular tower.

CHAPTER 5

NON-DESTRUCTIVE TECHNIQUE FOR THE EVALUATION OF THIN CYLINDRICAL SHELLS' BUCKLING CAPACITY

The reduction in the cylinders' axial buckling capacity depends on the shape and the size of the imperfections that are present in the cylinders. Thus, *a priori* knowledge about the imperfections is required for the capacity prediction. However, measuring imperfections is a difficult, expensive, and time-consuming adventure. This makes the prediction of shells' capacity difficult, if not impossible. This chapter proposes a procedure to predict the buckling capacity of thin cylinders based on the feedback of probe force-displacement curves of axially loaded cylinders. The proposed procedure is computationally implemented on a thin perfect cylinder ($R/t \approx 286$) and on an imperfect cylinder with varying imperfection amplitude. In this proposed method, thin cylindrical shells are probed under different axial loads to explore the probing profile. Probe force-displacement curves contain significant information, which can be used to predict the buckling capacity of thin cylinders [69–72, 75]. We address the issues of extracting information from probe force-displacement curves and using this information to predict the capacity. In addition, we investigate the roles of probing location, imperfections amplitude, and background imperfections on the accuracy of the prediction.

5.1 Description of the procedure and its application on a perfect cylindrical shell

The proposed procedure takes advantage of the stability landscape of axially loaded cylinders [70, 72]. The method consists of three steps: 1) cylinders are put under axial load F_a, 2) these axially loaded cylinders are probed in radial direction at the location of a pre-existing imperfection, and 3) the peak probe force F_p^{max} and the corresponding axial load F_a are recorded and are used to predict the axial capacity. There are two constraints on the axial load F_a: 1) F_a is less than the axial capacity of the cylinders, and 2) the peak probe force F_p^{max} exists if the cylinders are probed. The constraint on the probing is that the probe displacement $D_p < 5t$, where t is the thickness of cylinders. These three steps of the procedure are iterated with increasing axial load F_a till the predicted axial capacity F_{pre} is converged. The convergence criterion is $\mid F_{pre} - F_A^0 \mid < 0.1F_{pre}$, where F_{pre} is the predicted capacity and F_a is the last axial load. We are using this convergence criterion because this is giving accurate prediction, any other criteria could be used if that gives a good prediction.

Initially, we put the cylinder under axial load $F_A^0 = 0.5\kappa P_c$, where κ is the knock-down factor of the cylinder and P_c is the theoretical axial buckling capacity of the perfect cylinder. The values of P_c, and κ are:

$$P_c = \frac{2\pi E t^2}{\sqrt{3(1-\nu^2)}} \tag{24}$$

$$\kappa = 1 - 0.901(1 - \exp(\frac{\sqrt{R/t}}{16})) \tag{25}$$

This initial value makes sure that the axial load is less than the capacity of the cylinder, the first constraint on F_a. This is true because F_a is less than half of the

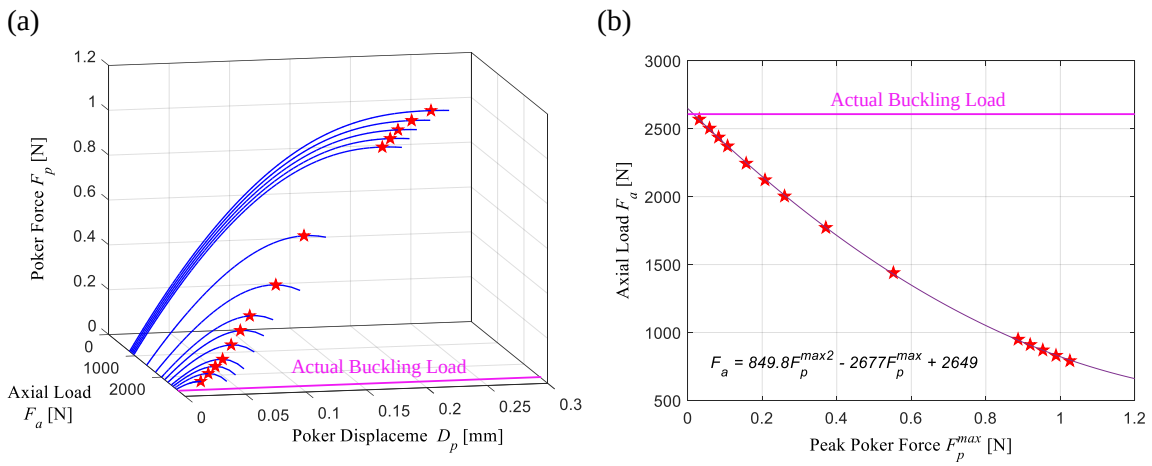

Figure 5.1: (a) Three-dimensional phase space of axial load F_a, probe displacement D_p, and probe force F_p. This force landscape is obtained by implementing the proposed procedure. The prediction is converged after 11 iterations. (b) The axial load F_a and corresponding peak probe force F_p^{max} along with their quadratic curve fitting. The predicted capacity, where the quadratic curve intercepts Y axis, of the cylinder F_{pre} is 2648.7 N, whereas the actual capacity of the cylinder F_{act} is 2584.7 N and is shown in red asterisk.

expected capacity (assuming the cylinder is imperfect) of the cylinder that is κP_c. To enforce the second constraint on F_a, we probe the cylinder that is under axial load $F_a = 0.5kP_c$. The probing is done at the location of the worst imperfection, where the amplitude of imperfection is maximum, with the constraint $D_p < 5t$. If F_p^{max} exists in the probe force then F_a and F_p^{max} will be $F_{a,1}$ and $F_{p,1}^{max}$, the first data set for the axial force and peak probe force that is used for the capacity prediction. If F_p^{max} does not exist in the probe force then F_a is increased by 10%, and the cylinder is probed again at the worst imperfect location. This iteration is continued till we find the peak F_p^{max} in probe force.

In the proposed procedure, a minimum of five pairs of $\{F^a; F_p^{max}\}$ are needed for the capacity prediction. Once we have the first data set $\{F_{a,1}; F_{p,1}^{max}\}$, we can find the next four data sets $\{F_{a,2}; F_{p,2}^{max}\}$, $\{F_{a,3}; F_{p,3}^{max}\}$, $\{F_{a,4}; F_{p,4}^{max}\}$, and $\{F_{a,5}; F_{p,5}^{max}\}$ following Eqn. (26).

$$F_{a,i} = F_{a,i-1} + 0.05F_{a,1} \tag{26}$$

$F_{p,i}^{max}$ is the peak probe force of the cylinder that is axially loaded under $F_{a,i}$. After having the five data sets, we predict the capacity of the cylinder by quadratic curve fitting of these data sets. The predicted capacity F_{pre} is the value of Y axis where the quadratic curve intercepts it assuming F_a corresponds to Y axis, and F_p^{max} corresponds to X axis. If the convergence criterion $\mid F_{pre} - F^a \mid < 0.1F_{pre}$ is satisfied, F_{pre} will be the capacity of the cylinder. Otherwise, a new data set $\{F_{a,i+1}, F_{p,i+1}^{max}\}$ is added following Eqn. (27).

$$F_{a,i+1} = F_{a,i} + cF_{pre} \tag{27}$$

$F_{p,i+1}^{max}$ is peak probe force corresponds to $F_{a,i+1}$, and c is a constant whose value depends on $\mid F_{pre} - F_a \mid$. The values of c are 0.25, 0.20, 0.15, 0.10, and 0.05; for $\mid F_{pre} - F_a \mid > 0.50F_{pre}$, $\mid F_{pre} - F_a \mid > 0.40F_{pre}$, $\mid F_{pre} - F_a \mid > 0.30F_{pre}$, $\mid F_{pre} - F_a \mid > 0.20F_{pre}$, and $\mid F_{pre} - F_a \mid > 0.10F_{pre}$ respectively. $\mid F_{pre} - F_a \mid < 0.10F_{pre}$ is the convergence criteria; the iteration stops at this point, and F_{pre} will be the predicted capacity of the cylinder.

To illustrate the proposed procedure, we apply this computationally using FEA package ABAQUS [80] on a perfect cylinder that represents mini Coke cans (7.5 fl oz), made of aluminum as shown in figure 5.2. The dimensions and material properties of the cylinder are given in Table 5.1. We use these cans because they are easily available for the experiments. The modeling technique follows the one presented in Ref. [95]. The mesh for the models was created by user-written codes using $S4R$ elements with an element size of 0.91 mm, about $0.54\sqrt{Rt}$, in both axial and circumferential directions. The boundary conditions at the ends of the cylinder are applied using the

Figure 5.2: A mini Coke can (7.5 fl oz) made of aluminum. This Coke can is used to illustrate the proposed procedure for predicting the capacity.

same procedure as in Ref. [95] with rigid links, which connect the central node to the nodes at the ends of the cylinder. Further, we simplified our modeling assuming the cross-sections of cans are circular throughout the length, which is a slight deviation from the real cans. This does not affect our analysis as here the purpose is the evaluation of the proposed procedure not to emulate the experiments exactly. For a perfect cylinder, probing can be done anywhere, as there is no imperfection. However, we probe in the middle of the cylinder to avoid the effects of boundaries on the results. For step 1 of the procedure, geometrically nonlinear static analysis is used to put the cylinder under proscribed axial load, and for step 2, the arc-length based Riks method [91] is used to probe the cylinder in the radial direction in the middle.

Figure 5.1a shows the force landscape—a three-dimensional phase space of axial load F_a, probe displacement D_p, and probe force F_p— of the cylinder. This force landscape is obtained by implementing the proposed procedure. The prediction is

Table 5.1: Dimensions and material properties of mini Coke cans (7.5 fl oz)

E (GPa)	R (mm)	ν	t (μm)	L (mm)
68.95	286	0.3	100	107

converged after 11 iteration, and thus 11 probe force-displacement plots are shown. In figure 5.1b, the axial load F_a and corresponding peak probe force F_p^{max} is shown along with their quadratic curve fitting (polynomial fit of order 2). The predicted capacity, where the quadratic curve intercepts Y axis, of the cylinder F_{pre} is 2648.7 N, whereas the actual capacity of the cylinder F_{act} is 2584.7 N, which is obtained computationally and is shown in figure 5.1b in red asterisk.

The percentage difference between the F_{pre} and F_{act} is 2.5% ($\frac{|F_{act}-F_{pre}|}{F_{act}} \times 100$); this shows that the proposed procedure is predicting the capacity of a perfect cylinder accurately. However, the real test of the procedure is when it predicts the capacity of imperfect cylinders because all real structures are imperfect. This is the subject of the next section.

5.2 Application of the procedure on imperfect cylindrical shells

To apply the proposed procedure on imperfect cylinders, we induce a local dimple imperfection in the middle of the perfect cylinder. The dimple imperfection is modeled as a two-dimensional normal distribution function following Ref. [89] and Ref. [1]. The mathematical description of the dimple imperfection is:

$$w = -\delta e^{-\left(\frac{x-x_0}{L_1}\right)^2} e^{-\left(\frac{\theta-\theta_0}{\theta_1}\right)^2} \tag{28}$$

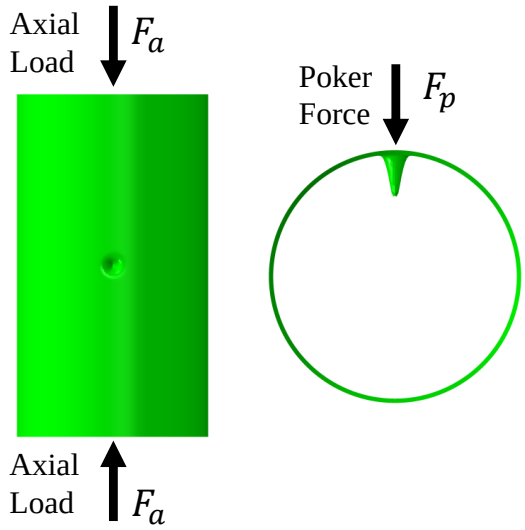

Figure 5.3: Imperfect cylinder along with axial load (F_a) and poker force (F_p). The dimple is modeled as a two-dimensional normal distribution following Ref. [89] and Ref. [1] and is located in the middle of the cylinder. The probing is done in the middle of the dimple because it is the worst imperfect location. The amplitude of dimple is scaled up so that it is visible; however, in our analyses, the amplitude is of the order the thickness of the cylinder, and it is difficult to visually distinguish the imperfect cylinder from the perfect one.

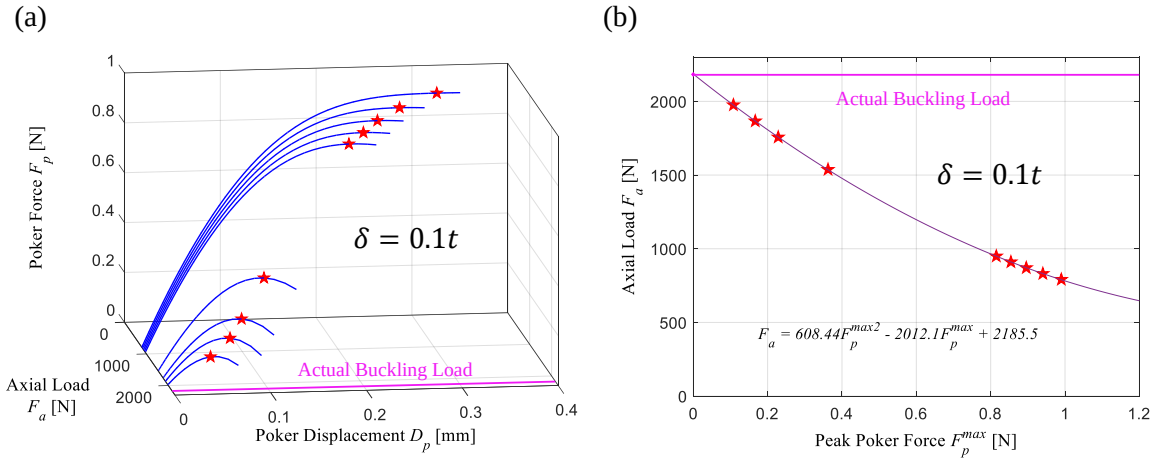

Figure 5.4: (a) Three-dimensional phase space of axial load F_a, probe displacement D_p, and probe force F_p. This force is obtained by implementing the proposed procedure. The prediction is converged after 9 iteration. (b) The axial load F_a and corresponding peak probe force F_p^{max} along with their quadratic curve fitting. The predicted capacity, where the quadratic curve intercepts Y axis, of the imperfect cylinder F_{pre} is 2185.5 N, whereas the actual capacity of the cylinder F_{act} is 2183.0 N and is shown in red asterisk.

Where w represents the deviation from the original position in the radial direction, δ is the amplitude of the imperfection, x and θ are the axial and circumferential coordinates, (x_0, θ_0) are the center of the dimple whose values are chosen such that the dimple is located in the middle of the cylinder. L_1, and θ_1 are the parameters that dictate the length (in the axial direction) and the width (in the circumferential direction) of the dimple. In this study, the value of L_1 and θ_1 are 0.55λ and $0.55\lambda/R$ [1], where λ is the half-wavelength of classical axisymmetric buckling mode of the cylindrical shell under axial load whose value is [79]:

$$\lambda = \pi\sqrt{\frac{Rt}{\sqrt{12(1-\nu^2)}}} \tag{29}$$

This dimple is induced in the perfect cylinder whose dimensions are given in Table 5.1. Figure 5.3 shows the dimple-like imperfect cylinder along with axial load F_a and probe force F_p that is applied radially inward in the middle of the dimple. In this figure, the amplitude of dimple is scaled up so that it is visible; however, in our analyses, the amplitude is of the order the thickness of the cylinder, and it is difficult to visually distinguish the imperfect cylinder from the perfect one.

We apply the proposed procedure computationally using FEA package ABAQUS [80] on the imperfect cylinder. For step 2 of the procedure, the probing is done in the middle of the dimple. The output of the procedure for imperfection amplitude $\delta = 0.1t$ is shown in figure 5.4. Figure 5.4a shows the force landscape, and figure 5.4b shows the axial load F_a and corresponding peak probe force F_p^{max} along with the quadratic curve fitting (polynomial fit of order 2). The predicted capacity of the cylinder F_{pre} is 2185.5 N, which is the value of Y axis where the quadratic curve intercepts it in figure 5.4b. The actual capacity of the cylinder F_{act}, obtain by Finite Element Analysis of the cylinder, is 2183.0 N that is 0.11% less than F_{pre}. Again,

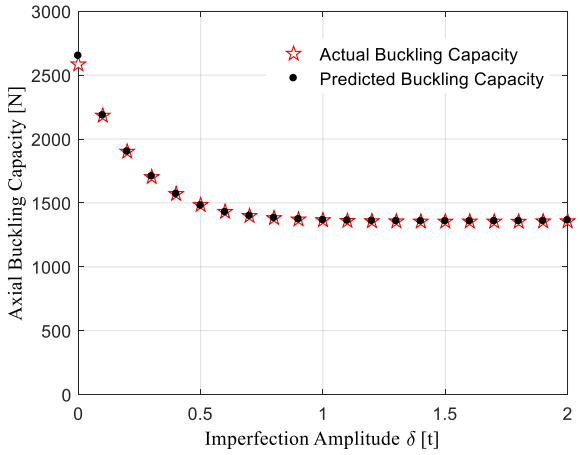

Figure 5.5: Actual F_{act}, and predicted F_{pre} capacities of the dimple imperfect cylinders. F_{act} is found by Finite Element Analysis, while F_{pre} is calculated using the proposed procedure. The predictions are quite accurate as the differences between F_{act} and F_{pre} are very small for all the imperfect cylinders that are considered ($\delta \leq 2t$).

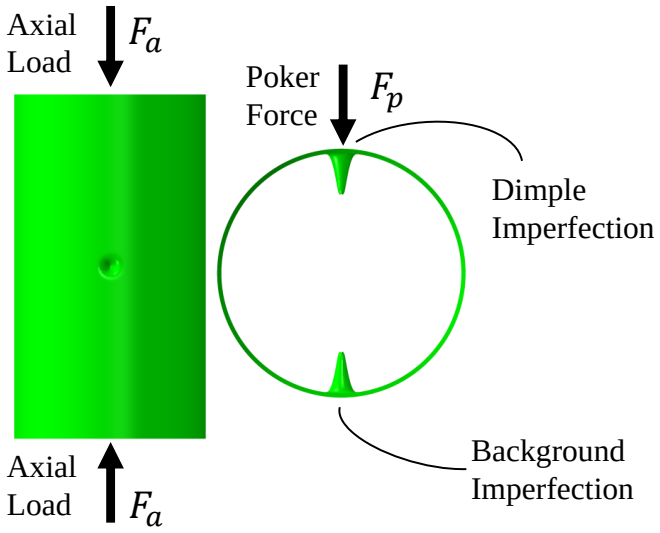

Figure 5.6: The Can with two dimple imperfections along with axial load (F^A) and poker force (F_p). The dimples are modeled as a two-dimensional normal distribution following Ref. [89] and Ref. [1] and located in the middle of the cylinder and dramatically opposite direction. We call the first dimple as dimple imperfection and the second dimple as background imperfection. The probing is done in the middle of the dimple imperfection. The amplitude of dimple is scaled up so that it is visible; however, in our analyses, the amplitudes are of the order the thickness of the Can.

the proposed procedure is predicting the capacity accurately of the imperfect cylinder with imperfection amplitude $\delta = 0.1t$.

The prediction procedure is also implemented on imperfect cylinders with higher imperfection amplitude. In figure 5.5, the predicted capacities and the actual capacities of imperfect cylinders are shown against the amplitude of the imperfection. It can be seen that the procedure is predicting the capacity of the imperfect cylinders accurately for higher imperfection amplitude ($0 < \delta \leq 2t$). We again emphasize that in all these computations the probing is done in the middle of the cylinder. This location is not known prior for real structures. The importance and implications of this location will be discussed in section-6 along with the effect of probing location, and the resilience of the procedure.

5.3 Application of the procedure on the Imperfect cylindrical shells having background imperfections

For a cylindrical shells have more than one dimples, the proposed procedure is predicting the capacity accurately when probing is done in the middle of the dominating dimple. However, the procedure, always, over-predicts the capacity when probing is done in the middle of the small dimple. This over-prediction is due to the presence of other dominating imperfections, we call it background imperfections. These background imperfections, when they are dominating, dictate the capacity of the cans. Consequently, for the small amplitude dimple, the prediction overestimates the capacity. Whereas for the high amplitude dimple, the prediction is accurate.

To illustrate this phenomenon of dominating imperfection further, we simulate the can having two dimples: we call the first dimple as dimple imperfection and the second dimple as background imperfection. These two dimples are shown in

figure 5.6. In this figure, the amplitude of the dimples are scaled up so that it is visible; however, in our analyses, the amplitudes are of the order the thickness of the cylinder. Figure 5.7a shows the actual capacities, found by FEA analysis, of this can with varying background and dimple imperfections. Figure 5.7a makes it clear that the imperfection, which has a high amplitude, dictates the capacity of the can. For example, when the background is zero, the capacity depends on the dimple imperfection amplitude (X-axis) as the capacity is reducing with an increase in the dimple imperfection amplitude But, for the background imperfection $0.2t$, the curve is flat till the dimple imperfection amplitude is less than $0.2t$ because the capacity is decided by the background imperfection. Similarly, for the background imperfection $0.5t$, the curve is flat until the background imperfection is less than $0.5t$. Further, for the background imperfection $2.0t$, the curve is always flat, and the variation of dimple imperfection amplitude does not affect the capacity as it is, always, less than $2.0t$. It is clear from this analysis that the capacity of cylinders is decided by the imperfection that has high imperfection amplitude. Here, we use a simple model for the background imperfection; in reality, background imperfections are very complex. Nevertheless, this simple model explains the concept of dominating imperfection.

Figure 5.7b shows the predicted capacity of the can; the predicted capacities are almost the same for all the cases irrespective to the background imperfection, and follow the actual capacity of the can without the background imperfection of figure 5.7a. It means that the probing can only gauge the imperfections that are near to the point of probing. And thus, the predicted capacity is accurate only if there is no other dominating imperfection away from the point of probing. The predicted capacity of figure 5.7b is accurate if the background imperfection amplitude is less than the dimple imperfection amplitude. Otherwise, the prediction overestimates the capacity. For example, when the background imperfection is $0.2t$ and dimple imperfection is $0.5t$,

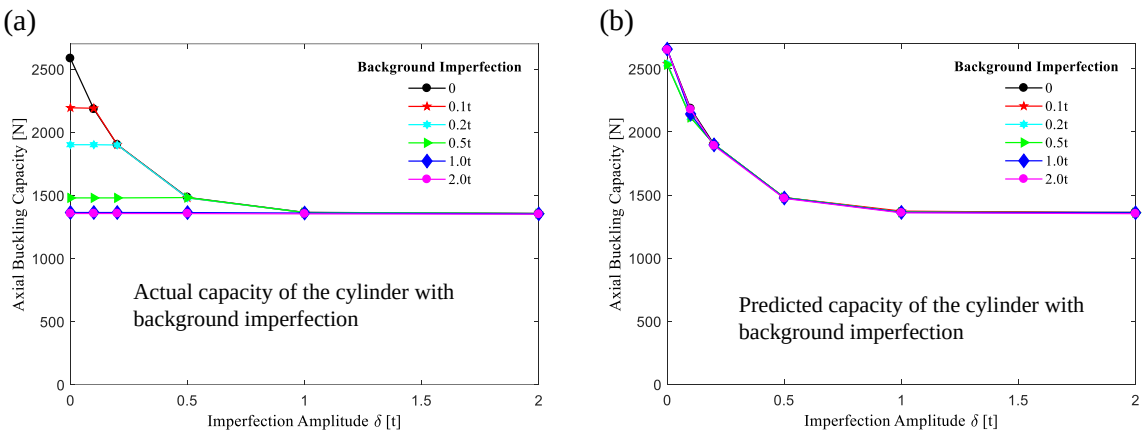

Figure 5.7: (a) Actual F_{act} capacity of the can with background imperfection. The amplitude of the background imperfection varies from 0 to $2.0t$. The $X-axis$ represents the amplitude of dimple imperfection that varies from 0 to $2.0t$. (b) Predicted capacities F_{pre} of the Can with background imperfection. For the prediction, probing is done in the middle of the dimple. The predicted capacity of F_{pre} is accurate if the background imperfection amplitude is less than the dimple imperfection amplitude. Otherwise, the prediction overestimates the capacity.

the predicted capacity (figure 5.7b) and actual capacity (figure 5.7a) are the same. But, when the background imperfection is $0.5t$ and dimple imperfection is $0.2t$, the predicted capacity (figure 5.7b) is more than the actual capacity (figure 5.7a). The same pattern is observed for all the cases.

This observation reflects the crucial role played by the location of probing. To further investigate this issue, we move the location of the probing away from the imperfection in the axial and circumferential directions. The results are presented in the next section.

5.4 Effect of the location of probing relative to the imperfections

In Section 5.3, we have demonstrated that the location of probing is of utmost importance for the accurate prediction of the buckling capacity of thin cylinders.

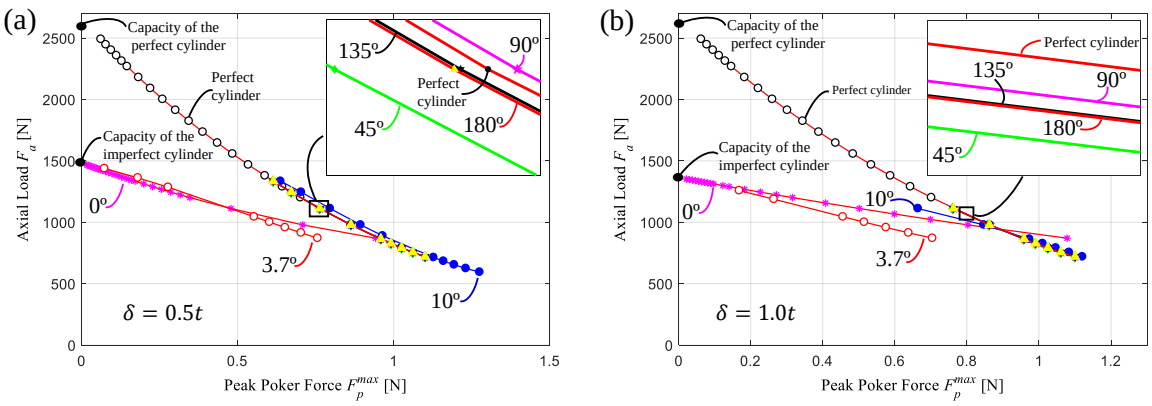

Figure 5.8: The axial load F_a and corresponding peak probe force F_p^{max} for the probing locations at $\theta = 0$, 3.7, 10, 45, 90, 135, and 180 relative to the middle of imperfection along the circumferential direction, for imperfection amplitudes $\delta = 0.5t$ (a), and $\delta = 1.0t$ (b). The plot for the perfect cylinder is also shown. The probing fails to recognize the presence of the imperfection for $\theta = 45$, 90, 135, and 180, and thus they do not predict the capacity accurately.

In this section, we further explore this issue, both computationally, by moving the probing location away from the imperfection in the axial and in the circumferential directions.

5.4.1 Computational study

We create a dimple-like imperfect cylinder similar to that described in Section 5.2 and shown in figure 5.3. First, we implemented the proposed procedure of Section 5.1, but we probed away from the middle of the dimple. We found that the proposed procedure is not yielding accurate results, and concluded that the procedure works only when the probing is done in the middle of the dominant imperfection (the imperfection that dictates the capacity of thin cylinders). Having asserted that now we address a more fundamental question: is it possible to predict the capacity of thin cylinders by probing away from the dominant imperfection? To answer this question, the axially loaded imperfect cylinder is probe away from the imperfection, and probing data is used to predict the capacity. Here, we emphasize that we are not following

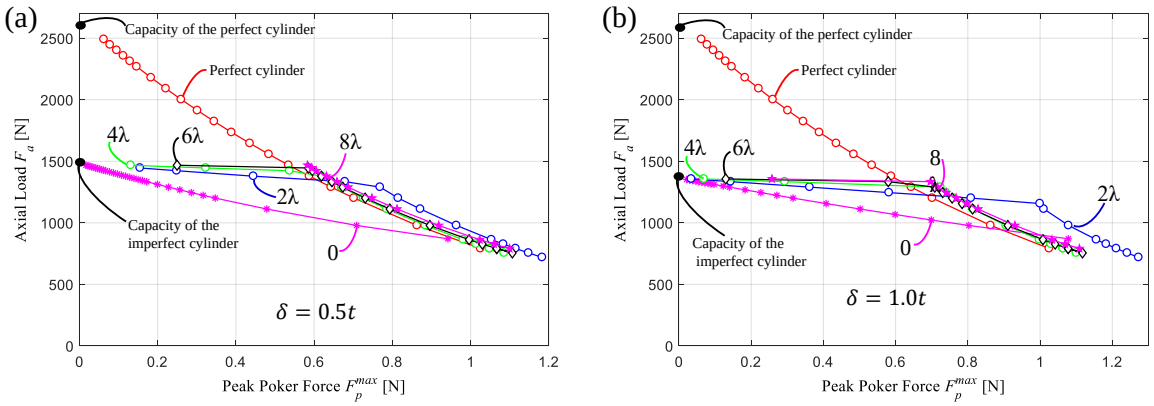

Figure 5.9: The axial load F_a and corresponding peak probe force F_p^{max} for the probing locations at $x = 0$, 2λ, 4λ, 6λ, and 8λ relative to the middle of imperfection along the axial direction, for imperfection amplitudes $\delta = 0.5t$ (a), and $\delta = 1.0t$ (b). The plot for the perfect cylinder is also shown. The probing fails to recognize the presence of the imperfection for $x = 2\lambda$, 4λ, 6λ, and 8λ, and thus they do not predict the capacity accurately.

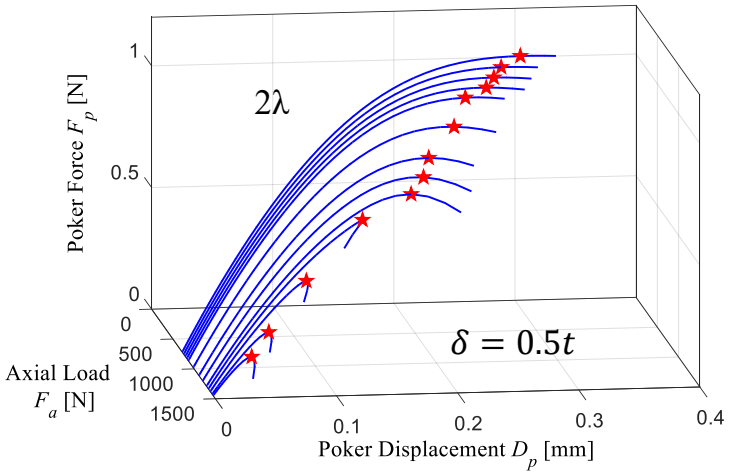

Figure 5.10: Three-dimensional phase space of axial load F_a, probe displacement D_p, and probe force F_p corresponds to $\delta = 0.5t$, and $x = 2\lambda$. In the last four plots, the probe returns before reaching the peak; this is a kind of buckling that makes the cylinder unstable. We cannot probe the cylinder under axial load that is near to the capacity of the cylinder. It also explains the reason behind the bending of the F_a and F_p^{max} plots in figure 5.9a. The bending is happening because the F_p^{max} is not the peak probe force, but the maximum probe force that can be achieved by probing at the higher F_a.

any specific scheme as the objective of this Section is to evaluate the possibility of prediction, and not to propose a procedure.

Figure 5.8 shows the plots of axial load F_a against the peak probe force F_p^{max} when the probing is done away from the middle of the imperfection along the circumferential direction, for the imperfection amplitude $\delta = 0.5t$, and $1.0t$. We chose 7 locations along the circumferential direction, i.e., $\theta = 0$, 3.7, 10, 45, 90, 135, and 180; where θ is the angular distant between the probing location and the middle of the imperfection. $\theta = 0$ represents when probing is done in the middle of the imperfection that yields accurate prediction. Figure 5.8 also shows the plot for the perfect cylinder.

For $\delta = 0.5t$, plots for $\theta = 10$, 45, 90, 135, and 180 follow the plot of the perfect cylinder; and the probing fails to recognize the presence of the imperfection. Consequently, they predict the capacity of the perfect cylinder instead of the imperfect cylinder; indeed, this what we found. These results indicate that the probing fails to recognize the presence of imperfection if it is done away from the region of influence of the imperfection. Here, we use the term 'region of influence' to describe a region near the imperfection such that if the probing is done outside this region, the presence of the imperfection is unrecognized. For example $\theta = 10$, 45, 90, 135, and 180, are outside from the region of influence in figure 5.7a. While for $\theta = 3.7$, the F_a and F_p^{max} plot matches, although not exactly, the plot of imperfect cylinder with $\theta = 0$. This means that when $\theta = 3.7$ the probing location lies in the region of influence of the imperfection and thus predicted value is near the exact value of the imperfect cylinder. It should be noted that when the probing is in the region of influence, this does not mean that the prediction will be accurate; this only means that the imperfection has some influence on the F_a and F_p^{max} plot. For imperfection amplitude $\delta = 1.0t$, we got a similar pattern as shown in figure 5.8b; only the region of influence is larger as the imperfection has an impact on the plot for $\theta = 10$.

Figure 5.9 shows the plots of axial load F_a against the peak probe force F_p^{max} when the probing is done away from the middle of the imperfection along the axial direction, for the imperfection amplitude $\delta = 0.5t$, and $1.0t$. We chose 5 locations along the axial direction, i.e., $x = 0$, λ, 2λ, 3λ, and 4λ; where x is the distance between the probing location and the middle of dimple, and λ is classical axisymmetric buckle half-wavelength for cylindrical shells under axial load as given in Eq. 29. $x = 0$ represents when probing is done in the middle of the imperfection that yields accurate prediction. Figure 5.9 also shows the plot for the perfect cylinder. For the four cases, $x = \lambda$, 2λ, 3λ, and 4λ, the F_a and F_p^{max} plots can be divided into two distinctive regions: the first region is when the plot follows the plot of the perfect cylinder, we call it region1, and the second region is when the plot bent sharply near the axial capacity of the imperfect cylinder, we call it region2. In region2, the plots are bending towards the actual capacity, and it seems that the capacity can be predicted. However, On a closer look, we find that it is not the case. We cannot use the data corresponding to higher F_a because the probing at the higher F_a makes the cylinder unstable.

Figure 5.10 shows the three-dimensional phase space of axial load F_a, probe displacement D_p, and probe force F_p corresponds to $\delta = 0.5t$, and $x = 2\lambda$. It can be seen that, for the last four plots, the probe returns before reaching the peak; this is a kind of buckling that makes the cylinder unstable. We cannot probe the cylinder under axial load that is near to the capacity of the imperfect cylinder. It also explains the reason behind the bending of the F_a and F_p^{max} plots corresponds to region2; this bending is happening because the F_p^{max} is not the peak probe force but the maximum probe force that can be achieved by probing at the higher F_a. As a result, the data corresponding to the region2 cannot be used for the prediction.

From these analyses, it is clear that the probing location relative to the imperfection is crucial information, and the prediction would be inaccurate if the probing is

away from the imperfection. These analyses also reveal some interesting phenomena: 1) there exists a region of influence of the imperfection, and if probing is in this region, the imperfection affects the probing profile, otherwise, the probing profile is the same as for the perfect cylinder. The area of this region of influence depends on the imperfection amplitude and shape. 2) If the probing is done near the axial capacity of the cylinders, the probing might causes the failure of the cylinders. Thus, some safety margin between the axial load and the capacity must be maintained.

5.5 Discussion

A nondestructive procedure is proposed to predict the buckling capacity of thin cylindrical shells. This procedure is implemented computationally on mini Coke cans. For the perfect, computational implementation of the procedure predict accurate results. The percentage difference between the predicted capacity F_{pre} and actual capacity F_{act} is 2.5% ($\frac{|F_{act}-F_{pre}|}{F_{act}} \times 100$); this shows that the proposed procedure is predicting the capacity of a perfect cylinder accurately. For the imperfect can, the computational implementation yields accurate results when the probing is done in the middle of the imperfection. The percentage difference between the F_{pre} and F_{act} is 0.11% for imperfection amplitude $\delta = 0.t$. For other imperfection amplitudes also we are getting very accurate predictions. However, the procedure over-predicts the capacity of the cans when the probing is done away from the imperfection; the probing fails to recognize the presence of imperfection and the predicted capacity is near to the capacity of the perfect cane instead of imperfection one. This demonstrates the crucial role played by the probing location. Another significant finding is the phenomenon of dominating imperfection: if more than one imperfection is present in the cylinder, the capacity is dictated by the dominating imperfection.

Overall, this study demonstrates many aspects of the probing of axially loaded

thin cylinder shells: 1) probing can be used to predict the buckling capacity of shells containing a dimple imperfection, 2) the probing location plays a crucial role in the accuracy of the prediction, and 3) a framework can be developed for non-destructive experiments to predict the buckling capacity of thin shells.

These results show that the prediction of imperfect cylinders is possible if the probing is done at the proper location. Although finding the proper location in a real cylinder is a challenge. Nevertheless, this study gives a hope that a framework can be developed for non-destructive experiments to predict the buckling capacity of thin shells.

CHAPTER 6

SUMMARY, CONCLUSIONS AND FUTURE WORK

6.1 Summary and concluding remarks

This thesis has addressed its four objectives: 1) understanding the bending behavior of thin steel cylindrical shells, and find rational knockdown factors within the range of slenderness used in tall wind turbine towers, 2) shedding new light into the response of imperfection insensitive wavy cylinders under uniform axial compression and bending, 3) implementing the idea of the wavy cylinders for making wind turbine towers, and assessing the practical utility of the wavy cylinders, and 4) developing a non-destructive technique for the evaluation of thin cylindrical shells buckling capacity.

It has been found that steel cylindrical shells ($60 < R/t < 120$) are highly imperfection sensitive under inelastic bending, and the strain-hardening model plays an impactful role on the bending behavior. Moreover, the presence of imperfections reduces the collapse curvature more than the reduction in peak moment. For the geometric imperfections, modal shape, dimple-like, unbiased, and biased have been used; and for the strain-hardening model, a bilinear one and three versions of the Ramberg-Osgood plasticity model have been used. Our analyses have illustrated that the biased imperfection is worst and the dimple-like imperfection is least worst among all the imperfections. We have observed that the bending behavior of thin steel cylindrical shells highly depends on the strain-hardening models. The moment capacity and the collapse curvature are minimum for the bilinear model and maximum

for Ramberg-Osgood model with $n = 9$ among all the models used. The significance of the strain-hardening model can be exemplified by the fact that the ratio of collapse curvature for $n = 9$ to bilinear is around 3 ($R/t = 60$), which demonstrates that the same cylinder could collapse at three times less curvature if the strain- hardening model changes. This is a very significant finding and suggests that the selection of a strain-hardening model is extremely important because it can highly overestimate or underestimate the collapse curvature and bending capacity.

For the wavy cylinders under axial compression, we have found that the dimple-like imperfection does not reduce the load-carrying capacity significantly in the range of imperfection amplitude considered in this study. This is aligned with the findings of Ning and Pellegrino [66, 67], although they considered eigenmode imperfections. Many factors are responsible for making wavy cylinders insensitive to imperfections: 1) reduction in effective radius of curvature [66], 2) stiffness introduced by waviness, and 3) periodic change in the direction of curvature that creates disharmony with the imperfection and consequently, reducing the impact of imperfections. These factors are engaged simultaneously to achieve the imperfection insensitivity. For the wavy cylinders under bending, we again have found that wavy cylindrical shells are insensitive to the imperfections and the presence of imperfections does not reduce the load-carrying capacity significantly. Previous studies [66, 67] revealed similar conclusions for thin cylindrical shells under axial compression. Based on the comparisons between the knockdown factors of the wavy cylinders and the circular cylinders we have reported that for small amplitudes of imperfection ($w_o < 0.3t$) the reduction in bending capacities is high for the circular cylinders compared to the insignificant reduction for the wavy cylinders. Apart from this, we have found that the bending capacities of wavy cylinders are higher than the bending capacities of the circular cylinders. The wave parameters, i.e., the wave amplitude A_r and the number of waves

N, play a crucial role to impact the knockdown factor. The effectiveness of the wavy cylinders increases as the number of waves and the wave amplitude increase. For the higher wave amplitudes and the higher number of waves, wavy cylinders are less sensitive to imperfections, and their bending capacities are high. Further, this study has revealed that the wavy cylinders perform better than the stiffened cylinders in terms of imperfection sensitivity and the volume of the material required.

To assess the practical applicability of wavy cylinders, we have chosen a 61 m NORDEX S70/1500 wind turbine tower of 1.5 MW capacity, and have converted it into a wavy tower by using sinusoidal waves along the circumference. The study has revealed that the reduction due to imperfections in the bending capacity of the wavy turbine tower is insignificant compared to the reduction in the circular tower. For imperfection amplitude, $w_0 = 0.1t$, and first eigen mode imperfection, the reduction in the wavy tower is 4.0%, while the reduction in the circular tower is 20%. A similar pattern has been found for all the other imperfections and imperfection amplitudes. This means imperfection insensitivity of individual tapered wavy cylinders is transferred to the wind turbine tower made of multiple tapered wavy cylinders. Moreover, the wavy tower can bear substantially more load than the circular towers, and the wavy tower is more economical in terms of the volume of material required. Besides, the effect of a realistic dimple-like imperfection on the bending capacity of the towers has been explored, and it has been found again that the wavy tower performed better than the circular tower.

We have proposed a nondestructive procedure to predict the buckling capacity of thin cylindrical shells. This procedure has been implemented computationally on mini Coke cans. For the perfect Coke cans, computational implementation of the procedure has predicted accurate results. The percentage difference between the predicted capacity F_{pre} and actual capacity F_{act} is 2.5% ($\frac{|F_{act}-F_{pre}|}{F_{act}} \times 100$); this shows

that the proposed procedure is predicting the capacity of a perfect cylinder accurately. For the imperfect can, the computational implementation has yielded accurate results when the probing is done in the middle of the imperfection. The percentage difference between the F_{pre} and F_{act} is 0.11% for imperfection amplitude $\delta = 0.t$. For other imperfection amplitudes also we have got accurate predictions. However, the procedure over-predicts the capacity of the cans when the probing is done away from the imperfection; the probing fails to recognize the presence of imperfection and the predicted capacity is near to the capacity of the perfect can instead of the imperfect one. This demonstrates the crucial role played by the probing location. Another significant finding is the phenomenon of dominating imperfection: if more than one imperfection is present in the cylinder, the capacity is dictated by the dominating imperfection.

6.2 Outlook and future work

The results of this study are very promising and have the potential to change the way thin cylindrical shells are designed. However, there are several limitations that need to be addressed before the industrial applications of the reported results. These limitations, along with the suggestions for future work, are listed below.

- The effect of residual stresses, combined loading, and discontinuity in cylindrical shells have not been studied in this thesis. Studies, directed to addressed these issues, will be fruitful and will help to improve the designing of thin cylindrical shells.

- Three main factors are responsible for making wavy cylinders insensitive to imperfections: 1) reduction in effective radius of curvature, 2) stiffness introduced by waviness, and 3) periodic change in the direction of curvature. The individ-

ual contributions of the three main factors have not been addressed. It would be interesting to understand the individual contributions and the mechanics behind the imperfection insensitivity; this helps to design efficient thin cylindrical shells.

- The manufacturing feasibility of wavy cross-sectional thin cylindrical shells has not been studied; in the future, this aspect can be explored.

- The wavy cylindrical shells have been investigated for their sensitivity to geometric imperfections; however, the effect of material imperfections and residual stresses has not been addressed. These are the natural next steps in this line of research.

- The proposed procedure for the non-destructive capacity prediction has not been implemented experimentally that is necessary for the verification of our results. In future, experiments could be done to explore the idea further; indeed, one of our collaborator is performing experiments on mini Coke cans.

A long journey has to be traveled before the findings of this study are realized in real engineering applications. Nonetheless, the results of this study open a new avenue to explore, which will help designers of cylindrical shells and tall wind turbine towers in particular. This study shows that if wavy cross-sectional cylindrical shells are used, the high imperfection sensitivity of thin cylindrical shells can be circumvented. Further, our work on the non-destructive technique gives a hope that a framework can be developed to predict the buckling capacity of thin shells without measuring the imperfection.

REFERENCES

[1] Yadav, K.K., Gerasimidis S., Instability of thin steel cylindrical shells under bending, Thin-Walled Structures (2019), 137: 151-166.

[2] Yadav, K.K., Gerasimidis, S., Imperfection Insensitivity of Thin Wavy Cylindrical Shells Under Axial Compression or Bending, Journal of Applied Mechanics (2020), 87(4):041003.

[3] Yadav, K.K., Gerasimidis, S., Imperfection insensitive thin cylindrical shells for next generation wind turbine towers, Journal of Constructional Steel Research (2020), 172: 106228.

[4] Yadav, K.K., Nicholas, C., Emmanuel, V., Rubinstein, S.M., Gerasimidis, S., A non-destructive technique for the evaluation of thin cylindrical shells axial buckling capacity, Manuscripts in preparation.

[5] Hsue-Shen, T., A theory for the buckling of thin shells, Journal of the Aeronautical Sciences (1942), 9(10): 373-384.

[6] Karman, T.v., The buckling of thin cylindrical shells under axial compression, Journal of the Aeronautical Sciences (1941), 8(8): 303-312.

[7] Karman, T.v., Hsue-Shen, T., The buckling of spherical shells by external pressure, Journal of the Aeronautical Sciences (1939), 7(2): 43-50.

[8] Koiter, W. T., The stability of elastic equilibrium Doctoral Thesis (1945), Deft University of Technology, Delft.

[9] Hutchinson, J. W., Axial buckling of pressurized imperfect cylindrical shells, AIAA journal (1965), 3(8): 1461-1466.

[10] Hutchinson, J. W., Buckling of imperfect cylindrical shells under axial compression and external pressure, AIAA journal (1965), 3(10): 1968-1970.

[11] Budiansky, B., Hutchinson, J. W., A survey of some buckling problems, AIAA journal (1966), 4(9): 1505-1510.

[12] Hutchinson, J. W., Koiter, W.T., Postbuckling theory, Appl. Mech. Rev (1970), 23(12): 1353-1366.

[13] Brush, D.O., Almroth, B.O., Buckling of bars, plates, and shells, McGraw-Hill, New York(1975).

[14] Calladine, C. R., Theory of shell structures, Cambridge university press (1989).

[15] Euro–Code, Design of steel structures- Part-1-6: Strength and Stability of Shell Structures, EUROPEAN STANDARD (2007), Brussels, Belgium.

[16] Khatri, D., Economics of taller wind towers, Renew Energy World North Am Mag (2010), 2(1): 3-10.

[17] van Es, S.H.,J., Gresnigt, A.M., Vasilikis, D., Karamanos, S.A., Ultimate bending capacity of spiral-welded steel tubes–Part II: Predictions, Thin-Walled Structures (2016), 102: 305-319.

[18] Abdullah, M., Shahabeddin, T., Angelina, J., Fariborz, M., Andrew, T.M., Eric, S., Benjamin, W.S. Modeling the Flexural Collapse of Thin-Walled Spirally Welded Tapered Tubes, Journal of Structural Engineering (2018), 144(2): 04017201.

[19] Guo, L., Yang, S., Jiao, H., Behavior of thin-walled circular hollow section tubes subjected to bending, Thin-walled structures (2013), 73: 281-289.

[20] Jonkman, J., Butterfield, S., Musial, W., Scott, G., Definition of a 5-MW Reference Wind Turbine for Offshore System Development, National Renewable Energy Laboratory (2009).

[21] Brazier, L. G., On the flexure of thin cylindrical shells and other "thin" sections, Proceedings of the Royal Society of London A: Mathematical, Physical and Engineering Sciences (1927), 116(773): 104-114.

[22] Wood, J. D., The flexure of a uniformly pressurized, circular, cylindrical shell, Journal of Applied Mechanics (1958), 25(12): 453-458.

[23] Reissner.,E., On finite bending of pressurized tubes, J. Appl. Mech (1959), 26: 386-392.

[24] Reissner, E., Weinitschke, H.J., Finite pure bending of circular cylindrical tubes, Quarterly of applied mathematics (1963), 20(4): 305-319.

[25] Thurston, G. A., Critical bending moment of circular cylindrical tubes, Journal of Applied Mechanics (1977), 44(1): 173-175.

[26] Boyle, J. T., The finite bending of curved pipes, International Journal of Solids and Structures (1981), 17(5): 515-529.

[27] Molyneaux, T., Li, L., Dynamic elastic instability of long circular cylindrical shells under pure bending, Thin-walled structures (1996), 24(2): 123-133.

[28] Clifford, S. A., Bending strength of tubing in the plastic range, Journal of the aeronautical sciences (1957), 24(8): 605-610.

[29] Kyriakides, S., Shaw, P.K., Response and stability of elastoplastic circular pipes under combined bending and external pressure, International Journal of Solids and Structures (1982), 18(11): 957-973.

[30] Shaw, P.K., Kyriakides, S., Inelastic analysis of thin-walled tubes under cyclic bending, International Journal of Solids and Structures (1985), 21(11): 1073-1100.

[31] Corona, E., Kyriakides, S., On the collapse of inelastic tubes under combined bending and pressure, International Journal of Solids and Structures (1988), 24(5): 505-535.

[32] Karamanos, S.A., Tassoulas, J.L., Stability of inelastic tubes under external pressure and bending, Journal of engineering mechanics (1991), 117(12): 2845-2861.

[33] Houliara, S., Karamanos, S.A., Buckling of Thin-Walled Long Steel Cylinders Subjected to Bending, Journal of pressure vessel technology (2011), 133(1): 011201.

[34] Axelrad, E. L., Flexure of thin-walled beams under large elastic displacements, Izvestiya Akademii Nauk SSSR, Otdelenie Tekhnicheskikh Nauk, Mekhanika i Mashinostroenie (1961), 3: 124-132.

[35] Hutchinson, J. W., Buckling and initial postbuckling behavior of oval cylindrical shells under axial compression, Journal of Applied Mechanics (1968), 35(1): 66-72.

[36] Fabian, O., Collapse of cylindrical, elastic tubes under combined bending, pressure and axial loads, International Journal of Solids and Structures (1977), 13(12): 1257–1270.

[37] Stephens, W. B., Starnes, J.H., JR., Almroth, B.O., Collapse of long cylindrical shells under combined bending and pressure loads, AIAA Journal (1975), 13(1): 20-25.

[38] Chen, Y.N., Kempner J., Buckling of oval cylindrical shells under compression and asymmetricbending, AIAA Journal (1976), 14(9): 1235-1240.

[39] Karamanos, S. A., Bending instabilities of elastic tubes, International Journal of Solids and Structures (2002), 39(8): 2059-2085.

[40] Li, L., Kettle, R., Nonlinear bending response and buckling of ring-stiffened cylindrical shells under pure bending, International journal of solids and structures (2002), 39(3): 765-781.

[41] Veldman, S.L., Wrinkling prediction of cylindrical and conical inflated cantilever beams under torsion and bending, Thin-walled structures (2006), 44(2): 211-215.

[42] Houliara, S., Karamanos, S.A., Buckling and post-buckling of long pressurized elastic thin-walled tubes under in-plane bending, International Journal of non-linear mechanics (2006), 41(4): 491-511.

[43] Polenta, V., Garvey, S.D., Chronopoulos, D, Long, A.C., Morvan, H.P., Optimal internal pressurisation of cylindrical shells for maximising their critical bending load, Thin-Walled Structures (2015), 87: 133-138.

[44] Mathon, C., Limam, A., Experimental collapse of thin cylindrical shells submitted to internal pressure and pure bending, Thin-Walled Structures (2006), 44(1): 39-50.

[45] Rotter, J.M., Sadowski, A.J., Chen, L., Nonlinear stability of thin elastic cylinders of different length under global bending, International Journal of Solids and Structures (2014), 51(15-16): 2826-2839.

[46] Reddy, B. D., An experimental study of the plastic buckling of circular cylinders in pure bending, International Journal of Solids and Structures (1979), 15(9): 669-683.

[47] Gellin, S., The plastic buckling of long cylindrical shells under pure bending, International Journal of Solids and Structures (1980), 16(5): 397-407.

[48] Fabian, O., Resilience and sustainability of civil infrastructure: toward a unified approach, Ocean Engineering (1981), 8(3): 295-330.

[49] Kyriakides, S., Ju, G.T., Bifurcation and localization instabilities in cylindrical shells under bendingI. Experiments, International Journal of Solids and Structures (1992), 29(9): 1117-1142.

[50] Ju, G.T., Kyriakides, S., Bifurcation and localization instabilities in cylindrical shells under bendingII. Predictions, International journal of solids and structures (1992), 29(9): 1143-1171.

[51] Karamanos, S.A., Tassoulas, J.L., Tubular members. I: Stability analysis and preliminary results, Journal of engineering mechanics (1996), 122(1): 64-71.

[52] Karamanos, S.A., Tassoulas, J.L., Tubular members. II: Local buckling and experimental verification, Journal of engineering mechanics (1996), 122(1): 72-78.

[53] van Es, S.H.,J., Gresnigt, A.M., Vasilikis, D., Karamanos, S.A., Ultimate bending capacity of spiral-welded steel tubes–part I: experiments, Thin-Walled Structures (2016), 102: 286-304.

[54] Fariborz, M., Andrew, T.M., Angelina, J., Abdullah, M., Shahabeddin, T., Eric, S., Benjamin, W.S., Imperfection measurements to predict buckling behavior of slender steel tubes, Thin-Walled Structures (2018), 123(0263-8231): 270-281.

[55] Angelina, J., Andrew, T.M., Shahabeddin, T., Abdullah, M., Eric, S., Nestor, A., Ben, W.S., Spirally welded steel wind towers: Buckling experiments, analyses, and research needs, Journal of Constructional Steel Research (2016), 125(0143-974X): 218-226.

[56] Angelina., J., Andrew, T.M., Fariborz, M., Abdullah, M., Shahabeddin, T., Eric, S., Benjamin, W.S., Large-Scale Bending Tests of Slender Tapered Spirally Welded Steel Tubes, Journal of Structural Engineering (2016), 142(12): 04016136.

[57] Yadav, K.K., Gerasimidis, S., On the investigation of the most critical shape imperfections for wind turbine tower shell structures, Proc. Annual Stability Conference, Structural Stability Research Council (2017), San Antonio, TX.

[58] Pueppke, N. B., Buckling Behavior of Spirally Welded Steel Tubes Master's Thesis (2014), Deft University of Technology, Delft.

[59] Wunderlich, W., Albertin, U., Analysis and load carrying behaviour of imperfection sensitive shells, International journal for numerical methods in engineering (2000), 47(1-3): 255-273.

[60] Deml, M., Wunderlich, W., Direct evaluation of the worstimperfection shape in shell buckling, Computer methods in applied mechanics and engineering (1997), 149(1-4): 201-222.

[61] Lee, C., Chang, K., Park, K., Shin, H., Kim, T., Bending resistance of girth-welded stainless steel circular hollow sections, Thin-Walled Structures (2013), 73: 174-184.

[62] Kiymaz, G., Strength and stability criteria for thin-walled stainless steel circular hollow section members under bending, Thin-walled structures (2005), 43(10): 1534-1549.

[63] Winterstetter, T.A, Schmidt, H., Stability of circular cylindrical steel shells under combined loading, Thin-Walled Structures (2002), 40(10): 893-910.

[64] Weingarten, V.I.,Seide, P., Peterson, J.P., Buckling of thin-walled circular cylinders, NASA SP-8007 (1968).

[65] Seide, P., Weingarten, V.I., Morgan, E.J., The development of design criteria for elastic stability of thin shell structures, TRW SPACE TECHNOLOGY LABS LOS ANGELES CA (1960).

[66] Ning, X., Pellegrino S., Imperfection-insensitive axially loaded thin cylindrical shells, International Journal of Solids and Structures (2015), 62: 39-51.

[67] Ning, X., Pellegrino S., Experiments on imperfection insensitive axially loaded cylindrical shells, International Journal of Solids and Structures (2017), 115-116: 73-86.

[68] Yadav, K.K., Gerasimidis S., Imperfection insensitivity of wavy cross-sectional thin cylindrical shells under bending, Proceedings of IASS Annual Symposia (2018), 25: 1-8.

[69] Thompson, J.M.T., Advances in Shell Buckling: Theory and Experiments, International Journal of Bifurcation and Chaos (2015), 25(01).

[70] Thompson, J.M.T., Hutchinson, J.W., Sieber, J., Shock-Sensitivity in Shell-Like Structures: With Simulations of Spherical Shell Buckling, International Journal of Bifurcation and Chaos (2016), 26(02).

[71] Thompson, J.M.T., Hutchinson, J.W., Sieber, J., Probing Shells Against Buckling: A Nondestructive Technique for Laboratory Testing, International Journal of Bifurcation and Chaos (2017), 27(14).

[72] Hutchinson, J.W., Thompson, J.M.T., Nonlinear Buckling Interaction for Spherical Shells Subject to Pressure and Probing Forces, Journal of Applied Mechanics (2017), 84(06).

[73] Emmanuel, V., Kreilos, T., Schneider, T.M., Rubinstein, S.M., Stability Landscape of Shell Buckling, Phys. Rev. Lett. (2017), 119(22).

[74] Haigui, F., Critical buckling load prediction of axially compressed cylindrical shell based on non-destructive probing method, Thin-Walled Structures (2019), 139: 91-104.

[75] Abramian, A., Emmanuel, V., Emilio, L., Rubinstein, S.M., Schneider, T.M., Non-destructive prediction of the buckling load of imperfect shells, Submitted

[76] Ning, X., Pellegrino S., Searching for imperfection insensitive externally pressurized near-spherical thin shells, International Journal of Solids and Structures (2018), 120: 49-67.

[77] Sadowski, A.J., Camara, A., Málaga-Chuquitaype, C., Dai, K., Seismic analysis of a tall metal wind turbine support tower with realistic geometric imperfections, Earthquake Engineering & Structural Dynamics (2017), 46(2): 201-219.

[78] Kyriakides, S., Corona, E., Mechanics of offshore pipelines: volume 1 buckling and collapse, Elsevier (2007), 1.

[79] Timoshenko, S.P., Gere, J.M., Theory of elastic stability. McGraw-Hill (1961).

[80] Simulia, ABAQUS theory manual, Dassault Systems Simulia Corporation (2012).

[81] Gerasimidis, S., Computational assessment of the residual stresses of a wind turbine tower steel shell and their effect on its buckling capacity, Proc. Annual Stability Conference, Structural Stability Research Council (2017), San Antonio, TX.

[82] Wullschleger, L., Numerical investigation of the buckling behaviour of axially compressed circular cylinders having parametric initial dimple imperfections Doctoral Thesis (2006), ETH, Zurich.

[83] Hutchinson, J. W., Buckling of spherical shells revisited, Proceedings of the Royal Society of London A: Mathematical, Physical and Engineering Sciences (2016), 472: 20160577.

[84] Rotter, J.M., Teng, J., Elastic Stability of Cylindrical Shells with Weld Depressions, Journal of Structural Engineering (1989), 115(5): 1244-1263.

[85] Lee, A., Jiménez, F.L., Marthelot, J., Hutchinson, J.W., Reis, P.M., The geometric role of precisely engineered imperfections on the critical buckling load of spherical elastic shells, Journal of Applied Mechanics (2016), 83(11): 111005.

[86] Sherman, D.R., TEST OF CIRCULAR STEEL TUBES IN BENDING, Journal of the Structural Division (1976), 102(11): 2181-2195.

[87] Elchalakani, M., Zhao, X.L., Grzebieta, R., Bending tests to determine slenderness limits for cold-formed circular hollow sections, Journal of Constructional Steel Research (2002), 58(11): 1407-1430.

[88] Hilburger, M.W., Lindell, M.C., Waters, W.A., Gardner, N.W., Test and Analysis of Buckling-Critical Stiffened Metallic Launch Vehicle Cylinders, Proc. AIAA/ASCE/AHS/ASC Structures, Structural Dynamics, and Materials Conference (2018).

[89] Gerasimidis, S., Virot, E., Hutchinson, J.W., Rubinstein, S.M., On Establishing Buckling Knockdowns for Imperfection-sensitive Shell Structures, Journal of Applied Mechanics (2018), 85(9): 091010.

[90] Seide, P., Weingarten V., On the buckling of circular cylindrical shells under pure bending, Journal of Applied Mechanics (1961), 28(1): 112-116.

[91] Riks, E., An incremental approach to the solution of snapping and buckling problems, International journal of solids and structures (1979), 15(7): 529-551.

[92] Jiménez, F.L., Marthelot, J., Lee, A., Hutchinson, J. W., Pedro, R.M., Technical brief: knockdown factor for the buckling of spherical shells containing large-amplitude geometric defects, Journal of Applied Mechanics (2017), 84(3).

[93] Marthelot, J., Jiménez F.L., Lee, A., Hutchinson, J.W., Pedro, R.M., Buckling of a pressurized hemispherical shell subjected to a probing force, Journal of Applied Mechanics (2017), 84(12).

[94] Yadav, K.K., Gerasimidis, S., Imperfection insensitive thin steel tubular shells under bending, Proceedings of the annual stability conference structural stability research council St. Louis, Missouri(2019).

[95] Haynie, W., Hilburger, M., Bogge, M., Maspoli. M., Kriegesmann, B., Validation of Lower-Bound Estimates for Compression-Loaded Cylindrical Shells, 53rd AIAA/ASME/ASCE/AHS/ASC Structures, Structural Dynamics and Materials Conference.